REPORT DOCUMENTATION PAGE

Form Approved
OMB No. 0704-0188

1. REPORT DATE *(DD-MM-YYYY)*	2. REPORT DATE	3.
	March 1999	Final Report

4. TITLE AND SUBTITLE
Nonlinear Interaction of Surge Waves with Ice Cover in River Channels

5a. CONTRACT NUMBER

5b. GRANT NUMBER
DAAG55-98-1-0520

5c. PROGRAM ELEMENT NUMBER

6. AUTHOR(S)
Shen, Hung Tao, Dr.
Xia, Xun, Research Assistant

5d. PROJECT NUMBER

5e. TASK NUMBER

5f. WORK UNIT NUMBER

7. PERFORMING ORGANIZATION NAME(S) AND ADDRESS(ES)
Clarkson University
Civil & Environmental Engineering, PO Box 5710
Potsdam, NY 13699-5710

8. PERFORMING ORGANIZATION REPORT NUMBER
375-661

9. SPONSORING/MONITORING AGENCY NAME(S) AND ADDRESS(ES)
Department of the Army
Army Research Office
PO Box 12211
Research Triangle Park, NC 27709-2211

10. SPONSOR/MONITOR'S ACRONYM(S)
ARO 39244.1-EV-II

11. SPONSORING/MONITORING AGENCY REPORT NUMBER

12. DISTRIBUTION AVAILABILITY STATEMENT
DISTRIBUTION STATEMENT A
Approved for Public Release
Distribution Unlimited

13. SUPPLEMENTARY NOTES

14. ABSTRACT
See Attached

15. SUBJECT TERMS

16. SECURITY CLASSIFICATION OF:			17. LIMITATION OF ABSTRACT	18. NUMBER OF PAGES	19a. NAME OF RESPONSIBLE PERSON
a. REPORT	b. ABSTRACT	c. THIS PAGE		102	Dr. Gina Lee-Glauser, Director of Research
					19b. TELEPONE NUMBER (*Include area code*) (315) 268-3765

Abstract

The interaction of water waves with an ice cover in river channels is studied using one-dimensional governing equations which describe fluid continuity, momentum, and the ice cover response. The ice cover is assumed to be a continuous, thin elastic plate. Both linearized and nonlinear forms of the above three equations are analyzed in this study.

The effects of a constant compressive axial force along an ice cover on the propagation characteristics of linear water waves, i.e. celerity, attenuation, and group velocity, are first investigated over the entire spectrum of wavelengths on the basis of linear stability theory. It is found that only when an axial force approaches a critical value and the wavelength is around $2\pi l$, where l is the characteristic length of the cover, the effect of the axial force is significant.

The nonlinear terms in the water equation, which are ignored in the linear theory, become significant in highly unsteady flows such as surges caused by ice jam releases. An analytical solution for the nonlinear shallow wave equations is obtained. The effects of ice inertia and an axial force on the nonlinear waves are examined.

The stresses induced in ice cover by both linear and nonlinear waves obtained from the above mentioned analysis are used to investigate the possible formation of closedly-spaced transverse cracks often observed during ice cover breakups. The formation of closedly-spaced transverse cracks is the key mechanism for river ice breakup and the initiation of breakup ice runs. The validity of the linear theory is found to be very limited. The nonlinear analysis provides results in close agreement with field observations. These results provide basic explanation of the formation mechanism of transverse cracks which initiate the breakup ice runs.

NONLINEAR INTERACTION OF SURGE WAVES WITH ICE COVER IN RIVER CHANNELS

Final Report
Submitted to
Army Research Office
for Grant No. DAAG55-98-1-0520

by

Hung Tao Shen

March 1999
Department of Civil and Environmental Engineering
Clarkson University
Potsdam, NY 13699-5710

Acknowledgements

This report was prepared by Xun Xia, Research Assistant, and Dr. Hung Tao Shen, Professor, Department of Civil and Environmental Engineering, Clarkson University. This study was partially supported by the U.S. Army Research Office through Grant No. DAAG55-98-1-0520, and the U.S. Army Cold Regions Research and Engineering Laboratory through Contract No. DACA89-94-K-0017.

Abstract

The interaction of water waves with an ice cover in river channels is studied using one-dimensional governing equations which describe fluid continuity, momentum, and the ice cover response. The ice cover is assumed to be a continuous, thin elastic plate. Both linearized and nonlinear forms of the above three equations are analyzed in this study.

The effects of a constant compressive axial force along an ice cover on the propagation characteristics of linear water waves, i.e. celerity, attenuation, and group velocity, are first investigated over the entire spectrum of wavelengths on the basis of linear stability theory. It is found that only when an axial force approaches a critical value and the wavelength is around $2\pi l$, where l is the characteristic length of the cover, the effect of the axial force is significant.

The nonlinear terms in the water equation, which are ignored in the linear theory, become significant in highly unsteady flows such as surges caused by ice jam releases. An analytical solution for the nonlinear shallow wave equations is obtained. The effects of ice inertia and an axial force on the nonlinear waves are examined.

The stresses induced in ice cover by both linear and nonlinear waves obtained from the above mentioned analysis are used to investigate the possible formation of closedly-spaced transverse cracks often observed during ice cover breakups. The formation of closedly-spaced transverse cracks is the key mechanism for river ice breakup and the initiation of breakup ice runs. The validity of the linear theory is found to be very limited. The nonlinear analysis provides results in close agreement with field observations. These results provide basic explanation of the formation mechanism of transverse cracks which initiate the breakup ice runs.

Contents

List of Tables

List of Figures

Chapter 1

Introduction

1.1 Background

The breakup of a river ice cover can generally be classified as a thermal breakup or a mechanical breakup. A thermal breakup is essentially a thermal meltout process with the floating ice cover deteriorating and melting in place with insignificant ice movement. This type of breakup occurs when the river discharge remains relatively steady during the spring breakup period. The physics of thermal breakup is relatively well understood. A mechanical breakup is the fragmentation of a floating river ice cover by hydraulic and mechanical forces associated with the ice rubble load and the changes in river discharge and water level. The driving forces that contribute to a mechanical breakup include: 1) frictional forces due to water current and wind; 2) streamwise component of the weight of the cover; 3) the longitudinal and vertical forces acting on the ice cover by the ice rubble in an ice run from upstream; and 4) pressure variation on the underside of the ice cover produced by the water wave.

A mechanical breakup often leads to severe ice runs. Breakup ice runs and the associated ice jams can be destructive to hydraulic structures and shoreline properties. In addition to these concerns, the problem of mechanical breakup is also important for winter operations of dams and hydropower stations, where the flow regulation is limited by the stability of the ice cover.

In the last ten years, significant progress has been made on the understanding of the

dynamics of ice runs and ice jams (Shen et al. 1990, 1993, Liu and Shen 1998). However, since a clear understanding of the mechanics of river ice breakup is not available, predictions of the occurrences of breakup ice runs and ice jams still can not be made. The lack of understanding the mechanics of river ice breakup is mainly due to the lack of understanding on the phenomena of fracture of an ice cover under the action of surge waves, which is the key to the initiation of ice runs from a floating ice cover.

1.2 Mechanical Breakup

Prowse and Demuth (1989) categorized mechanical breakup into pre-frontal and frontal modes. During the initial stage of the breakup, pre-frontal mode represents the breakup of an ice cover into large sections of ice sheets. Frontal mode represents failure coincident with the surge wave and ice runs during the later stage of the breakup. Early in spring, shortly after the beginning of spring runoff, uplift pressures develop on the underside of shore-fast ice cover. Longitudinal cracks form along the river. Based on the classical theory of beams on an elastic foundation, Billfalk (1981) and Beltaos (1985, 1990) developed theoretical explanations for the formation of longitudinal cracks along the river. These analyses assumed that the dynamic effects are negligible, and the longitudinal gradient of the uplift pressure is small.

The formation of longitudinal cracks is a prelude to the breakup. It is often followed by the formation of far-spaced transverse cracks. Shulyakovskii (1972) and Beltaos (1984) showed that in meandering channels transverse cracks can form, spaced in the order of 1000 times the cover thickness, due to the bending moment produced by the in-plane hydraulic forces. Beltaos (1990) defined the onset of breakup at a given site as the time when the local ice cover is set in motion. He derived the criterion for the onset of breakup based on the boundary constraints of the river plane geometry in allowing the movement of the large ice sheets formed by far-spaced transverse cracks. However, these movements are limited and usually do not lead to ice runs until closedly-spaced transverse cracks form when a surge wave passes by.

The theories of longitudinal and transverse crack formations discussed above may be

used to describe the pre-frontal modes. The frontal modes occur during the later stage of the breakup period, and leads to ice runs, which are caused by a rapid increase of river discharge either due to runoff increase or due to an ice jam release from upstream. The process is much more dynamic, and may not be analyzed with static formulations discussed above. Parkinson (1982) provided the following vivid account on the dynamics of ice cover fracture during the breakup event on the Liard-Mackenzie River from a surge wave acting on a competent ice cover:

> *Upon the arrival of the flood wave, there was a rapid rise of the cover. ...Cracks spaced at 50 to 200 m apart appeared across the ice cover, followed by small ridges of crushed ice formed along the cracks. Beyond this stage, ... the water level rise continued and the cover re-adjusted and moved slowly from 10 to 100 m, until it wedged against the shore again. This movement was accompanied by widespread breakage of the cover, with crack lines and associated ridging spaced at 10 to 50 m. This in-situ fracture of the ice cover when the front of the surge wave was passing occurred over long reaches of the river. The broken ice front was moving at a speed approximately equal to that of the free surface surge wave. The broken ice did not move downstream, and the water level returned to approximately the pre-flood level following the passage of the wave.... Prolonged ice run occurred only after the water level rose a couple days later to the point when the broken ice could be lifted and carried downstream.*

This description and similar observations by Gerard et al. (1984) and Prowse (1986) clearly show the importance of the effect of a surge wave on the formation of breakup ice runs. In their attempts to explain the formation of closedly-spaced transverse cracks due to a surge wave similar to that described above, Billfalk (1982) and Beltaos (1985) assumed static pressure distribution on the underside of the ice cover to represent the uplift due to surges and found that a water surface slope larger than 0.005 is required to break the ice cover. Such a large slope can not be found in rivers with an ice cover. Daly (1995) used linear analysis to study the interaction between river waves and ice cover, and suggested the possibility of the formation of cracks spaced at 10 m or less by waves in the gravity

wave range with small wave amplitude. This phenomenon was not observed in the field.

In this study, the linear analysis of Daly (1993, 1995) is extended to include the effect of an axial compressive force. The limitation of linear analysis is examined. A nonlinear analysis is carried out on the interaction of a floating river ice cover with shallow water waves, and the formation of transverse cracks during the passage of the waves.

Chapter 2

Governing Equations

It is commonly accepted that the effect of ice cover on water wave propagation in river channels is limited to the additional flow resistance due to the presence of an additional rough boundary and the reduction in flow cross section due to the ice cover submergence. Hydrostatic condition is considered to be valid. However, for a rapidly varying channel flow, the hydrostatic assumption may not be valid. The wave may be modified by the inertia and resistance to bending of the cover.

The governing equations for one-dimensional unsteady flow in a wide, rectangular ice-covered channel is presented in this chapter. The ice cover is assumed to be an intact, uniform, thin elastic plate. The ice-cover density and thickness are assumed to be constant in space and time. The fluid density changes in response to changes of fluid pressure.

2.1 Water Mass Conservation Equation

Considering a control volume in a one-dimensional channel as shown in Fig. 2.1, the mass conservation of water in the differential control volume is given as:

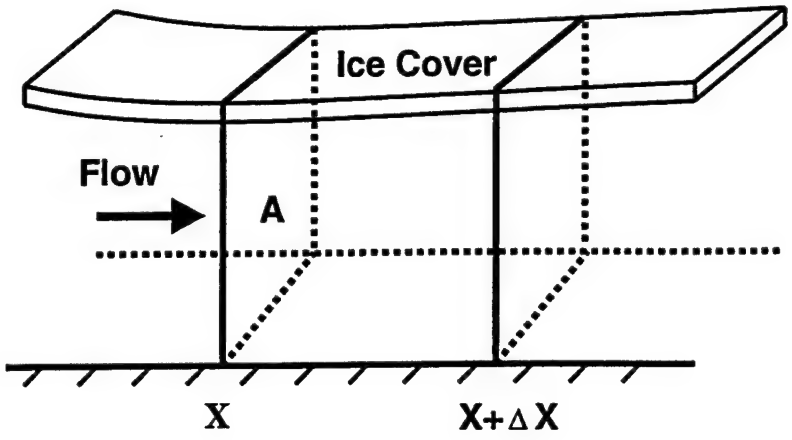

Figure 2.1: Differential element for mass conservation equation

$$[(\rho Au)_x - (\rho Au)_{x+\Delta x}]\Delta t = (\rho A \Delta x)_{t+\Delta t} - (\rho A \Delta x)_t$$

In differential form, this equation becomes

$$\frac{\partial(\rho A)}{\partial t} + \frac{\partial(\rho Au)}{\partial x} = 0$$

or

$$\frac{1}{\rho}\frac{D\rho}{Dt} + \frac{1}{A}\frac{DA}{Dt} + \frac{\partial u}{\partial x} = 0 \tag{2.1}$$

where $\frac{D}{Dt}$ = total derivative; x = longitudinal distance; t = time; A = channel cross-sectional area; u = cross section-averaged flow velocity; ρ = fluid density. If the flow is incompressible, Eq. 2.1 reduces to the traditional continuity equation for open channel flows.

Assuming that changes in fluid density are caused only by pressure deviations P' from hydrostatic, thus

$$\frac{1}{\rho}\frac{D\rho}{Dt} = \frac{1}{E_W}\frac{DP'}{Dt} \tag{2.2}$$

where E_W = bulk modulus of elasticity of water with a value of about $2.04 \times 10^9 N/m^2$ near 0^0C. Equations 2.1 and 2.2 give

$$\frac{1}{E_W}\frac{DP'}{Dt} + \frac{1}{A}\frac{DA}{Dt} + \frac{\partial u}{\partial x} = 0 \tag{2.3}$$

For a wide uniform rectangular channel,

$$\frac{1}{E_W}\frac{DP'}{Dt} + \frac{1}{d}\frac{Dd}{Dt} + \frac{\partial u}{\partial x} = 0 \tag{2.4}$$

where d = depth of flow from channel bottom to ice cover.

2.2 Water Momentum Equation

Considering a control volume of length Δx as shown in Fig. 2.2, the resultant force on the control volume in the longitudinal direction is

$$F_x = F_1 - F_2 + W_x - F_f = -\gamma \Delta x A \left[\frac{\partial}{\partial x}\left(d + z + \frac{\rho_i}{\rho}\eta + \frac{P'}{\rho g}\right) + \frac{\tau}{\gamma R}\right] \tag{2.5}$$

in which $R = \frac{A}{\bar{p}}$, hydraulic radius; τ = average shear stress due to the bed and ice cover; η = ice cover thickness; γ = unit weight of water. The term within the parenthesis is the piezometric head:

$$H = z + d + \frac{\rho_i}{\rho}\eta + \frac{P'}{\rho g} \tag{2.6}$$

The right-hand side terms of Eq. 2.5 can be derived as the following. The pressure forces acting on the control volume are

$$F_1 = AP_1 + \gamma A\overline{z} = AP_1' + g\rho_i\eta_1 A + \gamma A\overline{z}$$

$$F_2 = AP_2 + \gamma A\overline{z} + \gamma A\frac{\partial d}{\partial x} = AP_2' + g\rho_i\eta_2 A + \gamma A\overline{z} + \gamma A\frac{\partial d}{\partial x}\Delta x$$

where $\overline{z}$ = centroid of cross section A. The weight of water in the longitudinal direction is

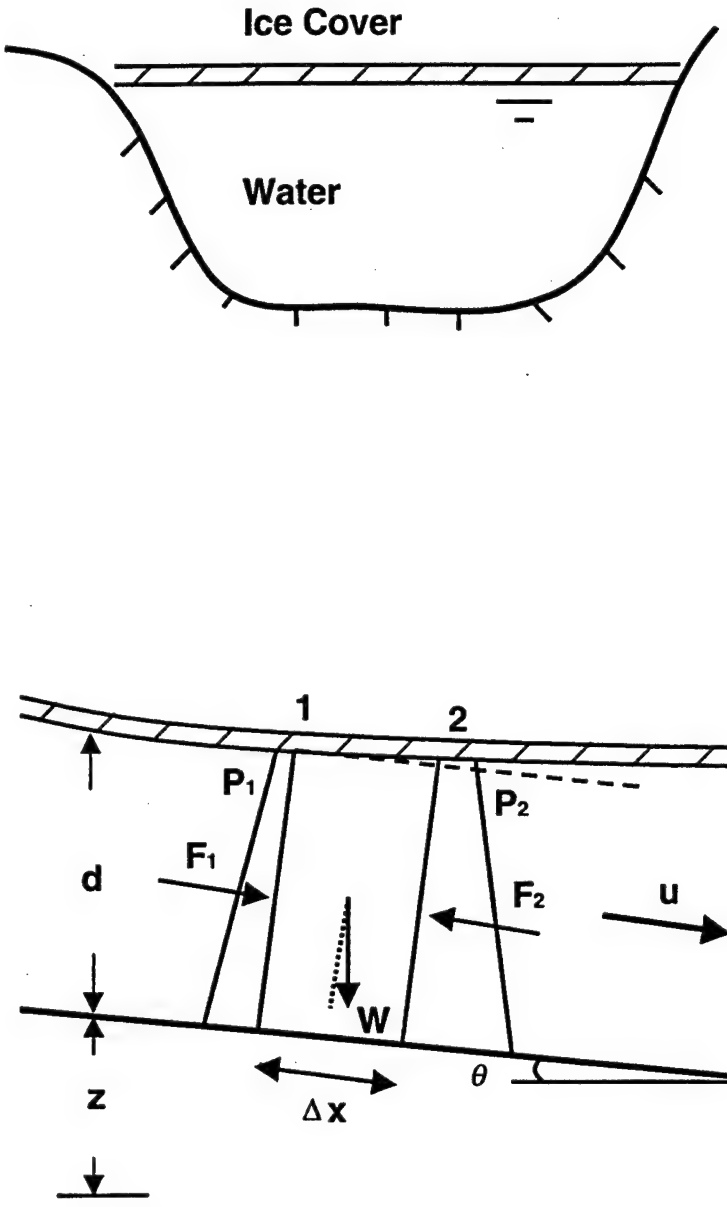

Figure 2.2: Definition sketch for momentum equation

$$W_x = \gamma A \Delta x \sin\theta = -\gamma A \Delta x \frac{\partial z}{\partial x}$$

where $\theta << 1$. The total friction

$$F_f = (\tau_b p_b + \tau_i p_i)\Delta x = \tau \bar{p} \Delta x$$

where $\bar{p}$ = wetted perimeter. According to Reynolds transport theorem:

$$\begin{aligned} F_x &= \frac{\partial}{\partial t}\int_x^{x+\Delta x} \rho u A dx + (\rho A u^2)_2 - (\rho A u^2)_1 \\ &= \left[\frac{\partial(\rho A)}{\partial t} + \frac{\partial(\rho A u)}{\partial x}\right] u\Delta x + \rho A \Delta x (\frac{\partial u}{\partial t} + u\frac{\partial u}{\partial x}) \\ &= \rho A \Delta x (\frac{\partial u}{\partial t} + u\frac{\partial u}{\partial x}) \end{aligned}$$

Defining the friction slope as

$$S_f = \frac{(\tau_b p_b + \tau_i p_i)}{\gamma A} \tag{2.7}$$

The momentum equation becomes

$$\frac{\partial u}{\partial t} + u\frac{\partial u}{\partial x} + g\frac{\partial H}{\partial x} + gS_f = 0 \tag{2.8}$$

When the vertical acceleration of the flow is significant, and the flow is incompressible, Eq. 2.8 becomes (Chaudhry 1993)

$$\frac{\partial u}{\partial t} + u\frac{\partial u}{\partial x} + g\frac{\partial H}{\partial x} + gS_f = \frac{d^2}{3}(\frac{\partial^3 u}{\partial x^2 \partial t} + u\frac{\partial^3 u}{\partial x^3}) \tag{2.9}$$

The Boussinesq's term on the right-hand side of Eq. 2.9 represents the effect of vertical acceleration, when the flow is not hydrostatic.

For a rectangular channel, the friction slope becomes

$$S_f = \frac{2\bar{\tau}}{\gamma d}$$

in which $\bar{\tau} = \frac{1}{2}(\tau_i + \tau_b) = \frac{\bar{f}}{8}\rho u^2$, and $\bar{f}$ = average friction factor of the bed and the ice cover. Noting that η and z do not vary with time, then the mass conservation equation (2.4) becomes

$$(1-\alpha)\left(\frac{\partial d}{\partial t} + u\frac{\partial d}{\partial x}\right) + \alpha\left(\frac{\partial H}{\partial t} + u\frac{\partial H}{\partial x} - u\frac{\partial z}{\partial x}\right) + d\frac{\partial u}{\partial x} = 0 \tag{2.10}$$

where $\alpha = \frac{\rho g d}{E_W}$. Since the celerity of acoustic wave $c_a = \sqrt{\frac{\frac{E_W}{\rho}}{1+\frac{E_W d}{E\eta}}} \simeq \sqrt{\frac{E_W}{\rho}}$ and the celerity of gravity wave $c = \sqrt{gd}$, the parameter α can be approximated by $\alpha \simeq \frac{c^2}{c_a^2}$.

If $\alpha \simeq 0$, i.e. $c \ll c_a$, the incompressible, hydrostatic flow condition prevails, and Eq. 2.10 reduces to the conventional momentum equation for open channel flow with a floating cover.

$$\frac{Dd}{Dt} + d\frac{\partial u}{\partial x} = 0 \tag{2.11}$$

2.3 Ice Cover Response Equation

The ice cover is assumed to be a homogeneous thin, continuous elastic plate. A differential element of ice cover per unit width, as shown in Fig. 2.3, is subjected to the hydrodynamic pressure, P, on the underside of the cover from the underlying water, in addition to water drag, wind drag and gravity. The cover is also subjected to an axial force resulting from the combination of fluid drag force, the component of the gravitational force in the longitudinal direction resulting from the slope of the water surface, and the loading at the upstream end of the intact cover due to ice rubble and fractured ice cover. This axial force is partially balanced by the intermittent bank resistance on the cover along the longitudinal shore cracks.

The momentum equation for the ice element in the x-direction, neglecting longitudinal inertia, is

$$F(x) - (F(x) + \frac{\partial F}{\partial x}\Delta x) + \Delta x\tau_x + \Delta x\eta\rho_i g\sin\theta = 0$$

or

$$\frac{\partial F}{\partial x} = \tau_x + \eta\rho_i g\sin\theta$$

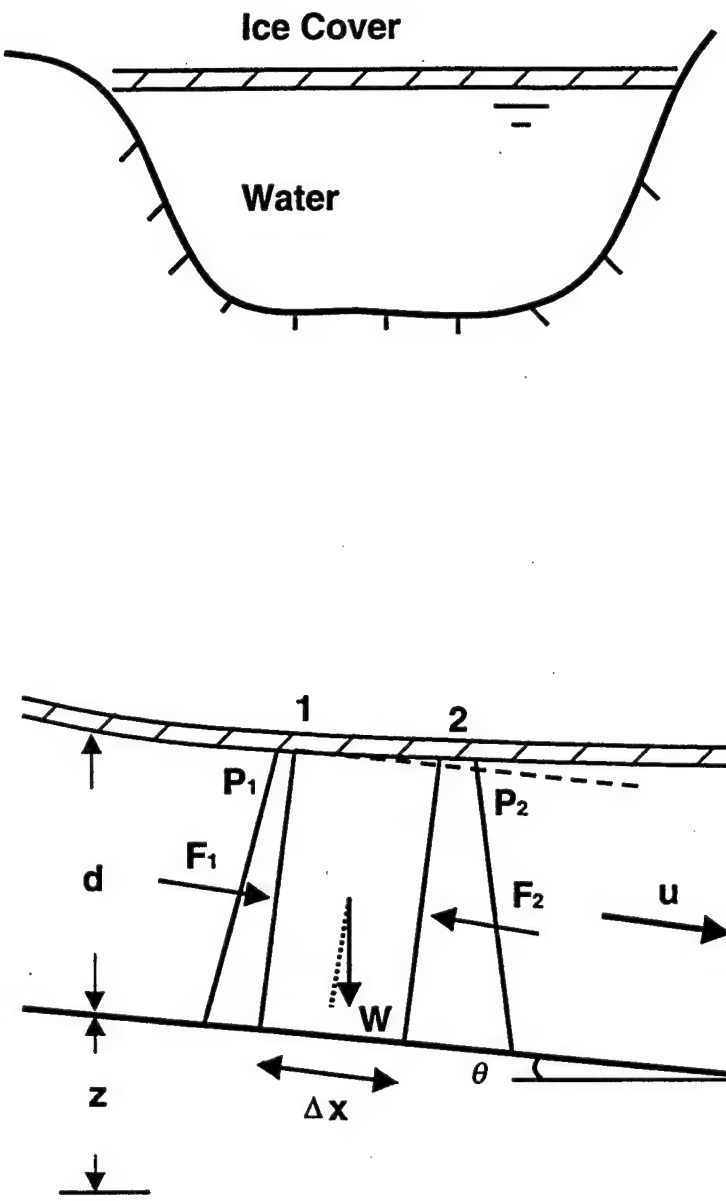

Figure 2.2: Definition sketch for momentum equation

where τ_x is the x-component of $\tau = \tau_W + \tau_a - \tau_b$; τ_W and τ_a are shear stresses on ice due to current and wind, respectively; and $\tau_b = \tau_B/B$ with τ_B = bank friction force per unit cover length; and B = cover width; $F(x)$ is the compressive axial force per unit width. The axial force $F(x)$ may be assumed to be a constant N for a uniform channel with constant τ_a and τ_W, except near the leading edge of the ice cover.

The momentum equation for the element in vertical direction is

$$V(x) - (V(x) + \frac{\partial V}{\partial x}\Delta x) - \Delta x \eta \rho_i g \cos\theta + \Delta x P(x) = \rho_i \eta \Delta x \frac{\partial^2 d}{\partial t^2}$$

in which, $P(x)$ is the uplift pressure at the interface.

For $\theta << 1$, this equation becomes

$$\frac{\partial V}{\partial x} + \eta \rho_i g - P(x) = -\rho_i \eta \frac{\partial^2 d}{\partial t^2} \tag{2.12}$$

in which, P(x)=$P'(x) + \eta\rho_i g$ is the net upward pressure on the underside of the ice cover at its deformed state. The pressure $P(x)$ is a combination of the hydrodynamic pressure $P(x)$ and the net buoyancy (Beltaos 1990).

Taking moment with respect to O gives:

$$-M(x) + (M(x) + \frac{\partial M}{\partial x}\Delta x) + (V(x) + \frac{\partial V}{\partial x}\Delta x)\Delta x$$
$$-F(x)\Delta x \frac{\partial d}{\partial x} + g\rho_i \eta \Delta x \frac{\Delta x}{2} - P(x)\Delta x \frac{\Delta x}{2} = 0$$

i.e.

$$\frac{\partial M}{\partial x} + V - F(x)\frac{\partial d}{\partial x} = 0$$

or

$$\frac{\partial^2 M}{\partial x^2} + \frac{\partial V}{\partial x} - F(x)\frac{\partial^2 d}{\partial x^2} - \frac{\partial F}{\partial x}\frac{\partial d}{\partial x} = 0 \tag{2.13}$$

For a thin plate, the bending moment is related to the curvature of the deflection curve of the plate (Ugural 1995), i.e. $M = -\frac{EI}{1-\nu^2}\frac{1}{r}$. For small deformations ($|\ \frac{\partial d}{\partial x}\ | \ll 1$), the curvature $\frac{1}{r} = \frac{\partial^2 d/\partial x^2}{[1+(\partial d/\partial x)^2]^{3/2}} = \frac{\partial^2 d}{\partial x^2} + (-\frac{3}{2})(\frac{\partial d}{\partial x})^2 \frac{\partial^2 d}{\partial x^2} + ... \approx \frac{\partial^2 d}{\partial x^2}$. Thus M can be approximated by $M = -\frac{EI}{1-\nu^2}\frac{\partial^2 d}{\partial x^2}$. Assuming $F(x)$ as a constant N. Equations. 2.12 and 2.13 give the following ice cover equation of motion:

$$\frac{EI}{1-\nu^2}\frac{\partial^4 d}{\partial x^4} + \rho_i \eta \frac{\partial^2 d}{\partial t^2} - P'(x) + N\frac{\partial^2 d}{\partial x^2} = 0 \tag{2.14}$$

or

$$\frac{\rho_i \eta}{\rho g}\frac{\partial^2 d}{\partial t^2} + l^4 \frac{\partial^4 d}{\partial x^4} - \frac{P'(x)}{\rho g} + \frac{N}{\rho g}\frac{\partial^2 d}{\partial x^2} = 0 \tag{2.15}$$

in which,

$$l = \left[\frac{EI}{\rho g(1-\nu^2)}\right]^{1/4} = \left[\frac{\eta^3 E}{12\rho g(1-\nu^2)}\right]^{1/4} \tag{2.16}$$

The characteristic length of the ice cover, l, represents the stiffness of the cover. This equation is the same as the equation for elastic plate on an elastic foundation with modulus $k = \rho g$. The elastic modulus of ice, E, is in the range of $0.4 \sim 9.8$ GPa, and the Poisson's ratio $\nu = 0.35$ (Daly 1993).

Equations 2.14 or 2.15 has been linearized based on the assumption

$$(\frac{\partial d}{\partial x})^2 \ll 1 \tag{2.17}$$

This implies that the nonlinear term $(\frac{\partial d}{\partial x})^2 \frac{\partial^2 d}{\partial x^2}$ is of an order smaller than the term $\frac{\partial^2 d}{\partial x^2}$ in the expression for the ice cover curvature $\frac{1}{r}$. The validity of this approximation will be discussed in Sections 3.2.3, 4.2.2 and 4.2.4.

Chapter 3

Linearized Model

In this chapter, wave propagation in ice-covered channels will be analyzed using the method of linear perturbation, in which the waves are represented by sinusoidal perturbations. The length of waves can be varied from very long kinematic flood waves to very short pressure waves. The general approach follows that of Ponce and Simons (1997), who analyzed the wave propagation in open channels. Daly (1993, 1995) studied the fracture of the ice cover by river waves, using the same approach. In Daly's analysis, the axial force acting along the cover was neglected. The purpose of the present chapter is to introduce the effect of the axial force acting along the cover and to examine the validity of the linear theory in the analysis of the breakup of ice cover due to wave-ice cover interaction.

3.1 Linear Perturbation Analysis

The governing equations 2.8, 2.10, and 2.15 must satisfy the unperturbed steady uniform flow condition for which $u = u_0$, $d = d_0$, $H = H_0$, and $\tau = \tau_0$ as well as the perturbed flow for which $u = u_0 + u'$, $d = d_0 + d'$, $H = H_0 + H'$, and $\tau = \tau_0 + \tau'$, where superscripted variables represent a small perturbation to the steady uniform flow. The gradients of the steady uniform variables are zero in x and t except that

$$\frac{\partial H_0}{\partial x} = \frac{\partial z}{\partial x} = -S_0 = -\frac{2\tau_0}{\rho g d_0} \tag{3.1}$$

Since the perturbations in ice thickness η and bed elevation z are not allowed, $H_0 = z + d_0 + \frac{\rho_i}{\rho}\eta$ for the hydrostatic condition. Equation 2.6 gives $H' = H - H_0$ as:

$$H' = d' + \frac{P'}{\rho g} \tag{3.2}$$

Substituting the perturbed variables into Eqs. 2.6, 2.9 and 2.12 and subtracting the undisturbed equations yield the following linearized perturbation equations after neglecting higher-order terms:

$$(1-\alpha_0)(\frac{\partial d'}{\partial t} + u_0\frac{\partial d'}{\partial x}) + \alpha_0(\frac{\partial H'}{\partial t} + u_0\frac{\partial H'}{\partial x}) + d_0\frac{\partial u'}{\partial x} = 0 \tag{3.3}$$

$$\frac{\partial u'}{\partial t} + u_0\frac{\partial u'}{\partial x} + g\frac{\partial H'}{\partial x} + gS_0(\frac{2u'}{u_0} - \frac{d'}{d_0}) = 0 \tag{3.4}$$

$$\frac{\rho_i\eta}{\rho g}\frac{\partial^2 d'}{\partial t^2} + l^4\frac{\partial^4 d'}{\partial x^4} - (H' - d') + \frac{N}{\rho g}\frac{\partial^2 d'}{\partial x^2} = 0 \tag{3.5}$$

In order to provide a convenient way to examine the various wave models, Eq. 3.4 is recasted as

$$\frac{l_c}{g}\frac{\partial u'}{\partial t} + \frac{au_0}{g}\frac{\partial u'}{\partial x} + p\frac{\partial H'}{\partial x} + kS_0(\frac{2u'}{u_0} - \frac{d'}{d_0}) = 0 \tag{3.6}$$

in which l_c, a, p, k are integers that can take a value of either 0 or 1 , depending on which terms are used to describe the wave motion.

If the flow is assumed to be incompressible, the effect of including the vertical inertia of water may be analyzed by using a linearized Boussinesq's approximation. The above equation becomes (Chaudhry 1993):

$$\frac{l_c}{g}\frac{\partial u'}{\partial t} + \frac{au_0}{g}\frac{\partial u'}{\partial x} + p\frac{\partial H'}{\partial x} + kS_0(\frac{2u'}{u_0} - \frac{d'}{d_0}) - \bar{b}\frac{d_0^2}{3g}(\frac{\partial^3 u'}{\partial x^2 \partial t} + u_0\frac{\partial^3 u'}{\partial x^3}) = 0 \tag{3.7}$$

in which $\bar{b}$ is an integer that can take a value of either 0 or 1.

The propagation of shallow water waves is controlled by the balance of the various forces included in the momentum equation. In Eq. 3.7, the first term represents the local inertia term, the second term represents the convective inertia term, the third term represents the pressure differential term, the fourth term accounts for the friction and bed slopes, and the fifth term represents the vertical inertia of water. Various wave models can be constructed, depending on which of these terms is assumed to be negligible when compared with the remaining terms. The wave models are: (1) Kinematic wave, $l_c = a = p = \bar{b} = 0, k = 1$; (2) diffusion wave, $l_c = a = \bar{b} = 0, p = k = 1$; (3) steady dynamic wave, $l_c = \bar{b} = 0, a = p = k = 1$; (4) gravity wave, $l_c = a = p = 1, k = \bar{b} = 0$; (5) dynamic wave, $l_c = a = p = k = 1$, $\bar{b} = 0$; and (6) Boussinesq's approximation, $l_c = a = p = k = \bar{b} = 1$.

Assuming the perturbations are in the following exponential form :

$$\frac{d'}{d_0} = \hat{d}e^{[i(\sigma\hat{x}-\beta\hat{t})]} \tag{3.8}$$

$$\frac{u'}{u_0} = \hat{u}e^{[i(\sigma\hat{x}-\beta\hat{t})]} \tag{3.9}$$

$$\frac{H'}{d_0} = \hat{H}e^{[i(\sigma\hat{x}-\beta\hat{t})]} \tag{3.10}$$

in which $\hat{d}$, $\hat{u}$, and $\hat{H}$ = dimensionless amplitudes; $\hat{x}$, $\hat{t}$ = dimensionless space and time coordinates; σ = a dimensionless wave number; and β = a dimensionless complex wave propagation factor. These dimensionless variables are defined as the following:

$$\sigma = \left(\frac{2\pi}{L}\right) L_0 \tag{3.11}$$

$$\hat{x} = \frac{x}{L_0} \tag{3.12}$$

$$\hat{t} = \frac{tu_0}{L_0} \tag{3.13}$$

where $L_0 = \frac{d_0}{S_0}$, a longitudinal length scale; and $\beta = \beta_R + i\beta_I$. The imaginary part describes the dimensionless wave amplitude $\hat{d}e^{\beta_I\hat{t}}$.

By defining the real part of β as

$$\beta_R = \frac{2\pi}{T}\frac{L_0}{u_0} \tag{3.14}$$

the dimensionless wave celerity $\hat{c}$ can be written as

$$\hat{c} = \frac{\beta_R}{\sigma} \tag{3.15}$$

where $\hat{c} = \frac{c}{u_0}$, and the wave celerity $c = \frac{L}{T}$, in which L = wave length and T = wave period.

Substituting (3.7), (3.8), and (3.9) into (3.3), (3.5), and (3.6) results in the following set of equations:

$$\begin{bmatrix} i\sigma p & 2k + iF^2[(a\sigma - l_c\beta) + b\sigma^2(\sigma - \beta)] & -k \\ \alpha(\sigma - \beta) & \sigma & (1-\alpha)(\sigma - \beta) \\ -1 & 0 & Y \end{bmatrix} \begin{bmatrix} \hat{H} \\ \hat{u} \\ \hat{d} \end{bmatrix} = 0 \tag{3.16}$$

where

$$Y = -\eta_0 F_r^2 (\frac{d_0}{L_0})^2 \beta^2 + l_0^4 \sigma^4 + 1 - N_0 \sigma^2 \tag{3.17}$$

and

$$N_0 = \frac{N}{\rho g L_0^2} \tag{3.18}$$

$$F_r = \frac{u_0}{\sqrt{g d_0}} \tag{3.19}$$

$$\eta_0 = \frac{\rho_i}{\rho}\frac{\eta}{d_0} \tag{3.20}$$

$$l_0 = \frac{l}{L_0} \tag{3.21}$$

$$b = \frac{1}{3}(\frac{d_0}{L_0})^2 \bar{b} = \frac{1}{3} S_0^2 \bar{b} \tag{3.22}$$

Equation 3.16 constitute a homogeneous system of linear equations in the unknowns $\hat{H}$, $\hat{u}$ and $\hat{d}$. For the solution to be nontrivial, the determinant of the coefficient matrix must vanish. The determinant is a fourth-degree polynomial of β with complex coefficients. The wave dispersion relation can be obtained from the determinant matrix:

$$\sum_{j=1}^{5}(p_j + iq_j)\beta^{j-1} = 0 \tag{3.23}$$

where

$$\begin{aligned}
p_1 &= k(-2l_0^4\sigma^5\alpha - 3\sigma) + k(2\alpha N_0\sigma^3) \\
p_2 &= k(2 + 2\alpha l_0^4\sigma^4) + k(-2N_0\sigma^2\alpha) \\
p_3 &= k(2\lambda F_r^2\alpha\sigma) \\
p_4 &= k(-2\lambda F_r^2\alpha) \\
p_5 &= 0
\end{aligned} \tag{3.24}$$

and,

$$\begin{aligned}
q_1 &= p\sigma^2 + pl_0^4\sigma^6 - a(F_r^2 l_0^4\sigma^6\alpha) - aF_r^2\sigma^2 - N_0\sigma^4(p - a\alpha F_r^2) - b\sigma^4 F_r^2(\alpha l_0^4\sigma^4 - \alpha N_0\sigma^2 + 1) \\
q_2 &= (l_c + a)(F_r^2\sigma) + (l_c + a)(F_r^2 l_0^4\sigma^5\alpha) + (l_c + a)(-N_0 F_r^2\sigma^3\alpha) + 2b\sigma^3 F_r^2(\alpha l_0^4\sigma^4 - \alpha N_0\sigma^2 + 1) \\
q_3 &= a\lambda F_r^4\sigma^2\alpha - p\lambda F_r^2\sigma^2 - l_c F_r^2 - l_c(\alpha l_0^4\sigma^4 F_r^2) + l_c(\alpha F_r^2 N_0\sigma^2) \\
&\quad -b\sigma^2 F_r^2[\alpha l_0^4\sigma^4 - \alpha N_0\sigma^2 + 1 + \sigma^2(-\alpha\eta_0 F_r^2(\frac{d_0}{L_0})^2)] \\
q_4 &= -(a + l_c)\lambda F_r^4\sigma\alpha - 2b\alpha\eta_0\sigma^3 F_r^2(\frac{d_0}{L_0})^2 \\
q_5 &= l_c\lambda F_r^4\alpha + b\alpha\eta_0\sigma^2 F_r^2(\frac{d_0}{L_0})^2
\end{aligned} \tag{3.25}$$

In Eq.3.23, β can be analytically solved as a function of σ, which can be used to analyze wave celerity and attenuation under ice-covered conditions.

A computer code is developed to calculate the four complex roots of Eq. 3.23 using the IMSL routine DZPOCC. Before doing this, Eq. 3.23 is recasted by introducing

$$\beta^* = \frac{\beta}{\sigma}[1 + (\alpha F_r^2)^{-\frac{1}{2}}]^{-1} \tag{3.26}$$

and recognizing that the wave number σ can be defined by

$$\frac{2\pi l}{L} = \sigma l_0 \tag{3.27}$$

In general, four roots exist in Eq 3.23. Two of them describe the propagation of free waves in an infinite continuously supported plate, and are not relevant to the present investigation. The remaining two roots describe two waves propagating along two characteristic paths.

3.2 Analysis of Results

3.2.1 Wave Celerity

The propagation characteristics of various types of water waves in open channels were discussed in detail by Ponce and Simons (1977). The solution of Ponce and Simons (1977) can be considered as a special case of ice-covered channels with $\eta = l = N = \bar{b} = 0$. The propagation celerity for open-water conditions as a function of Froude number and wave number are shown in Fig. 3.1, which is the same as Fig. 1 of Ponce and Simon (1977).

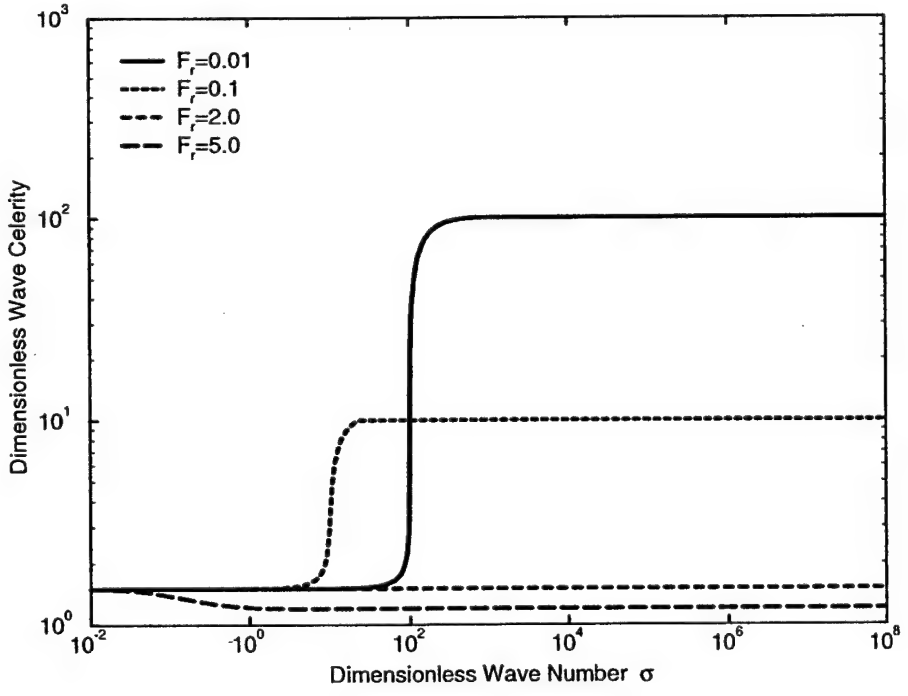

Figure 3.1: Dimensionless wave celerity as function of dimensionless wave number in open water channel

This figure shows that there are three bands in the wave number spectrum for the dynamic model: (1) a gravity band corresponding to large wave numbers, in which $\hat{c}$ is $1 + \frac{1}{F_r}$, independent of σ; (2) a kinematic band corresponding to small wave numbers, in which $\hat{c}$ is a constant equal to 3/2. and (3) a dynamic band corresponding to intermediate values of wave number, in which $\hat{c}$ varies with both σ and F_r.

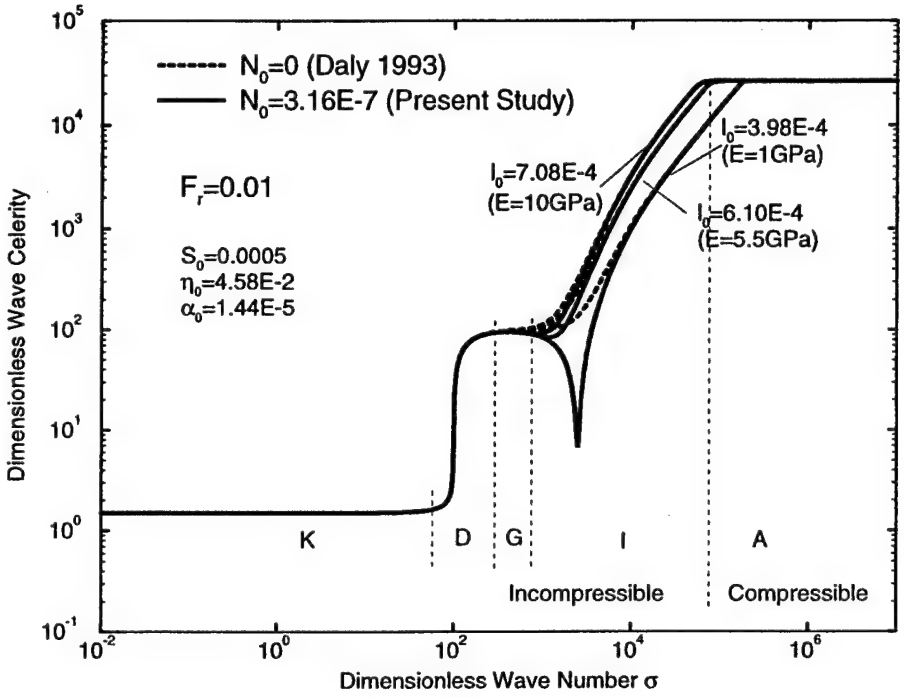

Figure 3.2: Effect of axial force on the dimensionless wave celerity in ice-covered channel.

Under ice-covered condition, the variation of wave celerity is shown in Fig. 3.2. The dimensionless wave celerity is calculated by using the first root of Eq. 3.23, which represents the "primary wave" propagating in the downstream direction (Ponce and Simoms 1977).

As pointed out by Daly (1993), there are five well-defined bands in the wave number spectrum for ice-covered channels. As shown in Fig. 3.2, the first band from the left, corresponding to small values of dimensionless wave number, was identified as the kinematic band (K), which has a wave celerity $\hat{c} = \frac{3}{2}$, or $c = \frac{3}{2}u_0$, in which the gravity and frictional forces dominate. The next band to the right, corresponding to larger dimensionless wave numbers, is the the dynamic band (D) over which $\hat{c}$ changes rapidly and is a function of both σ and F_r, in which the gravity, frictional, and inertial forces dominate. With a further

increase in the dimensionless wave number, the gravity band (G), in which the gravity and inertial forces dominate, is found. The wave celerity is only a function of F_r. For the wave propagating downstream, $\hat{c} = 1 + \frac{1}{F_r}$, or $c = u_0 + (gd_0)^{1/2}$. This is analogous to the open-water gravity wave celerity. These three bands, i.e. kinematic, dynamic, and gravity bands, define the quasi-open-channel range. The wave celerity is not affected by the existence of the ice cover, and independent of variations in the ice properties. The governing equations could be simplified by dropping the ice cover equation and let $P' = 0$. The ice cover can be considered as floating at hydrostatic equilibrium over the range of quasi-open-channel.

Immediately above the quasi-open-channel range, the ice-covered channel wave celerity begin to deviate from the corresponding open-water wave celerity in the gravity wave band, in which the gravity, inertial, and ice-cover bending and inertial forces dominate. This band can be used to define the limit of quasi-open-channel range. Daly (1993) found in this band, which is named as the ice-coupled band (I), the dimensionless wave celerity deviates sharply from the open water condition and is a function of nondimensional wave number, the Froude number, and the characteristic length of ice.

A further increase in the dimensionless wave number leads to the acoustic band. It is only in this band that water is considered as compressible and the wave celerity are equal to the acoustic wave velocity in water as if waves were propagating in a closed elastic conduit. The dimensionless wave celerity in this band is independent of the dimensionless wave number and the ice properties and is a function of F_r and α only, $\hat{c} = 1 \pm \frac{1}{F_r \alpha^{1/2}}$. The wave celerity is $c = u_0 \pm (\frac{E_w}{\rho})^{1/2} = u_0 + c_a$.

The propagation of wave in a floating ice plate is governed by two restoring forces produced by elastic bending of the plate and the tendency of gravity to make the upper surface of the supporting water horizontal. The compressive axial force acts against these restoring forces. Figure 3.2 shows the effect of the axial force for three different values of l_0 corresponding to $E = 1$ GPa, 5.5 GPa, and 10 GPa. This shows that an axial force in the ice plate may sharply decrease the dimensionless wave celerity in the gravity band and the ice-coupled band. Addition figures for different values of F_r are given in Appendix C as Figs. C.1 and C.2. These figures show that the increase in the elastic modulus of the ice cover can reduce the effect of axial force on the wave celerity.

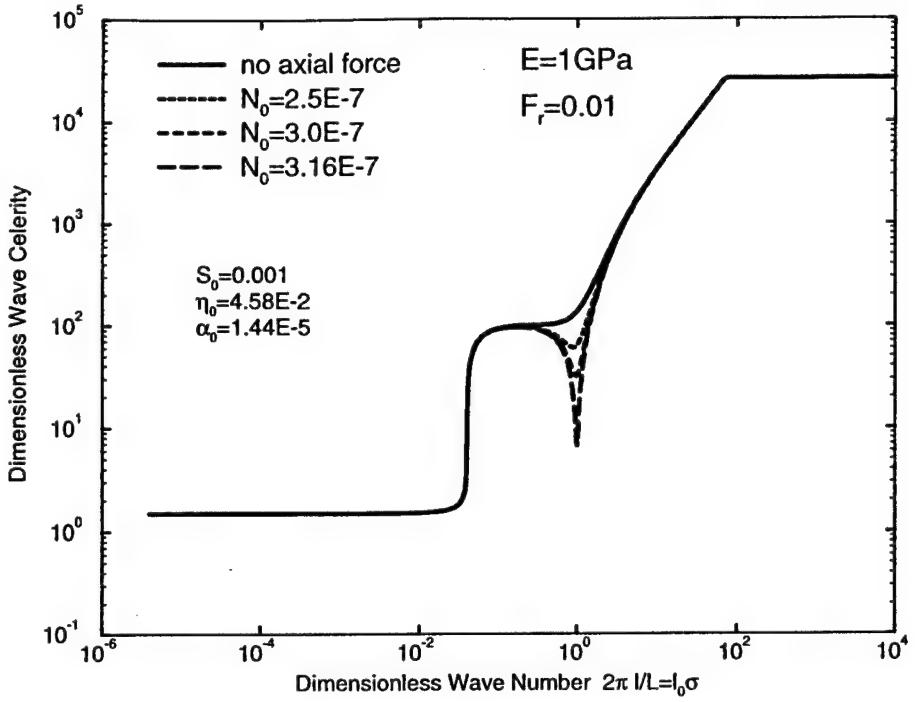

Figure 3.3: Dimensionless wave celerity in ice-covered channel with different axial forces.

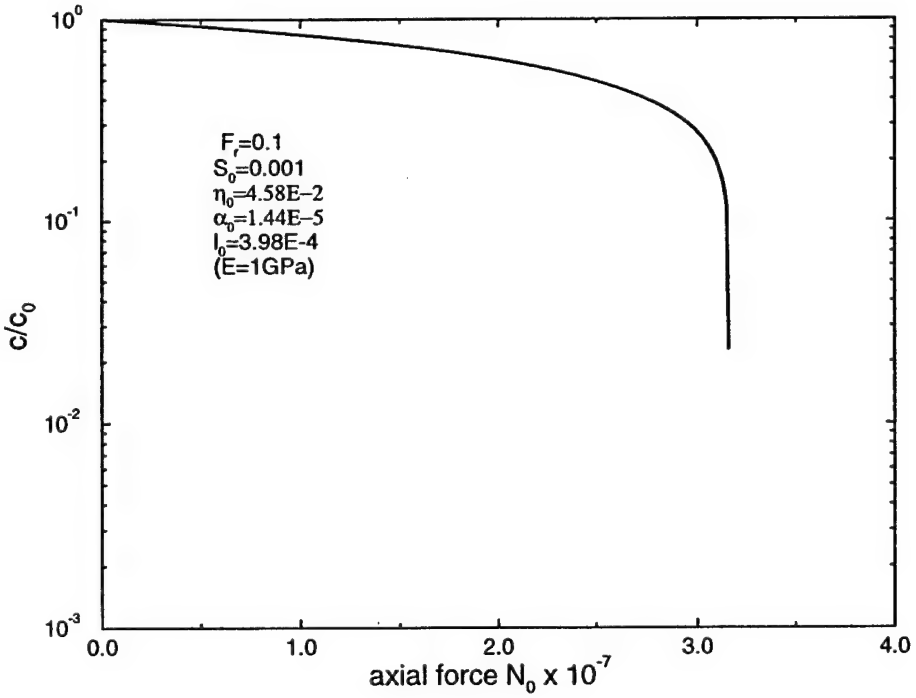

Figure 3.4: Variation of the wave celerity with axial forces, c, relative to that without axial force, C_0, at $\frac{2\pi l}{L} = 1$.

The influence of the magnitude of the axial force on wave celerity can be seen in Fig. 3.3, as well as Fig. C.3 to C.11 for different F_r and E values. Figure 3.4 shows that this effect on wave celerity becomes significant only when the magnitude of the axial force reaches the critical axial force, N_{cr}, defined in section 3.2.3. The ice thickness does not have considerable effect on the wave celerity, as shown in Fig. 3.5.

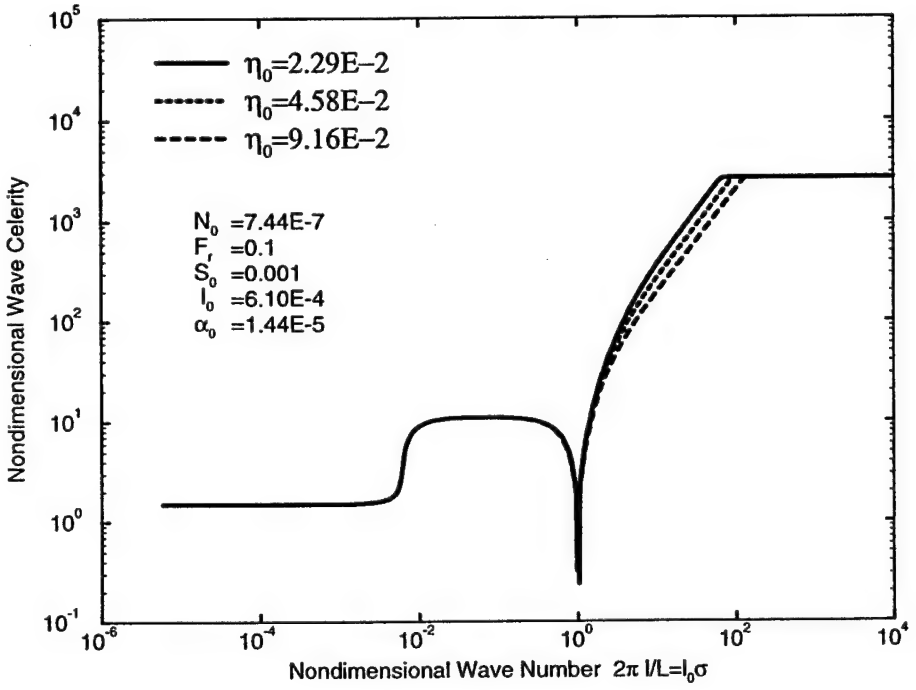

Figure 3.5: Effect of ice cover thickness on dimensionless wave celerity in ice-covered channel

3.2.2 Wave Attenuation

The wave attenuation is described by the dimensionless amplitude $\hat{d}e^{\beta_I \hat{t}}$. The wave decay can be quantified by the logarithmic decrement of the wave amplitude over a duration $\frac{L_0}{c}$. It is defined as $\delta = ln(a_1) - ln(a_0)$, where a_1 and a_0 = amplitudes at a time period $\left(\frac{L_0}{c}\right)$ apart. Based on Eq. 3.13, this leads to

$$\delta = ln\left(\frac{a_1}{a_0}\right) = ln\left(e^{\beta_I\left(\frac{L_0}{c}\frac{u_0}{L_0}\right)}\right) = \beta_I \frac{u_0}{c} = \frac{\beta_I}{\beta_R}\sigma \tag{3.28}$$

Figure 3.6 as well as Figs. C.12 and C.13 depict that the natural decrement, δ, of wave amplitude is always negative for the case considered here, indicating that waves propagating

in ice-covered channels are always attenuated as they progress. Over the quasi-open-channel range, the ice-covered wave attenuation is analogous to the open-water wave attenuation. The decrement δ has its minimum value at the lowest nondimensional wave numbers in the kinematic band and reaches a maximum value in the dynamic band. The value of δ closes to a constant $-\frac{1}{F(F+1)}$ in the gravity band and is much larger than that in kinematic band. Again, similar to the wave celerity, the wave attenuation deviates sharply from the quasi-open-channel attenuation in the ice influenced bands. The attenuation of ice-coupled waves decreases with the increasing wave number and reaches a minimum at a nondimensional wave number slightly less than the limit of the acoustic band. In the acoustic band, δ is a constant that is approximately $-\frac{\alpha^{\frac{1}{2}}}{F}$. It is noted that dynamic and gravity waves will be subjected to strong attenuation, whereas kinematic waves, ice-coupled waves at higher wave numbers, and acoustic waves will be subjected to small attenuation. Figure 3.6 shows that the axial force increases the wave attenuation in the transition zone between the gravity band and ice-coupled band.

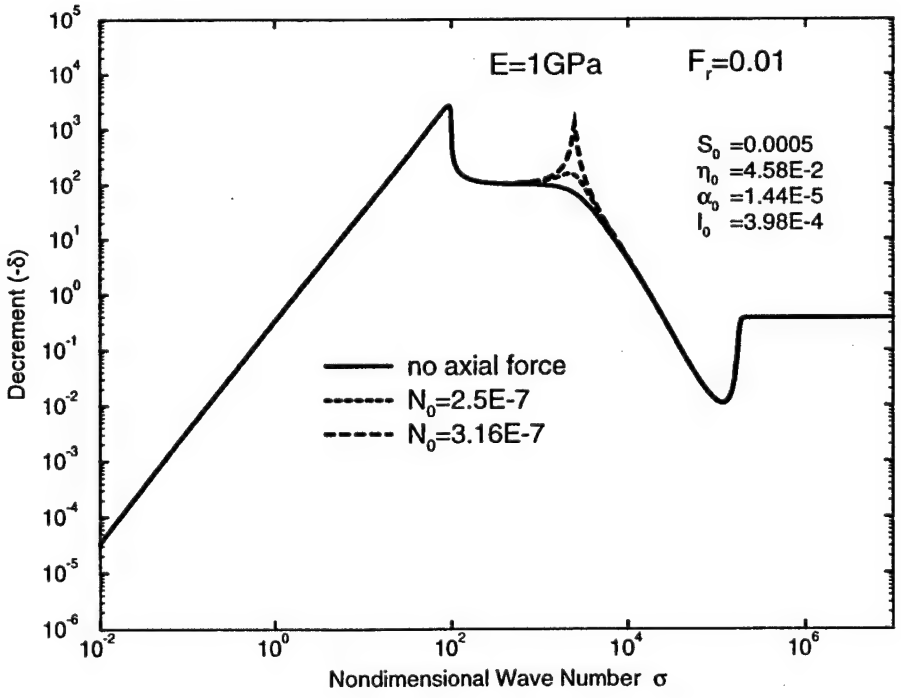

Figure 3.6: Effect of axial forces on natural decrement

3.2.3 Ice Cover Response

Assuming that the floating ice cover is subjected to hydrostatic pressure only, the following elastic plate equation can be obtained from Eq. 2.8 and 2.15.

$$\frac{\rho_i \eta}{\rho g}\frac{\partial^2 d'}{\partial t^2} + l^4\frac{\partial^4 d'}{\partial x^4} + d' + \frac{N}{\rho g}\frac{\partial^2 d'}{\partial x^2} = 0 \tag{3.29}$$

This is the equation of elastic plate supported by a massless Winkler foundation. The free or homogeneous wave celerity , C_H, in the ice cover can be obtained by substitution of Eq. 3.8 into Eq. 3.29 as

$$C_H = \left(\frac{\rho g}{\rho_i \eta}\right)^{\frac{1}{2}}\left[l^4\left(\frac{2\pi}{L}\right)^2 + \left(\frac{L}{2\pi}\right)^2 - \frac{N}{\rho g}\right]^{\frac{1}{2}} \tag{3.30}$$

This shows the compressive axial force can reduce the homogeneous wave celerity. The wavelength L_{min}, at which the minimum homogeneous wave celerity occurs, is found from $\frac{\partial C_H}{\partial(\frac{2\pi l}{L})} = 0$:

$$L_{min} = 2\pi l \tag{3.31}$$

and the minimum homogeneous wave celerity is

$$C_{Hmin} = \left(\frac{\rho g}{\rho_i \eta}\right)^{\frac{1}{2}} l\left(2 - \frac{N_0}{l_0^2}\right)^{\frac{1}{2}} \tag{3.32}$$

When $C_H = 0$, the minimum value of N obtained from Eq. 3.30 using the condition $\frac{\partial N}{\partial(\frac{2\pi}{L})} = 0$ is again $L = 2\pi l$. This minimum value of N is

$$N_{min}|_{C_H=0} = 2\rho g l^2 = 2\sqrt{\rho g E I} = N_{cr} \tag{3.33}$$

which is the critical buckling load of the infinite beam (Hetenyi 1955). Equation 3.32 shows that C_{Hmin} decreases with increasing N and C_{Hmin} becomes zero when $N = N_{cr}$. i.e. $N_0 = 2l_0^2$.

It is well known that when $N > N_{cr}$ the beam shape is not straight i.e. the assumption used for Eq. 2.14 is not satisfied. Hence Eqs. 2.15 and 3.29 are not applicable (Kerr 1972). For this case the necessary analysis is very involved and is beyond the scope of this study. In the following analysis, we will only consider conditions with $N < N_{cr}$.

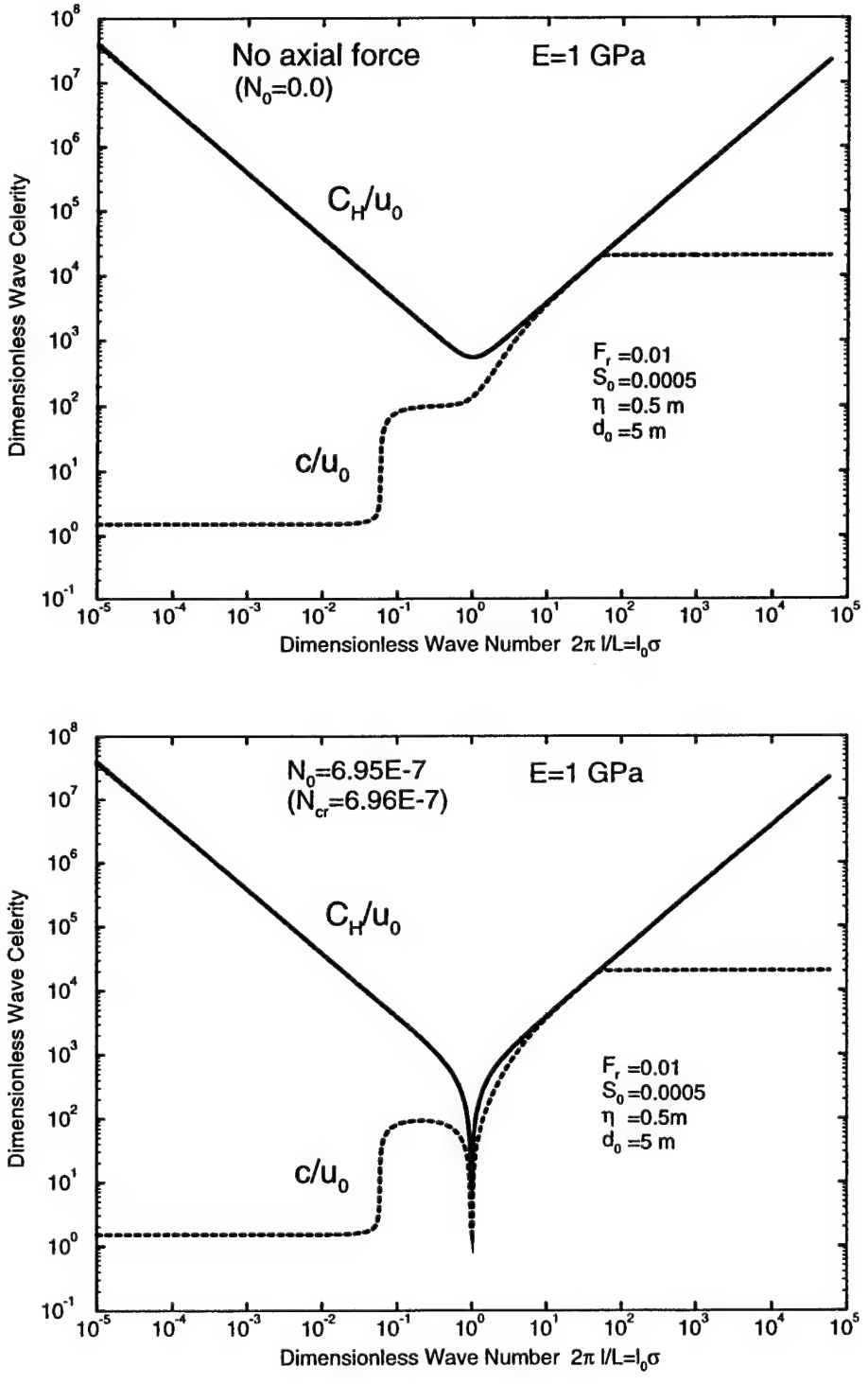

Figure 3.7: Dimensionless free-wave celerity C_H and dimensionless wave celerity $\hat{c}$ in ice-covered channel as functions of dimensionless wave number

The ice cover response is described by Eq. 3.5. By substituting Eqs. 3.8 and 3.10 for the dynamic pressure $P' = \rho g(H' - d')$ into Eq. 3.5, the relationship between the amplitude of the propagating wave $\hat{H}$ and the response of the ice cover $\hat{d}$ can be obtained:

$$\frac{\hat{d}}{\hat{H}} = \left(\frac{\rho g}{\rho_i \eta}\right)\left(\frac{L}{2\pi}\right)^2 \frac{1}{C_H^2 - c^2} \tag{3.34}$$

or

$$\frac{\hat{d}}{\hat{H}} = \left(\frac{L}{2\pi l}\right)^2 \left[\left(\frac{2\pi l}{L}\right)^2 + \left(\frac{L}{2\pi l}\right)^2 - \frac{N_0}{l_0^2}\right]^{-1} \left[1 - \frac{c^2}{C_H^2}\right]^{-1} \tag{3.35}$$

Since $\left[\left(\frac{2\pi l}{L}\right)^2 + \left(\frac{L}{2\pi l}\right)^2\right] \geq 2$, and reaches its minimum value of 2 when $L = L_{min} = 2\pi l$, the maximum ice response d' is approached at the wavelength of $L = 2\pi l$.

Equation 3.32 can be rewritten as

$$\frac{\hat{d}}{\hat{H}} = \frac{1}{\left[1 + \left(\frac{L}{2\pi l}\right)^4 - \frac{N_0}{l_0^2}\left(\frac{2\pi l}{L}\right)^2\right]} \frac{1}{\left[1 - \frac{c^2}{C_H^2}\right]} \tag{3.36}$$

This shows that when $c = C_H$, the ice cover response $\hat{d}$ approaches infinite. The assumption of Eq. 2.14 and the small wave amplitude assumption will be violated. When the axial force is zero, Fig. 3.7 as well as C.14 to C.18 showed that $c < C_H$ over the entire spectrum of possible wavelength, although c closely approaches C_H in the ice-coupled band at wave numbers just below the acoustic band. Because of the resolution of Fig 3.7, it may appear that c and C_H are equal in this range, as pointed out by Daly (1993). The cover response $\hat{d}$ approaches $\hat{H}$ when the wave length L is much larger than $2\pi l$, and approaches zero when L is much less than $2\pi l$. When the axial force is not zero and $N < N_{cr}$, c is still less than C_H. When $N \to N_{cr}$, c and C_H approach zero at wavelength $L = 2\pi l$ as shown in Fig. 3.7, and $\hat{d}$ approaches infinity. This shows the possibility of cover fracture at a wave length $2\pi l$ as N approaches N_{cr}. However, the linear perturbation analysis may not be valid as $\hat{d}$ approaches infinity.

To further the analysis, the bending stress in the ice cover is examined. The bending stress S_x in the ice cover at a distance z from the neutral axial produced by waves propagating in the longitudinal direction is

$$S_x = -\frac{Ez}{1-\nu^2}\frac{\partial^2 d'}{\partial x^2} \tag{3.37}$$

The maximum bending stress in the ice cover $S_{x,max}$ is at the top and the bottom of the ice sheet, $z = \pm\frac{\eta}{2}$.

$$S_{x,max} = -\frac{E}{1-\nu^2}\frac{\eta}{2}\frac{\partial^2 d'}{\partial x^2} \tag{3.38}$$

By substituting Eq. 3.8 for d' and then relating $\hat{d}$ to $\hat{H}$ by Eq. 3.35, the maximum stress

$$S_{x,max} = \frac{\hat{H} d_0 E}{1-\nu^2}\frac{\eta}{2}\left[l^4\left(\frac{2\pi}{L}\right)^2 + \left(\frac{L}{2\pi}\right)^2 - \frac{N}{\rho g}\right]^{-1}\left[1 - \frac{c^2}{C_H^2}\right]^{-1} \tag{3.39}$$

Equation 3.39 and 3.30 gives

$$S_{xmax} = \frac{\hat{H} d_0 E}{1-\nu^2}\frac{\eta}{2}\frac{1}{\left[l^4\left(\frac{2\pi}{L}\right)^2 + \left(\frac{L}{2\pi}\right)^2 - \frac{N}{\rho g} - \frac{\rho_i \eta}{\rho g}c^2\right]} \tag{3.40}$$

For an ice cover with a maximum flexural strength S_{Xb} , the minimum wave amplitude to cause cover crack at any wavelength is then obtained as

$$a_{min} = d_0 \hat{H}_{min}(L) = \frac{2S_{Xb}(1-\nu^2)}{E\eta} l^2 \left[\left(\frac{2\pi l}{L}\right)^2 + \left(\frac{L}{2\pi l}\right)^2 - \frac{N}{\rho g l^2}\right]\left[1 - \frac{c^2}{C_H^2}\right] \tag{3.41}$$

where $\frac{N}{\rho g l^2} = \frac{N_0}{l_0^2}$. The amplitude $a_{min}(L)$ is shown in Fig. 3.8 as well as C.19 to C.23 as a function of the dimensionless wave number $\frac{2\pi l}{L} = l_0\sigma$. These figures show that when the axial force increases, the amplitude of the propagating wave required to fracture the cover decreases when the wave length is in the vicinity of $2\pi l$. The amplitude $a_{min}(L)$ has a well-defined global minimum value at the wavelength $L_{min} = 2\pi l$. In addition, $a_{min}(L)$ rapidly approaches zero when the axial force approaches the critical buckling load N_{cr} for a homogeneous wave. This means that, under the assumptions of linear perturbation theory, when the ice cover is subjected to the critical axial force, it will be fractured.

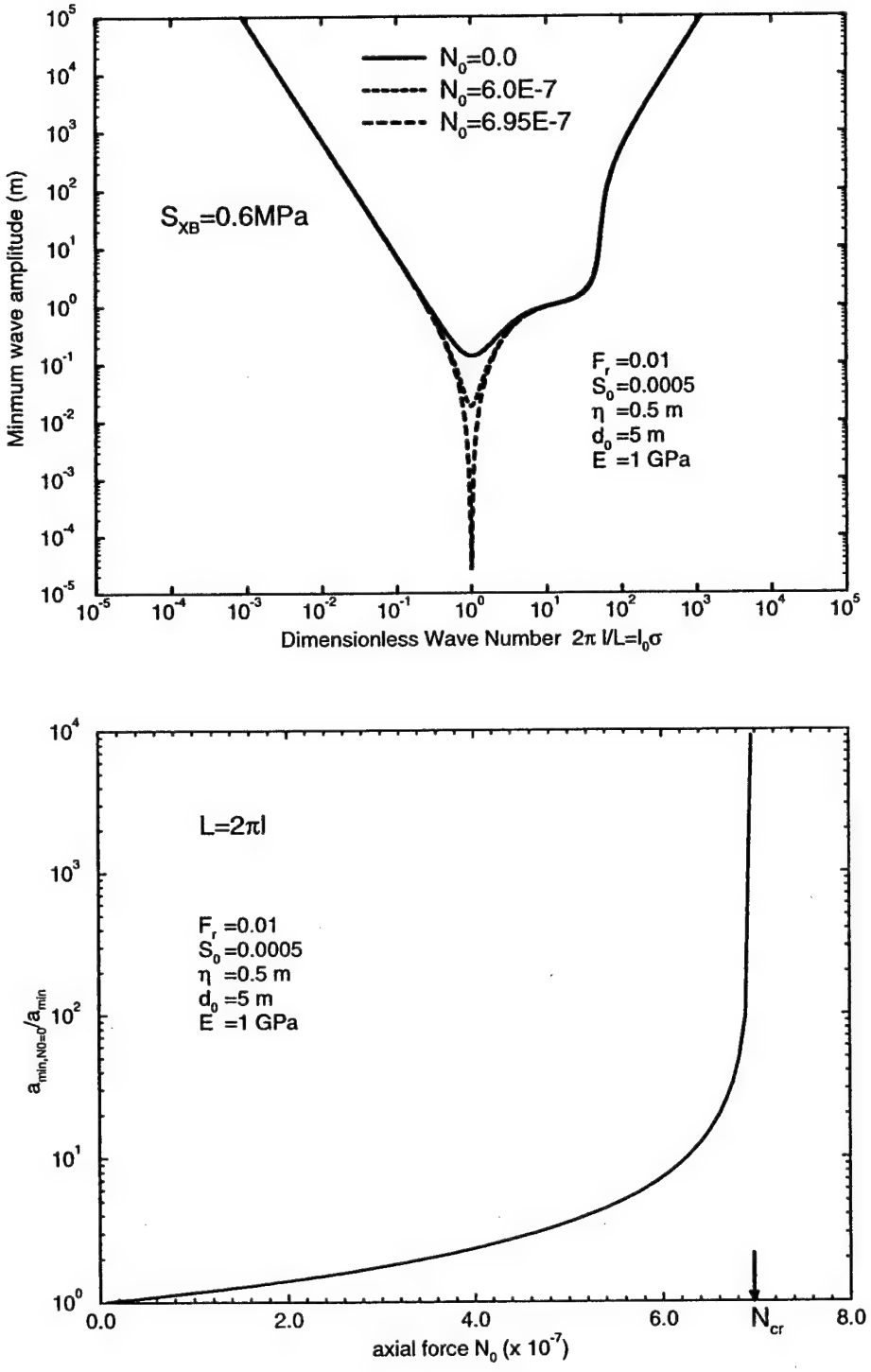

Figure 3.8: (a) Minimum wave amplitude (m) required to fail an ice cover of 0.5 m thick; (b) Effect of an axial force on the minimum wave amplitude.

Considering that the axial force is related to the length of ice cover, D, over which there is no bank support, then Eq. 3.33 gives

$$N_{cr} = 2\rho g l^2 = \frac{1}{2} D d_0 \rho g S_0$$

Using a value of $l = 5$ m from Fig. 4.6, $S_0 = 5 \times 10^{-4}$, $d_0 = 5$ m, then $D = 40$ km. This shows that the axial force rarely reaches the critical value in the field condition for natural river ice cover. Without an axial force, the wave amplitude required to cause an ice cover to crack is $O(0.1m)$ at the wavelength of $2\pi l$ (Daly 1995). Hence, for both cases with or without axial load the term $(\frac{\partial d}{\partial x})^2 \ll 1$, and the small deformation assumption used in Eq. 2.14 is satisfied.

3.2.4 Effect of Boussinesq's term

The one-dimensional depth-averaged momentum, Eq. 2.8 or 3.4 are based on the assumption of hydrostatic pressure distribution. When the wave number is large, the vertical acceleration of the flow may be significant. Since the preceding discussions showed that the fracture of an intact ice cover will occur at a wave length of $2\pi l$, the compressibility of water associated with the acoustic band need not be considered. This assumption is further supported by the fact that longitudinal cracks, formed long before the fracture of cover by propagating waves, enable the release of excess pressure under the cover. The effect of the vertical inertia of fluid may be expressed by a linearized Boussinesq approximation as in Eq. 2.9 or 3.7. Steffler and Hicks (1994) analyzed linearized Boussinesq's equation and discussed the effect of vertical water inertia on wave celerity when there is no axial force. When $l_c = a = p = k = \hat{b} = 1$ is chosen in Eq. 3.7, the effect of the Boussinesq's term is considered, i.e.

$$\frac{1}{g}\frac{\partial u'}{\partial t} + \frac{u_0}{g}\frac{\partial u'}{\partial x} + \frac{\partial H'}{\partial x} + S_0\left(\frac{2u'}{u_0} - \frac{d'}{d_0}\right) - \frac{d_0^2}{3g}\left(\frac{\partial^3 u'}{\partial x^2 \partial t} + u_0\frac{\partial^3 u'}{\partial x^3}\right) = 0 \qquad (3.42)$$

As shown in Figs. 3.9, C.24 and C.25 the vertical inertia of the water causes a reduction in celerity. However, it does not reduce minimum wave amplitude required to fail the ice cover, as shown in Fig. 3.10.

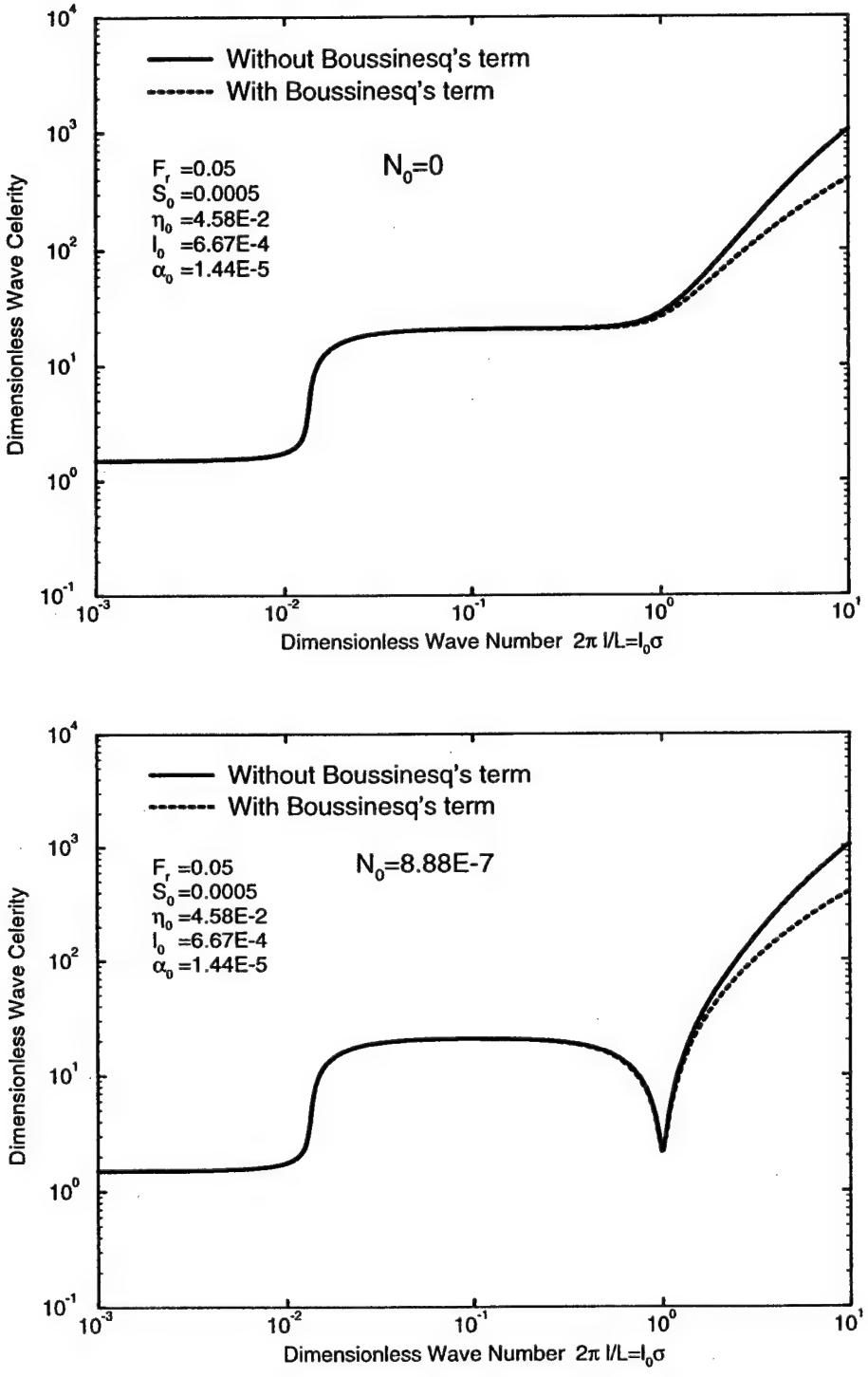

Figure 3.9: (a)Effect of Boussinesq's term: without axial force, Steffler and Hicks (1994); (b) with an axial force.

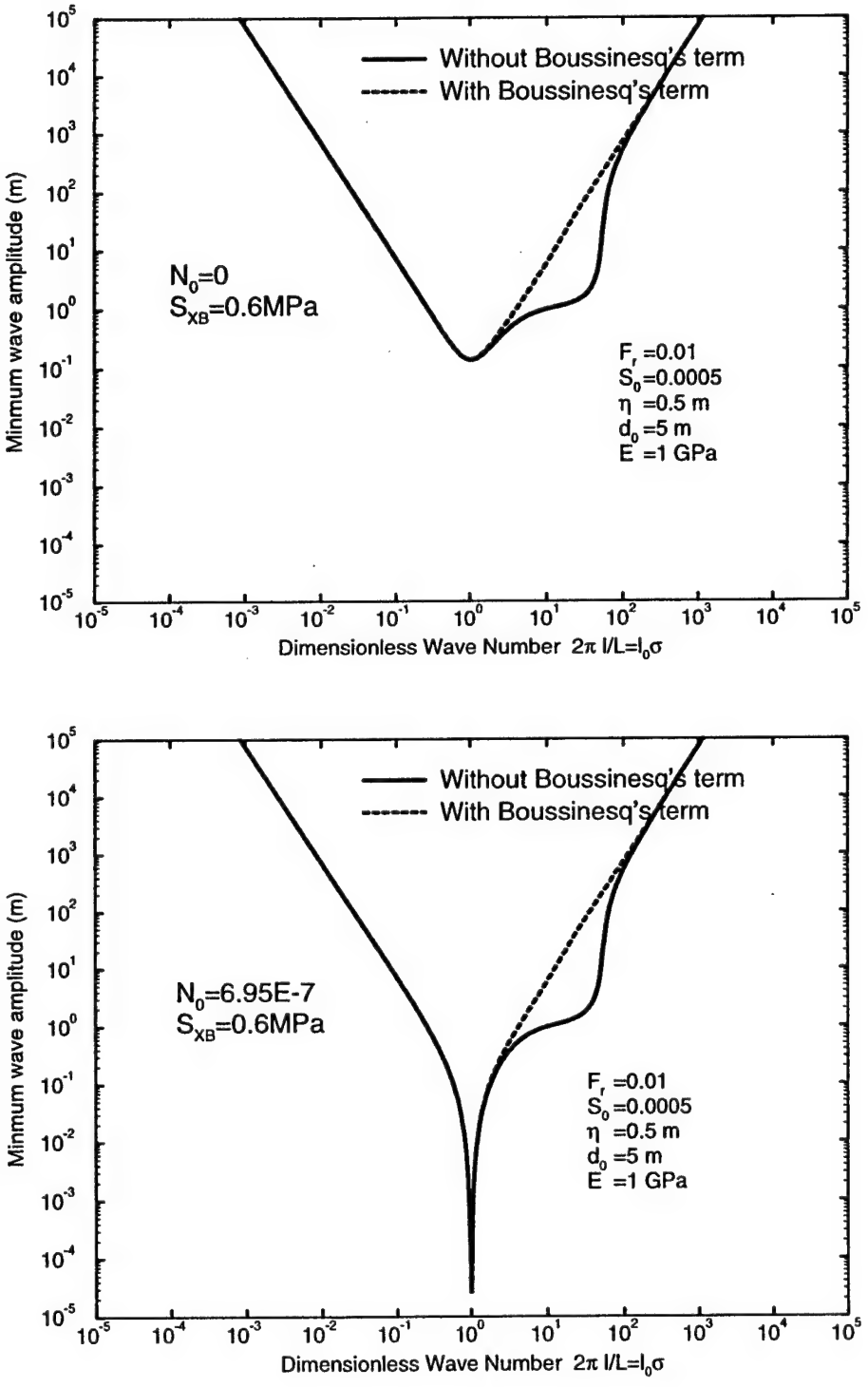

Figure 3.10: Effect of vertical inertia of the water on the minimum wave amplitude required to fail an ice cover of 0.5 m thick

Since the nonlinear term is important when the vertical inertia of water is significant, Eq. 3.42, which neglected the nonlinear term, is not strictly correct. Neglecting the friction and bed slope and using the following dimensionless variables

$$x^* = \frac{x}{L_0}, \quad d^* = \frac{d}{a}, \quad t^* = \frac{ct}{L_0}, \quad u^* = \frac{d_0 u}{ac} \tag{3.43}$$

Eq. 2.9 can be written in a nondimensional form as

$$\frac{\partial u^*}{\partial t^*} + \frac{\partial d^*}{\partial x^*} + Fr\frac{\partial u^*}{\partial x^*} + \varepsilon u^*\frac{\partial u^*}{\partial x^*} - \varepsilon_1\frac{\partial^3 u^*}{\partial t^* \partial x^{*2}} = 0 \tag{3.44}$$

where $\varepsilon = \frac{a}{d_0}$ and $\varepsilon_1 = \frac{d_0^2}{3L_0^2}$. If these two parameters are of the same order, the nonlinear term $u^*\frac{\partial u^*}{\partial x^*}$ should be considered.

3.2.5 Group Velocity

The group velocity plays a fundamental role in wave propagation since wave energy propagates at this velocity. In dimensionless form, the group velocity $\hat{U}$ is

$$\hat{U} = \frac{d\beta_R}{d\sigma} = \hat{c} + \sigma\frac{d\hat{c}}{d\sigma} \tag{3.45}$$

When $\hat{c}$ is independent of σ in the wave number spectrum, the wave is not dispersive. Therefore, the group velocity and wave celerity are the same in kinematic, gravity, or acoustic bands. In the two bands where $\hat{c}$ is a function of σ, i.e. dynamic and ice-coupled bands, the waves are highly dispersive. Thus, the group velocity and wave celerity differ as shown in Fig. 3.11 as well as C.26 to C.28. Without the axial force, the group velocity always exceeds the wave celerity. However, with a large enough axial force, the group velocity may approach zero.

When group velocity varies in the wave propagation direction from a positive value to a small value, there will be an accumulation of wave energy. An infinite wave train of initially constant amplitude entering from a distance, would attain singular amplitude where it encountered a place of zero group velocity. From Fig. 3.11, The group velocity can reach zero just around the wave length $2\pi l$ over the entire spectrum. This is another explanation for waves with length near $2\pi l$ can break ice cover easily.

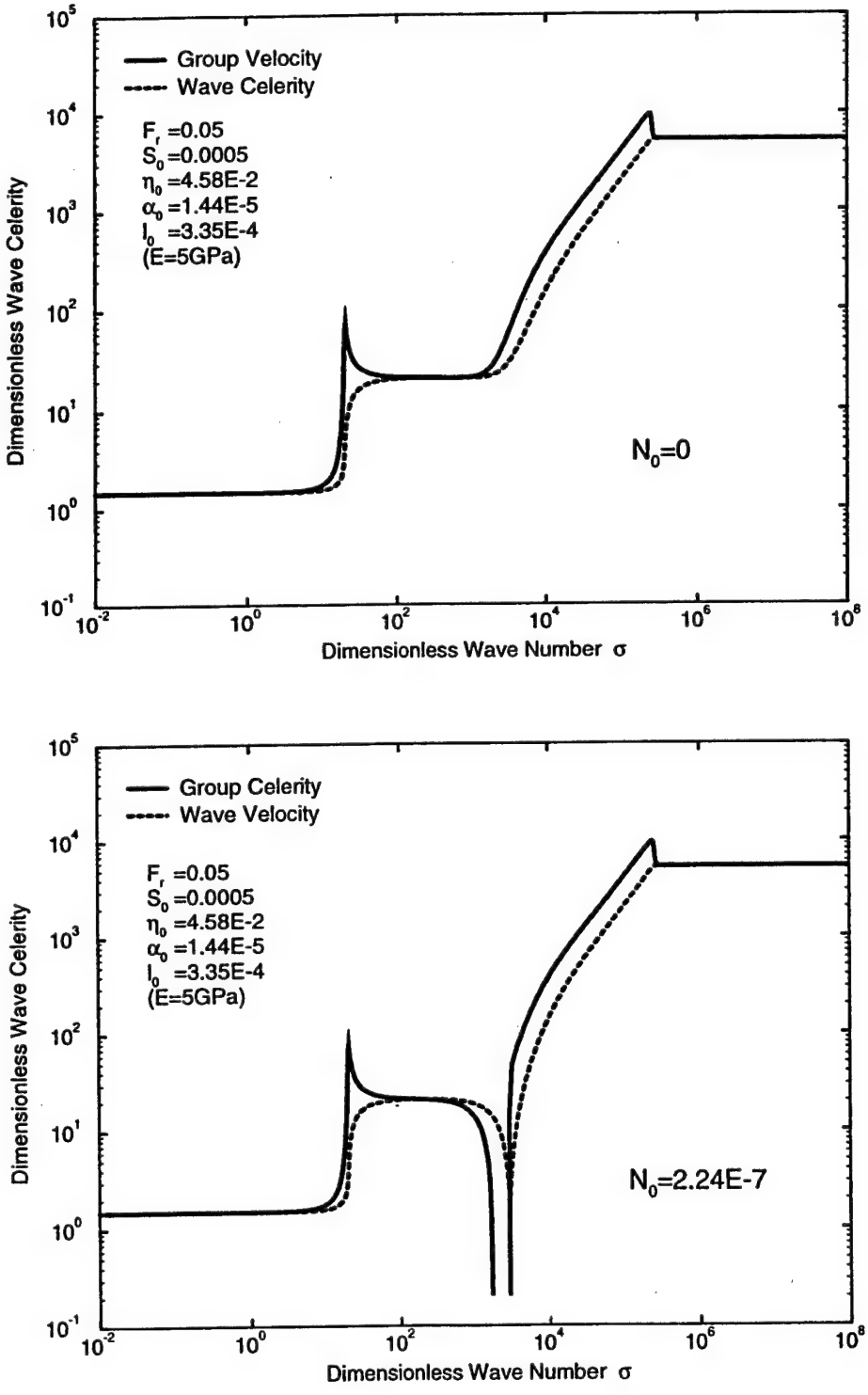

Figure 3.11: Dimensionless wave celerity and group velocity as functions of dimensionless wave number

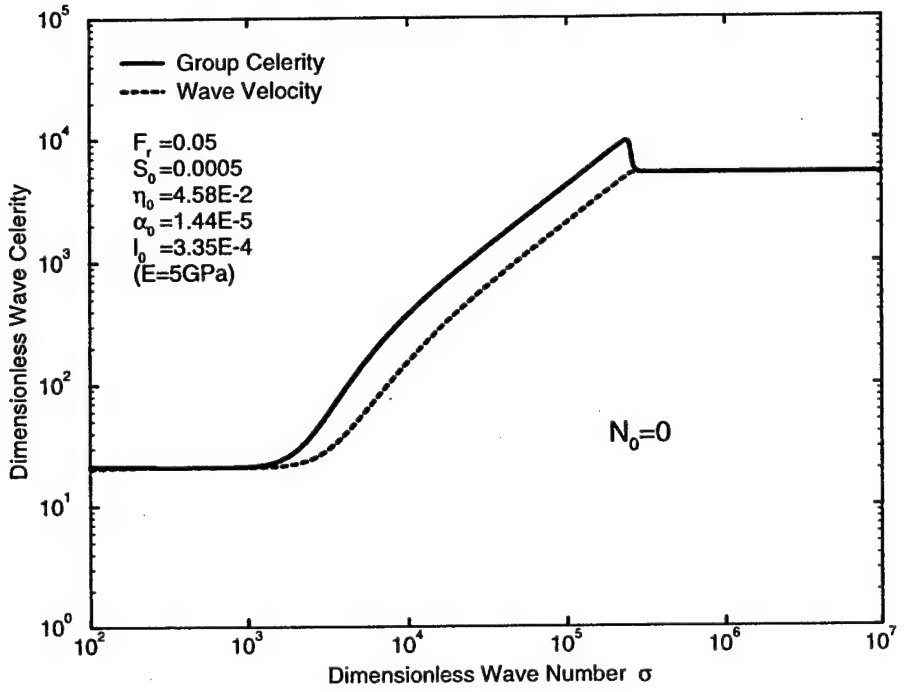

Figure 3.12: Enlarged plot of the wave celerity and group velocity plot in Fig. 3.11

3.3 Summary and Conclusions

In this chapter, the effect of an axial force along the ice cover on the interaction of water waves with ice cover in a uniform channel is analyzed using the linear perturbation theory. The linear theory is valid only for small amplitude waves, i.e. the order of nonlinear terms is much less than that of linear terms. The present analysis shows that the axial force can greatly reduce the wave celerity in the ice-coupled band of the wave number spectrum. The wave attenuation in the transition zone between the gravity band and the ice-coupled band increases with the axial force. The fracture of ice cover will occur at a wavelength of $2\pi l$ as in the case of zero axial force analyzed by Daly (1995). This means that if the cover does not fracture at a wavelength of $2\pi l$, it will then not fracture. This implies that the compressibility of water can be neglected in the analysis of ice cover breakup. The present analysis also shows that the minimum wave amplitude that is required to fracture the ice cover rapidly approaches zero when the axial force approaches the critical buckling load of a floating elastic plate and the wave length approaches $2\pi l$. The linear analysis is therefore valid for cases with a large axial force. The validity of the linear theory for zero axial force needs to be further examined and will be discussed in the Section 4.1 along with the nonlinear analysis.

Chapter 4

Nonlinear Model

The linear analysis determined the asymptotic ice cover response to propagating waves by sinusoidal perturbations of various wavelengths and amplitudes. It showed that waves with a wavelength near the characteristic length of the ice cover are most likely to induce transverse cracks. Surges that occurred during the ice jam release may make the nonlinear term $u' \frac{\partial u'}{\partial x}$ in Eq.2.9 significant and not negligible. No field data on water waves underneath a river ice cover is available for determining the dominate wave types which cause the ice breakup. To circumvent this lack of information, the governing equations describing the propagation of waves under a floating ice cover will be investigated in this chapter by considering nonlinear terms of the water wave equations.

4.1 Governing Equations

The compressibility of water is not important when the ice cover is separated from the banks after the formation of the longitudinal cracks. The linear analysis also showed that the compressibility is not responsible for the formation of transverse cracks, therefore the water is considered to be incompressible in the following analysis. The linear analysis showed that friction and bed slope contribute only to kinematic waves. Therefore, the bed and cover friction can be assumed to be small and the bed slope is negligible. Thus the mass conservation equation 2.11, the momentum equation 2.8 and the elastic ice cover equation 2.14 can be written as:

$$\frac{\partial d}{\partial t} + \frac{\partial (ud)}{\partial x} = 0 \tag{4.1}$$

$$\frac{\partial u}{\partial t} + u\frac{\partial u}{\partial x} + g\frac{\partial d}{\partial x} + \frac{1}{\rho}\frac{\partial P'}{\partial x} = 0 \tag{4.2}$$

$$\frac{EI}{1-\nu^2}\frac{\partial^4 d}{\partial x^4} + \rho_i \eta \frac{\partial^2 d}{\partial t^2} + N\frac{\partial^2 d}{\partial x^2} - P' = 0 \tag{4.3}$$

Let $u = u_0 + u'$ and $d = d_0 + d'$, where u_0 and d_0 are constants, representing the uniform flow, then Eqs. 4.1, 4.2 and 4.3 give

$$\frac{\partial d'}{\partial t} + u_0\frac{\partial d'}{\partial x} + d_0\frac{\partial u'}{\partial x} + \frac{\partial (u'd')}{\partial x} = 0 \tag{4.4}$$

$$\frac{\partial u'}{\partial t} + u_0\frac{\partial u'}{\partial x} + u'\frac{\partial u'}{\partial x} + g\frac{\partial d'}{\partial x} + \frac{1}{\rho}\frac{\partial P'}{\partial x} = 0 \tag{4.5}$$

$$\frac{EI}{1-\nu^2}\frac{\partial^4 d'}{\partial x^4} + \rho_i \eta \frac{\partial^2 d'}{\partial t^2} + N\frac{\partial^2 d'}{\partial x^2} - P' = 0 \tag{4.6}$$

Let $x' = x - u_0 t$ and $t' = t$, thus $\frac{\partial}{\partial x} = \frac{\partial}{\partial x'}$ and $\frac{\partial}{\partial t} = \frac{\partial}{\partial t'} - u_0\frac{\partial}{\partial x'}$. After combining Eqs. 4.5 and 4.6, this set of equations after dropping the primes becomes,

$$\frac{\partial d}{\partial t} + d_0\frac{\partial u}{\partial x} + \frac{\partial (ud)}{\partial x} = 0 \tag{4.7}$$

$$\frac{\partial u}{\partial t} + u\frac{\partial u}{\partial x} + g\frac{\partial d}{\partial x} + \frac{EI}{(1-\nu^2)\rho}\frac{\partial^5 d}{\partial x^5} + \frac{\rho_i \eta}{\rho}\left(\frac{\partial^3 d}{\partial t^2 \partial x} - 2u_0\frac{\partial^3 d}{\partial t \partial x^2} + u_0^2\frac{\partial^3 d}{\partial x^3}\right) + \frac{N}{\rho}\frac{\partial^3 d}{\partial x^3} = 0 \tag{4.8}$$

It is convenient to introduce the following dimensionless parameters to characterize the nonlinear shallow water waves based on a horizontal length scale L_0, a vertical length scale d_0, and the wave amplitude a.

$$Fr = \frac{u_0}{\sqrt{gd_0}}, \varepsilon = \frac{a}{d_0}, \delta = \frac{EI}{(1-\nu^2)\rho g L_0^4} = \frac{l^4}{L_0^4}, \gamma = \frac{\rho_i}{\rho}\frac{d_0 \eta}{L_0^2}, N_0 = \frac{N}{\rho g L_0^2} \tag{4.9}$$

The meaning of the first two parameters are well known, i.e. Froude number and dimensionless wave amplitude. The last three parameters are dimensionless ice cover stiffness, ice cover inertia, and axial force. In addition, variables in Eqs. 4.7 and 4.8 can also be nondimensionlized as:

$$x^* = \frac{x}{L_0}, \quad d^* = \frac{d}{a}, \quad t^* = \frac{ct}{L_0}, \quad u^* = \frac{d_0 u}{ac} \tag{4.10}$$

in which, $c = \sqrt{gd_0}$.

In terms of the preceding nondimensional variables and parameters, Eqs. 4.7 and 4.8 can be written in the nondimensional form as,

$$\frac{\partial d^*}{\partial t^*} + \frac{\partial u^*}{\partial x^*} + \varepsilon \frac{\partial (u^* d^*)}{\partial x^*} = 0 \tag{4.11}$$

$$\frac{\partial u^*}{\partial t^*} + \frac{\partial d^*}{\partial x^*} + \varepsilon u^* \frac{\partial u^*}{\partial x^*} + \delta \frac{\partial^5 d^*}{\partial^5 x^*} + N_0 \frac{\partial^3 d^*}{\partial^3 x^*} + \gamma \left(\frac{\partial^3 d^*}{\partial t^{*2} \partial x^*} - 2Fr \frac{\partial^3 d^*}{\partial t^* \partial x^{*2}} + Fr^2 \frac{\partial^3 d^*}{\partial x^{*3}} \right) = 0 \tag{4.12}$$

It should be noted that Eqs. 4.11 and 4.12 are similar to the well-known Boussinnesq equation (Debnath 1994, Mei 1983), albeit more complicated. In Eq. 4.12 the third term is the nonlinear term, and the terms following it are dispersion terms. Daly's (1995) linear analysis showed that waves with a wavelength of $2\pi l$ having an amplitude in the order of O(0.1 m) can cause transverse cracks to form even when $N_0 = 0$. In such a case, the order of ice stiffness parameter $\delta = (\frac{l}{L_0})^4 = (\frac{1}{2\pi})^4$ is 0.001, and the order of small amplitude parameter ε is 0.01 or larger. The nonlinear term in Eq. 4.12 is comparable to the ice stiffness term, thus can not be neglected. The linear analysis is therefore not valid.

We look for a solution, correct to the first order in ε and δ, in the form

$$u^* = d^* + \varepsilon Q_1 + \delta Q_2 + O(\varepsilon^2 + \delta^2) \tag{4.13}$$

where Q_1 and Q_2 are functions of d^* and its derivatives. Consequently, since $d^*_{t^*} = -d^*_{x^*} + O(\varepsilon, \delta)$, Eqs. 4.11 and 4.12 become

$$d^*_{t^*} + d^*_{x^*} + \varepsilon d^* d^*_{x^*} + \varepsilon \left(d^* d^*_{x^*} + \frac{\partial Q_1}{\partial x^*} \right) + \delta \frac{\partial Q_2}{\partial x^*} + O(\varepsilon^2, \varepsilon\delta) = 0 \tag{4.14}$$

$$d^*_{t^*} + d^*_{x^*} + \varepsilon d^* d^*_{x^*} - \varepsilon \frac{\partial Q_1}{\partial x^*} + \delta(-\frac{\partial Q_2}{\partial x^*} + \frac{\partial P^*}{\partial x^*}) + O(\varepsilon^2, \varepsilon\delta) = 0 \tag{4.15}$$

where $P^* = \frac{\partial^4 d^*}{\partial^4 x^*} + \frac{\gamma}{\delta}(\frac{\partial^2 d^*}{\partial t^{*2}} - 2Fr\frac{\partial^2 d^*}{\partial t^* \partial x^*} + Fr^2\frac{\partial^2 d^*}{\partial x^{*2}}) + \frac{N_0}{\delta}\frac{\partial^2 d^*}{\partial x^{*2}}$. These two equations must be consistent so that we stipulate

$$\begin{aligned} Q_1 &= -\frac{d^{*2}}{4} \\ Q_2 &= \frac{P^*}{2} \end{aligned} \tag{4.16}$$

Consequently, we obtain a single equation for d^* accurate to the first order, by neglecting terms of order ε^2 and $\delta\varepsilon$ or higher:

$$d^*_{t^*} + d^*_{x^*} + \frac{3}{2}\varepsilon d^*_{x^*} d^* + \frac{\delta}{2} d^*_{x^* x^* x^* x^* x^*} + \frac{\gamma}{2}(1+Fr)^2 d^*_{x^* x^* x^*} + \frac{N_0}{2} d^*_{x^* x^* x^*} = 0 \tag{4.17}$$

and a relation between u^* and d^*:

$$u^* = d^* + \varepsilon(-\frac{d^{*2}}{4}) + \delta\frac{P^*}{2} \tag{4.18}$$

It is noted that the neglected nonlinear terms in the ice cover response equation Eq. 2.14 $(\frac{\partial d}{\partial x})^2 = \varepsilon^2(\frac{d_0}{L_0})^2(\frac{\partial d^*}{\partial x^*})^2 \leq \varepsilon^2$. Therefore, the assumption of $\frac{1}{r} = \frac{\partial^2 d}{\partial x^2}$ is acceptable.

Equation 4.17 expressed in dimensional form is

$$\frac{1}{c} d_t + d_x + \frac{3}{2d_0} d d_x + \frac{l^4}{2} d_{xxxxx} + \frac{\rho_i}{2\rho} d_0 \eta (1+Fr)^2 d_{xxx} + \frac{N}{2\rho g} d_{xxx} = 0 \tag{4.19}$$

The first two terms, $d_t + c d_x$, describe wave evolution at the shallow water speed $c = \sqrt{g d_0}$, the third term with coefficient $\frac{3c}{2d_0}$ represents a nonlinear wave steepening. These term are the same as those in the KdV equation for free-surface shallow water waves. The rest of the terms are all dispersion terms due to ice cover bending, inertia of ice cover, and the axial force along the cover. Thus, similar to the KdV equation, Eq. 4.19 is a balance between time evolution, nonlinearity and dispersion.

We now seek a steady progress wave solution of Eq. 4.19 traveling to the downstream. The solution is stationary in the reference frame ζ so that $d = d(\zeta)$, $\zeta = x - Ut$. Substituting this into Eq. 4.19, we obtain

$$(1 - \frac{U}{c}) d' + \frac{3}{2d_0} d d' + \frac{l^4}{2} d'''' + \frac{\rho_i}{2\rho} d_0 \eta (1+Fr)^2 d''' + \frac{N}{2\rho g} d''' = 0 \tag{4.20}$$

where $' = \frac{d}{d\zeta}$. Integrating with respect to ζ, we get

$$A + (1 - \frac{U}{c})d + \frac{3}{4d_0}d^2 + \frac{l^4}{2}d'''' + \frac{\rho_i}{2\rho}d_0\eta(1+Fr)^2 d'' + \frac{N}{2\rho g}d'' = 0 \tag{4.21}$$

Where A is an integration constant to be determined.

4.2 Solutions

4.2.1 Solution of the Simplified Equation

We will first solve the following simplified equation by ignoring the axial force and the inertia of ice cover terms

$$A + (1 - \frac{U}{c})d + \frac{3}{4d_0}d^2 + \frac{l^4}{2}d'''' = 0 \tag{4.22}$$

It is known that cnoidal waves with slowly varying amplitude are observed in rivers (Debnath 1994). By assuming a solution of the following form

$$d(\zeta) = -a\mathrm{cn}^4(\alpha\zeta, k) + b \tag{4.23}$$

where a is the wave height measured vertically from trough to crest and U is the wave celerity, both of these and constants α, b and k need to be determined. Since the net area occupied by fluid within a wavelength above the mean water level is zero:

$$\int_0^{Lw} d(x,t)dx = 0 \tag{4.24}$$

where the wavelength as shown in Appendix B is:

$$L_W = 2\alpha^{-1}\mathrm{K}(k) \tag{4.25}$$

and $\mathrm{K}(k)$ is the complete elliptic integral of the first kind.

Equation 4.22 gives

$$A + (1 - \frac{U}{c})d + \frac{3}{4d_0}d^2 = -\frac{l^4}{2}\alpha^4 d_{XXXX} \tag{4.26}$$

in which $X = \alpha\zeta$. The following procedure shows that Eq. 4.23 satisfies Eq. 4.26. The term $\alpha^4 d_{XXXX}$ and the left-hand terms of Eq. 4.26 can be written as:

$$\begin{aligned}\alpha^4 d_{XXXX} &= -a[840\alpha^4 k^4 \mathrm{cn}^8(X) + 1040(-2k^4 + k^2)\alpha^4 \mathrm{cn}^6(X) \\ &\quad +32\alpha^4(53k^4 - 53k^2 + 8)\mathrm{cn}^4(X) + 240\alpha^4(-2k^4 + 3k^2 - 1)\mathrm{cn}^2(X) \\ &\quad +24\alpha^4(1-k^2)^2] \qquad (4.27)\end{aligned}$$

$$\begin{aligned}A + (1 - \frac{U}{c})d + \frac{3}{4d_0}d^2 &= \frac{3a^2}{4d_0}\mathrm{cn}^8(X) + [(1 - \frac{U}{c}) + \frac{3}{2d_0}b](-a)\mathrm{cn}^4(x) \\ &\quad +[A + (1 - \frac{U}{c})b + \frac{3}{4d_0}b^2] \qquad (4.28)\end{aligned}$$

The procedure of deriving $(\mathrm{cn}^4)_{XXXX}$ is shown in Appendix B. By equating the coefficients of the polynomial of cn on both sides of Eq. 4.26, the following five equations should be satisfied by determining values of, or relationships between, a, α , b, k, A and U.

$$\frac{l^4\alpha^4}{2}a840k^4 = \frac{3}{4d_0}a^2 \qquad (4.29)$$

$$\frac{l^4\alpha^4}{2}a1040(-2k^4 + k^2) = 0 \qquad (4.30)$$

$$\frac{l^4\alpha^4}{2}a32(53k^4 - 53k^2 + 8) = (1 - \frac{U}{c} + \frac{3}{2d_0}b)(-a) \qquad (4.31)$$

$$\frac{l^4\alpha^4}{2}a240(-2k^4 + 3k^2 - 1) = 0 \qquad (4.32)$$

$$\frac{l^4\alpha^4}{2}a24(1-k^2)^2 = A + (1 - \frac{U}{c})b + \frac{3}{4d_0}b^2 \qquad (4.33)$$

Equations 4.30 and 4.32 give

$$k^2 = \frac{1}{2} \qquad (4.34)$$

Equation 4.29 yields

$$\alpha^4 = \frac{a}{140d_0 l^4} \qquad (4.35)$$

and, Eq. 4.24 yields

$$\int_0^{2\mathrm{K}(k)} -a\mathrm{cn}^4(y,k)dy + 2\mathrm{K}(k)b = 0 \qquad (4.36)$$

in which

$$y = \alpha x \qquad (4.37)$$

Using $k^2 = 1/2$ and Eq. B.32, Eq. 4.36 yields

$$b = \frac{1}{3}a \tag{4.38}$$

Equation 4.31 gives

$$U = (1 - \frac{1}{10}\frac{a}{d_0})c \tag{4.39}$$

Therefore, the wavelength is given by Eq. 4.25 as:

$$L_W = 2l(\frac{140d_0}{a})^{\frac{1}{4}}\mathrm{K}(\sqrt{\frac{1}{2}}) \tag{4.40}$$

in which

$$\mathrm{K}(\sqrt{\frac{1}{2}}) \approx 1.854 \tag{4.41}$$

The constant A is obtained from Eq. 4.33 as

$$A = -\frac{23a^2}{210d_0} \tag{4.42}$$

The final solution of Eq. 4.22 is

$$d(x,t) = a(\frac{1}{3} - \mathrm{cn}^4\left((\frac{a}{140d_0})^{\frac{1}{4}}\frac{(x-Ut)}{l}, \sqrt{\frac{1}{2}}\right)) \tag{4.43}$$

where wave speed U is given by Eq. 4.39

Equation 4.43 represents a train of periodic waves propagating at the speed of $U = (1 - 0.1\frac{a}{d_0})c$ in the ice-covered river channel. The shape, period, and wavelength of the wave are all functions of the wave amplitude a. Equation 4.40 shows that the wavelength decreases as the wave amplitude increases. Equation 4.44 shows that the celerity of the wave is smaller than c. The effect of ice cover on wave speed can be seen by comparing Eq. 4.44 with the solitary wave speed $U = c(1 + \frac{a}{2d_0})$, and cnoidal wave speed $U = c[1 + (a - \sqrt{\frac{3a}{4d_0^3}})/2d_0]$ for free surface waves (Debnath 1994). Equation 4.43 is an exact solution of Eq. 4.22, which is derived under the condition $\frac{a}{d_0} \ll 1$, for all positive a.

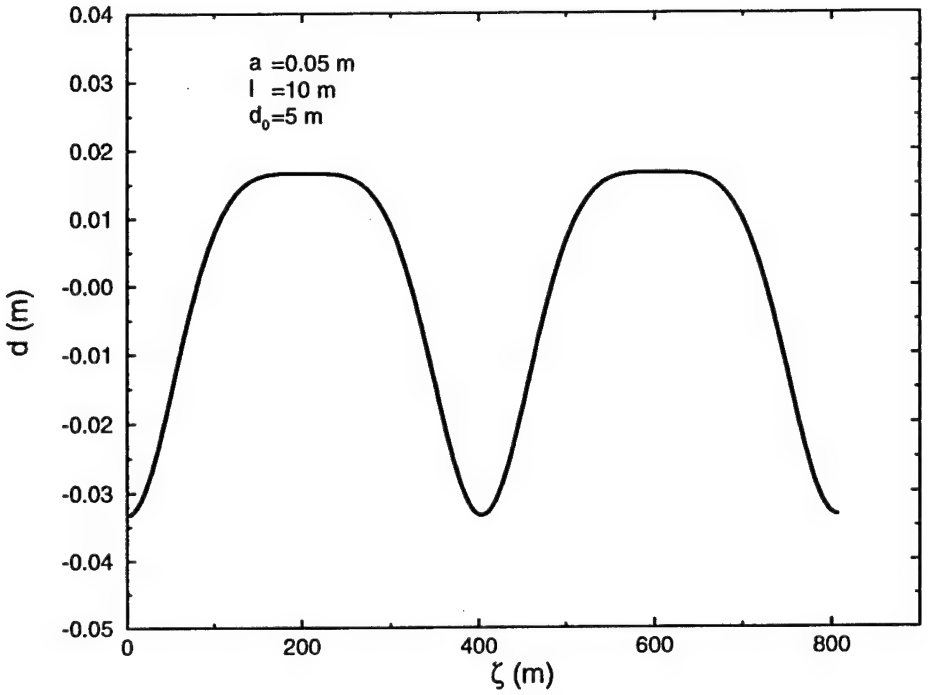

Figure 4.1: A typical wave profile under an ice cover; $\zeta = x - Ut$

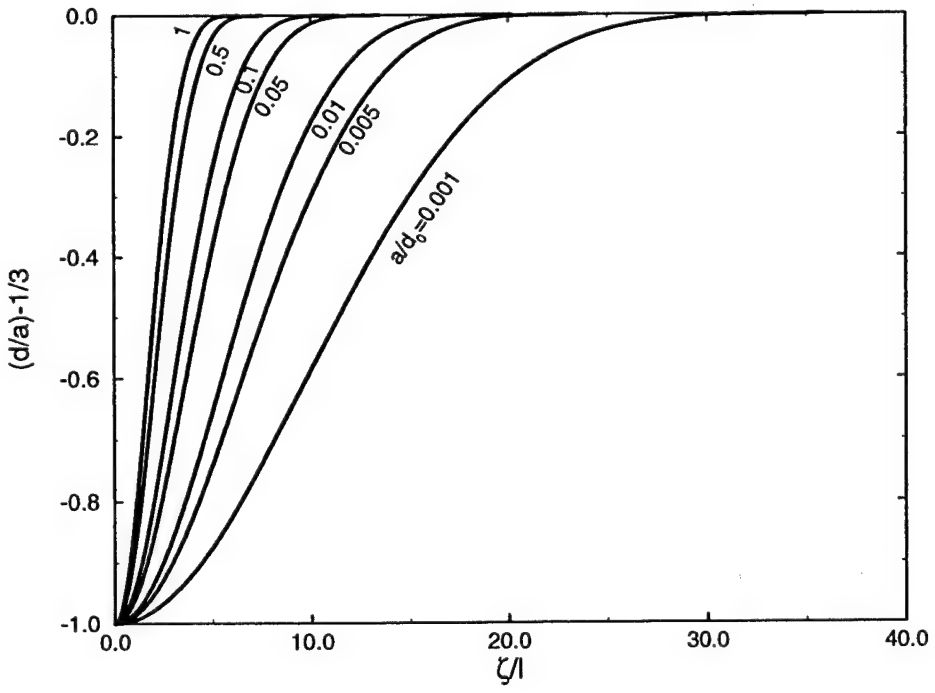

Figure 4.2: Profiles of the nonlinear waves under ice cover

Equations 4.43, 4.39 and 4.40 can be rewritten as

$$\frac{d}{a} = \frac{1}{3} - \mathrm{cn}^4\left(\left(\frac{1}{140}\frac{a}{d_0}\right)^{\frac{1}{4}}\frac{(x-Ut)}{l}, \sqrt{\frac{1}{2}}\right) \tag{4.44}$$

$$\frac{U}{c} = 1 - \frac{1}{10}\frac{a}{d_0} \tag{4.45}$$

and,

$$\frac{L_W}{l} = 2\left(\frac{140d_0}{a}\right)^{\frac{1}{4}}\mathrm{K}\left(\sqrt{\frac{1}{2}}\right) \tag{4.46}$$

A typical wave profile given by Eq. 4.44 is shown in Fig. 4.1. Figure 4.2 shows profiles of the nonlinear waves varying with the wave amplitude for the first half wavelength, obtained from Maple Version 4.

4.2.2 Application of Solutions for the Simplified Equation

The maximum bending stress S_{Xmax} in the ice cover is at the bottom of the ice sheet, $z = -\frac{\eta}{2}$. Eq. 3.37 becomes

$$S_{Xmax} = \frac{E}{1-\nu^2}\frac{\eta}{2}\frac{\partial^2 d}{\partial x^2} \tag{4.47}$$

Using Eqs. 4.43 and B.23 with $k^2 = \frac{1}{2}$, Eq. 4.47 gives

$$S_{Xmax} = -\frac{E}{1-\nu^2}\frac{\eta}{2}a\alpha^2\left(-10\mathrm{cn}^6\left(X, \sqrt{\frac{1}{2}}\right) + 6\mathrm{cn}^2\left(X, \sqrt{\frac{1}{2}}\right)\right) \tag{4.48}$$

in which, $X = \alpha\zeta = \left(\frac{a}{140d_0}\right)^{\frac{1}{4}}\frac{(x-Ut)}{l}$, as defined in Eq. 4.26. The profile of the function, $F_{cn} = -10\mathrm{cn}^6\left(X, \sqrt{\frac{1}{2}}\right) + 6\mathrm{cn}^2\left(X, \sqrt{\frac{1}{2}}\right)$, is shown in Fig. 4.3. Its minimum value is -4.

Substituting Eq. 4.35 for α in Eq. 4.4 yields

$$S_{Xmax} = \frac{E}{1-\nu^2}\frac{\eta}{l^2}\frac{a^{\frac{3}{2}}}{\sqrt{35d_0}} \tag{4.49}$$

For an ice cover with a maximum flexural strength S_{Xb}, the minimum wave amplitude which cause ice cover fracture is

$$a_{min} = \left(\frac{S_{Xb}(1-\nu^2)}{E\eta}l^2\sqrt{35d_0}\right)^{\frac{2}{3}} \tag{4.50}$$

or

$$\frac{a_{min}}{d_0} = \left(\sqrt{35}\frac{S_{Xb}(1-\nu^2)}{E}\frac{l^2}{d_0\eta}\right)^{\frac{2}{3}} \tag{4.52}$$

The value of elastic modulus of the channel ice cover E ranges from 0.4 to 9.8 GPa. The value of Poisson's ratio ν is estimated to be 0.35. The maximum flexural strength S_{Xb} is assumed to be 0.6 MPa, which the ice cover can withstand before a crack forms (Daly 1995). Equations 4.52, 4.39 and 4.40 are used to determine a_{min}, and corresponding values of U and L_W, i.e. L_{Wmax} based on these values. Sample values of the wave amplitude a_{min} required to cause the ice cover to crack, as well as other corresponding parameters, is shown in Table 4.1, where $l = (\frac{EI}{\rho g(1-\nu^2)})^{\frac{1}{4}} = (\frac{\eta^3 E}{12\rho g(1-\nu^2)})^{\frac{1}{4}}$.

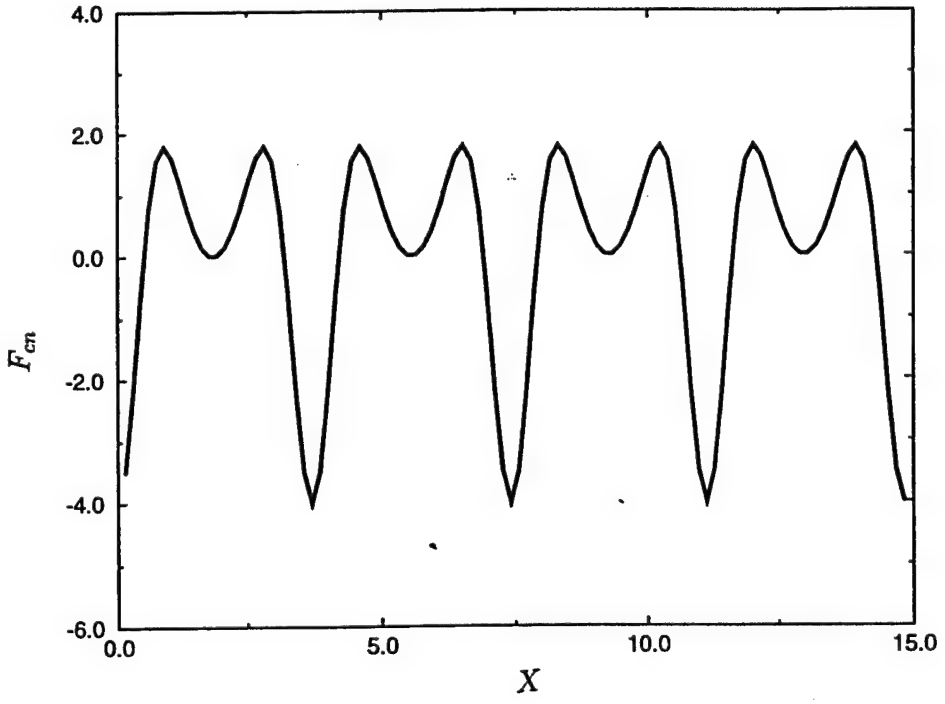

Figure 4.3: The profile of the function $-10\mathrm{cn}^6(X, \sqrt{\frac{1}{2}}) + 6\mathrm{cn}^2(X, \sqrt{\frac{1}{2}})$

If the amplitude of an incoming wave is larger than a_{min} or the wave length is less than L_{Wmax}, the wave will form transverse cracks in the ice cover. The linear model gives the result that the wave with wavelength near $2\pi l$, i.e. in the order of 10 m can generate sufficient amplitude to cause transverse cracks to form. However, The nonlinear

Table 4.1: Values for a_{min} and other corresponding parameters

d_0 (m)	E (GPa)	η (m)	l (m)	a_{min} (m)	U (m/s)	L_{Wmax} (m)
5	1	0.2	2.87	0.475	6.934	65.98
5	1	0.5	5.71	0.645	6.910	121.54
5	1	1.0	9.60	0.812	6.886	192.93
5	10	0.2	5.11	0.220	6.969	142.15
5	10	0.5	10.15	0.299	6.958	261.85
5	10	1.0	17.08	0.377	6.947	415.65
3	1	0.2	2.87	0.401	5.350	60.60
3	1	0.5	5.71	0.544	5.324	111.62
3	1	1.0	9.60	0.685	5.298	177.19
3	10	0.2	5.11	0.186	5.388	130.55
3	10	0.5	10.15	0.252	5.376	240.48
3	10	1.0	17.08	0.318	5.365	381.73

shown in Table 4.1. This is more consistent with the observations given by Parkinson(1982), Gerard et al. (1984), and Prowse (1986).

The relation between the wavelength and wave amplitude, Eq. 4.40, can be rearranged as:

$$\frac{a}{d_0} = 140(\frac{\mathrm{K}(\sqrt{\frac{1}{2}})}{\pi})^4(\frac{2\pi l}{L_W})^4 \tag{4.52}$$

This relationship is shown in Figs. 4.4 and 4.5.

Equations 4.23 and B.34 give

$$\begin{aligned} |\frac{\partial d}{\partial x}| &= a\alpha\,|\frac{d}{dx}\,\mathrm{cn}^4(x)\,| \\ &\leq \frac{4a^{5/4}}{(140d_0)^{1/4}l} \end{aligned} \tag{4.53}$$

Since the order of $|\frac{\partial d}{\partial x}|$ is O(0.1) for all cases in Table 4.1, the assumption used in deriving the plate equation, Eq.2.14 is justified.

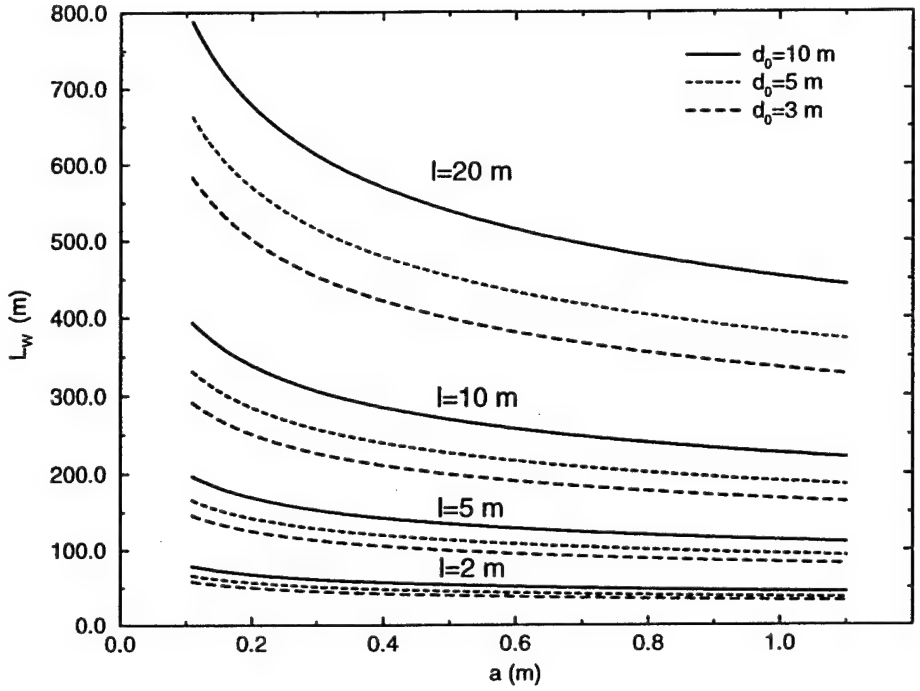

Figure 4.4: The relationship between wavelength and amplitude of nonlinear waves Eq. 4.40

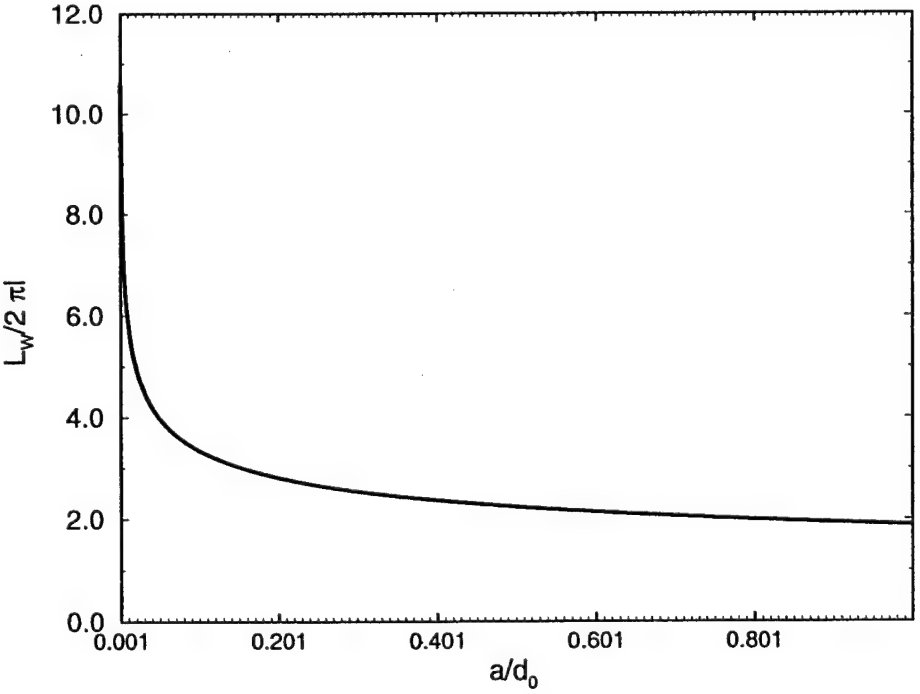

Figure 4.5: The relationship between wavelength and amplitude of nonlinear waves in dimensionless form Eq. 4.52

4.2.3 Solution of the Complete Equation

Now, we solve the complete equation 4.19. The idea is the same as that for the simplified case discussed in Sec. 4.2.1. Equation 4.21 is rearranged as the following:

$$A + (1 - \frac{U}{c})d + \frac{3}{4d_0}d^2 + \frac{1}{2}d'''' + \beta d'' = 0 \tag{4.54}$$

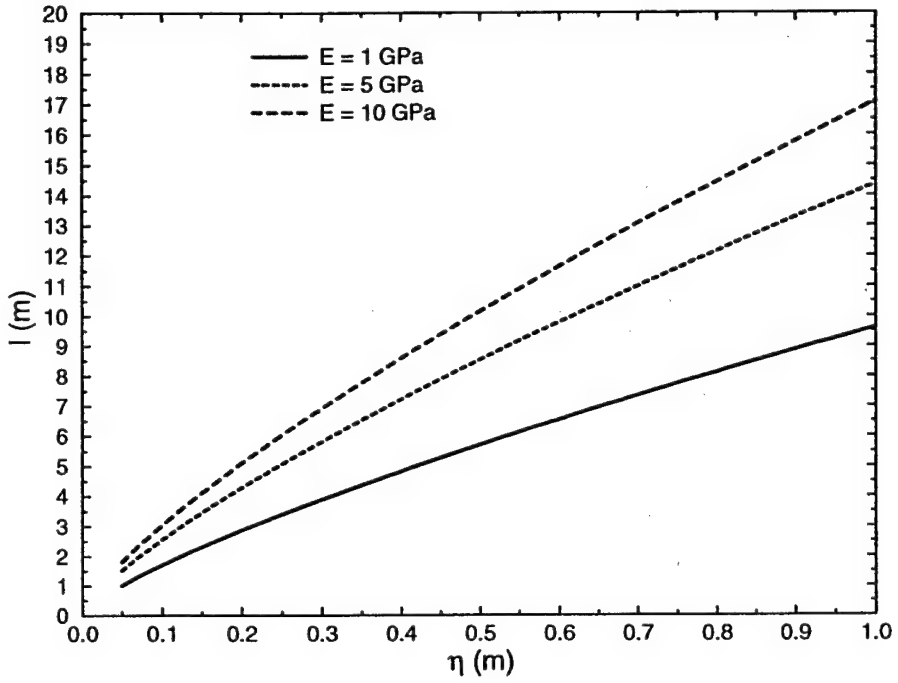

Figure 4.6: Characteristic length of ice cover

where $' = \frac{d}{d\xi}$, $\xi = \frac{\zeta}{l} = \frac{x-Ut}{l}$. The characteristic length $l = (\frac{\eta^3 E}{12\rho g(1-\nu^2)})^{\frac{1}{4}}$ is shown in Fig. 4.6. The parameter β is defined as $\beta = \frac{\rho_i}{2\rho}\frac{d_0\eta}{l^2}(1+Fr)^2 + \frac{N}{2\rho g l^2}$. The first term represents the ice inertia term, β_{ice}, which is shown in Fig. 4.7. The second term is the axial force β_{axial}. If N equals the maximum axial force N_{cr} defined in Eq. 3.33, then $\beta_{axial} = 1$.

Assuming the solution is in the following form

$$d(\zeta) = -a\mathrm{cn}^4(\alpha\xi, k) + b\mathrm{cn}^2(\alpha\xi, k) + g \tag{4.55}$$

i.e.

$$d(x,t) = -a\mathrm{cn}^4(\alpha\frac{x-Ut}{l}, k) + b\mathrm{cn}^2(\alpha\frac{x-Ut}{l}, k) + g$$

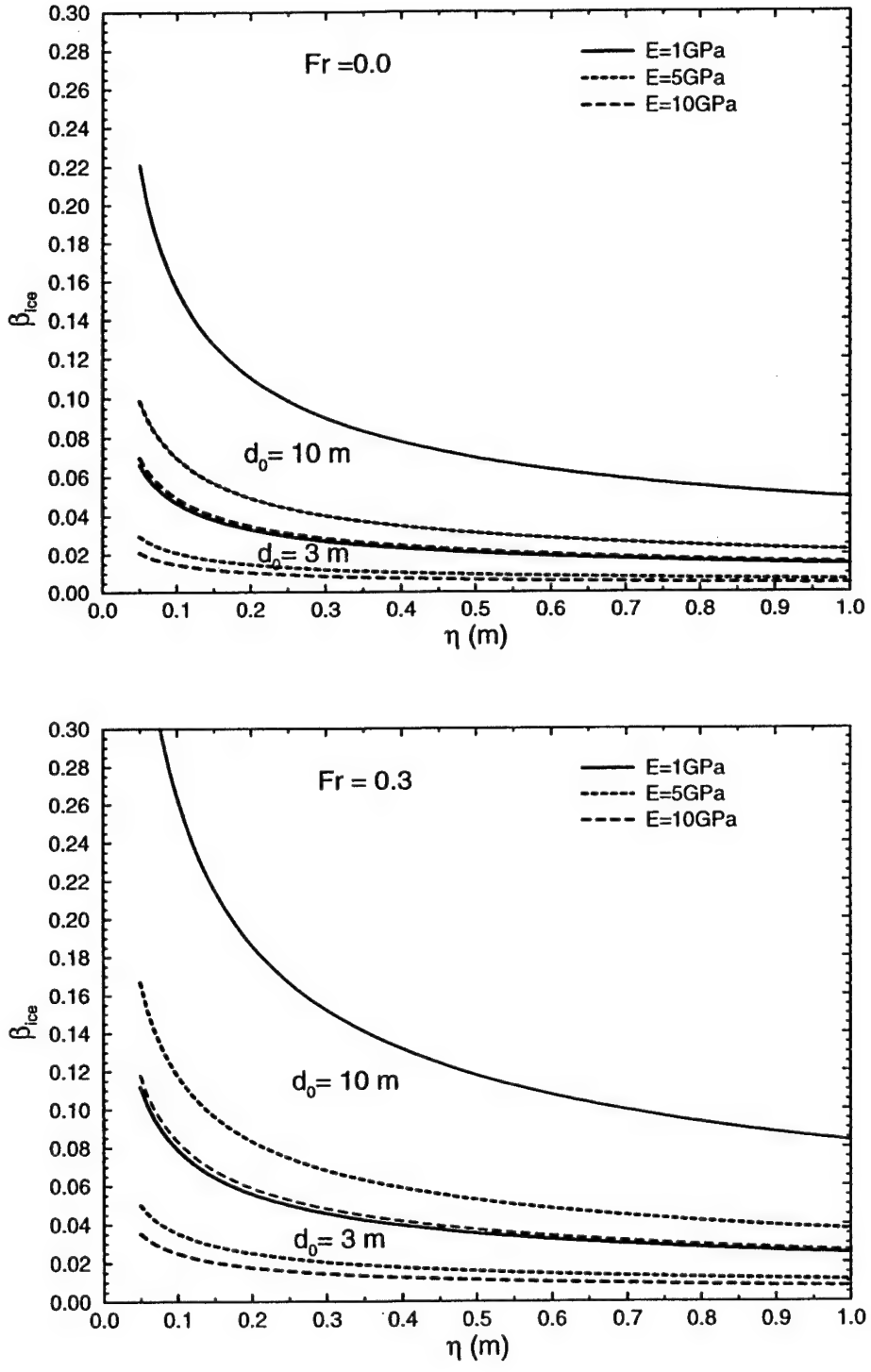

Figure 4.7: Values of the ice inertia term β_{ice}

where a, α, b, U, k and g are to be determined. The coefficient a, b, and α are different from those in Eq. 4.23. The wave height in Eq.4.55 is a combination of a and b.

Equation 4.54 can be rewritten as the following by letting $X = \alpha\xi$.

$$-[A + (1 - \frac{U}{c})d + \frac{3}{4d_0}d^2] = \frac{1}{2}\alpha^4 d_{XXXX} + \beta\alpha^2 d_{XX} \tag{4.56}$$

Equation 4.56 is similar to Eq.4.26, except for the last term. The right-hand side terms in Eq.4.56 can be obtained as the following by substituting Eq.4.55 into Eq.4.54. Expressions for cn^4_{XXXX} and cn^2_{XX} are derived in Appendix B.

$$\begin{aligned}
\frac{1}{2}\alpha^4 d_{XXXX} &= -a840\alpha^4\frac{1}{2}k^4\mathrm{cn}^8(X) \\
&\quad +[-a1040(-2k^4+k^2)\alpha^4\frac{1}{2} + b8\times 15k^4\alpha^4\frac{1}{2}]\mathrm{cn}^6(X) \\
&\quad +[-a32(53k^4-53k^2+8)\frac{1}{2}\alpha^4 + b8\times 15(-2k^4+k^2)\frac{1}{2}\alpha^4]\mathrm{cn}^4(X) \\
&\quad +[-a240\frac{1}{2}\alpha^4(-2k^4+3k^2-1) + b\frac{1}{2}\alpha^4 8(17k^4-17k^2+2)]\mathrm{cn}^2(X) \\
&\quad +(-a)24\frac{1}{2}\alpha^4(1-k^2)^2 + b\frac{1}{2}\alpha^4 8(-2k^4+3k^2-1) \qquad (4.57) \\
\beta\alpha^2 d_{XX} &= \alpha^2[\beta(20ak^2)\mathrm{cn}^6(X) \\
&\quad +\left(-a\beta 16(-1+2k^2) + b\beta(-6k^2)\right)\mathrm{cn}^4(X) \\
&\quad +\left(-a\beta 12(1-k^2) + b\beta 4(-1+2k^2)\right)\mathrm{cn}^2(X) \\
&\quad +b\beta 2(1-k^2)] \qquad (4.58)
\end{aligned}$$

The left-hand side terms can be obtained as:

$$\begin{aligned}
A + (1-\frac{U}{c})d + \frac{3d^2}{4d_0} &= \frac{3a^2}{4d_0}\mathrm{cn}^8(X) + \frac{3}{2d_0}(-a)b\mathrm{cn}^6(X) + [(1-\frac{U}{c})(-a) + \frac{3}{4d_0}(b^2+2(-a)g)]\mathrm{cn}^4(X) \\
&\quad +[(1-\frac{U}{c})b + \frac{3}{4d_0}2bg)]\mathrm{cn}^2(X) + (A + (1-\frac{U}{c})g + \frac{3g^2}{4d_0}) \qquad (4.59)
\end{aligned}$$

By equating the coefficients of polynomials of cn on the two sides of Eq. 4.56, The following five conditions are obtained for determining a, α, b, U, k and g, among which only one is an independent parameter.

$$-\frac{3}{4d_0}a^2 = -a840\alpha^4\frac{1}{2}k^4$$

$$-\frac{3}{4d_0}2(-a)b = (-a)1040(-2k^4+k^2)\alpha^4\frac{1}{2} + \alpha^4\frac{1}{2}b8\times 15k^4 + (20a\beta k^2)\alpha^2 \quad (4.60)$$

$$-[(1-\frac{U}{c})(-a)+\frac{3}{4d_0}(b^2+2(-a)g)] = (-a)32\alpha^4\frac{1}{2}(53k^4-53k^2+8)+b\frac{1}{2}\alpha^4 8\times 15(-2k^4+k^2) + (-a)\beta 16(-1+2k^2)\alpha^2 + b\beta(-6k^2)\alpha^2 \quad (4.61)$$

$$-[(1-\frac{U}{c})b+\frac{3}{4d_0}2bg)] = (-a)240\alpha^4\frac{1}{2}(-2k^4+3k^2-1)+b\alpha^4\frac{1}{2}8(17k^4-17k^2+2) + (-a)\beta 12(1-k^2)\alpha^2 + b\beta 4(-1+2k^2)\alpha^2 \quad (4.62)$$

$$-[\frac{A}{d_0}+(1-\frac{U}{c})\frac{g}{d_0}+\frac{3g^2}{4d_0^2}] = (-\frac{a}{d_0})24\alpha^4\frac{1}{2}(1-k^2)^2+\frac{b}{d_0}\alpha^4\frac{1}{2}8(-2k^4+3k^2-1) + \frac{b}{d_0}\beta 2(1-k^2)\alpha^2 \quad (4.63)$$

The integration constant A needs to be determined. Since the net area occupied by fluid within a wavelength above the mean water depth d_0 is zero:

$$\int_0^{Lw} d(x,t)dx = 0 \quad (4.64)$$

which implies

$$\int_0^{Lw}[-a\mathrm{cn}^4\left(\alpha\frac{(x-Ut)}{l},k\right)+b\mathrm{cn}^2\left(\alpha\frac{(x-Ut)}{l},k\right)+g]dx = 0 \quad (4.65)$$

where the wavelength (see Appendix B)

$$L_W = \frac{2l}{\alpha}\mathrm{K}(k) \quad (4.66)$$

Let

$$y = \alpha\frac{(x-Ut)}{l} \quad (4.67)$$

Equation 4.65 yields

$$-a\int_0^{2\mathrm{K}(k)}\mathrm{cn}^4(y,k)dy + b\int_0^{2\mathrm{K}(k)}\mathrm{cn}^2(y,k)dy + 2\mathrm{K}(k)g = 0 \quad (4.68)$$

Using Eqs. B.31 and B.32, Eq. 4.68 yields

$$\frac{g}{a} = \left(\frac{2(2k^2-1)}{3k^2}-\frac{b}{a}\right)\left(\frac{\mathrm{E}(k)}{\mathrm{K}(k)k^2}-\frac{1-k^2}{k^2}\right)+\frac{1-k^2}{3k^2} \quad (4.69)$$

The six equations, 4.59 to 4.63, and 4.69, are used to determine the constant A and five of the six parameters a, α, b ,U, k and g. Now, the parameter k, which varies between 0 and 1, is selected as the independent variable. Equations 4.59 to 4.62 give

$$\frac{a}{d_0} = 560k^4\alpha^4 \tag{4.70}$$

$$\frac{b}{d_0} = -\left(\frac{14\times 80}{3}(1-2k^2)\alpha^2 - \frac{14\times 40}{13\times 3}\beta\right)k^2\alpha^2 \tag{4.71}$$

$$\begin{aligned} -[(1-\frac{U}{c})+\frac{3g}{2d_0}] &= \left(16(53k^4-53k^2+8)+(40-\frac{70\times 8}{3})(1-2k^2)^2\right)\alpha^4 \\ &\quad +(-20+\frac{500}{3\times 13})(-2k^2+1)\beta\alpha^2 - \frac{2\times 31}{3\times 13^2}\beta^2 \equiv Q \end{aligned} \tag{4.72}$$

$$\begin{aligned} -[(1-\frac{U}{c})+\frac{3g}{2d_0}] &= \left(120\alpha^4(-2k^4+3k^2-1)+\beta 12(1-k^2)\alpha^2\right)\frac{3k^2\alpha^2}{2(-2k^2+1)\alpha^2-\frac{\beta}{13}} \\ &\quad +4(17k^4-17k^2+2)\alpha^4+4(-1+2k^2)\beta\alpha^2 \end{aligned} \tag{4.73}$$

After combining Eqs. 4.72 and 4.73 , we obtain the following equation for $\frac{\alpha^2}{\beta}$

$$C_3(\frac{\alpha^2}{\beta})^3 + C_2(\frac{\alpha^2}{\beta})^2 + C_1(\frac{\alpha^2}{\beta}) + C_0 = 0 \tag{4.74}$$

where

$$\begin{aligned} C_3 &= 3\times 120(-2k^4+3k^2-1)k^2 + 8(17k^4-17k^2+2)(-2k^2+1) \\ &\quad -2(-2k^2+1)\left(16(53k^4-53k^2+8)+(40-\frac{70\times 8}{3})(1-2k^2)^2\right) \\ C_2 &= [3k^2 12(1-k^2) - \frac{4}{13}(17k^4-17k^2+2) - 8(-1+2k^2)^2 \\ &\quad -2(-20+\frac{500}{3\times 13})(-2k^2+1)^2 \\ &\quad +\left(16(53k^4-53k^2+8)+(40-\frac{70\times 8}{3})(1-2k^2)^2\right)/13] \\ C_1 &= [\frac{4}{13}+(-20+\frac{500}{3\times 13})\frac{1}{13}+\frac{4\times 31}{3\times 13^2}](-2k^2+1) \\ C_0 &= -\frac{2\times 31}{3\times 13^3} \end{aligned}$$

Thus $\frac{\alpha^2}{\beta}$ is a function of k which can be obtained from Eq. 4.74. Furthermore, $\frac{\alpha^2}{\beta}$ should be the positive real roots of Eq. 4.74. Equations 4.70 and 4.71 yield

$$\frac{b}{a} = \frac{1}{39k^2\frac{\alpha^2}{\beta}} - \frac{2(1-2k^2)}{3k^2}$$

Thus Eq. 4.69 yields

$$\frac{g}{a} = \frac{-1}{39k^2\frac{\alpha^2}{\beta}}\left(\frac{\mathrm{E}(k)}{\mathrm{K}(k)k^2} - \frac{1-k^2}{k^2}\right) + \frac{1-k^2}{3k^2} \tag{4.75}$$

This shows that $\frac{g}{a}$ is a function of k and is independent on β. Eq. 4.72 is rearranged as the following,

$$\frac{U}{c} = 1 + \frac{3a}{2d_0}\frac{g}{a} + Q \tag{4.76}$$

where Q is the right-hand side term of Eq. 4.72 and is a function of k and β. Since $\frac{g}{a}$ can be replaced by Eq. 4.75, U is a function of k and β.

The following procedure is used to establish curves for a, b, U, g and α as functions of k for a selected value of the physical parameter β:

1. Select a physical parameter β;
2. Choose a value of k, which is in the range of 0 to 1;
3. Calculate $\frac{\alpha^2}{\beta}$ and α from Eq. 4.74;
4. Calculate coefficient a from Eq. 4.70;
5. Calculate b, g and U from Eqs. 4.71, 4.75, and 4.76, respectively, and the wave profile d from Eq. 4.55;
6. The wave length L_w can be calculated using Eq. B.9, i.e.

$$\frac{L_w}{l} = \frac{2}{\alpha}\mathrm{K}(k) \tag{4.77}$$

Figures 4.8 to 4.12 show the dimensionless parameters a, b, α, g and U as functions of k. Similar plots for α, a, b and g in dimension are shown in Appendix D. These figures show that, when $k \to 0$, thus $\alpha \to$ a constant which depends on the flow and ice cover condition l and β, and $a \to 0$, $b \to 0$. The result approaches that of linear equation. When $k \to \sqrt{\frac{1}{2}}$, α , a and b all approach positive infinity. In this case, the result approaches that of the simplified equation.

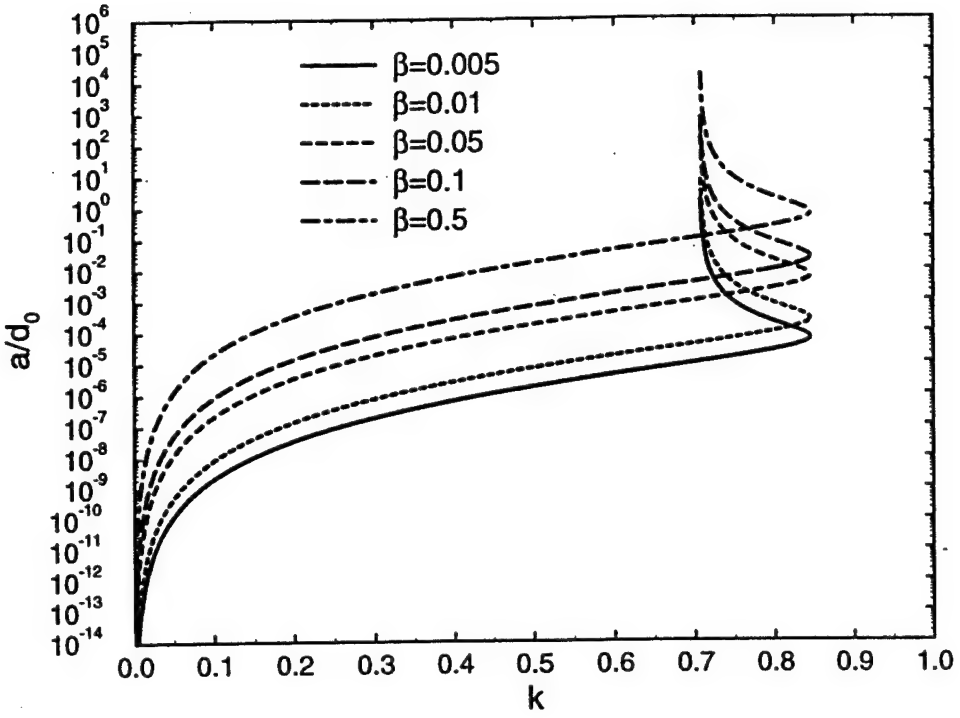

Figure 4.8: Variation of parameter a with k

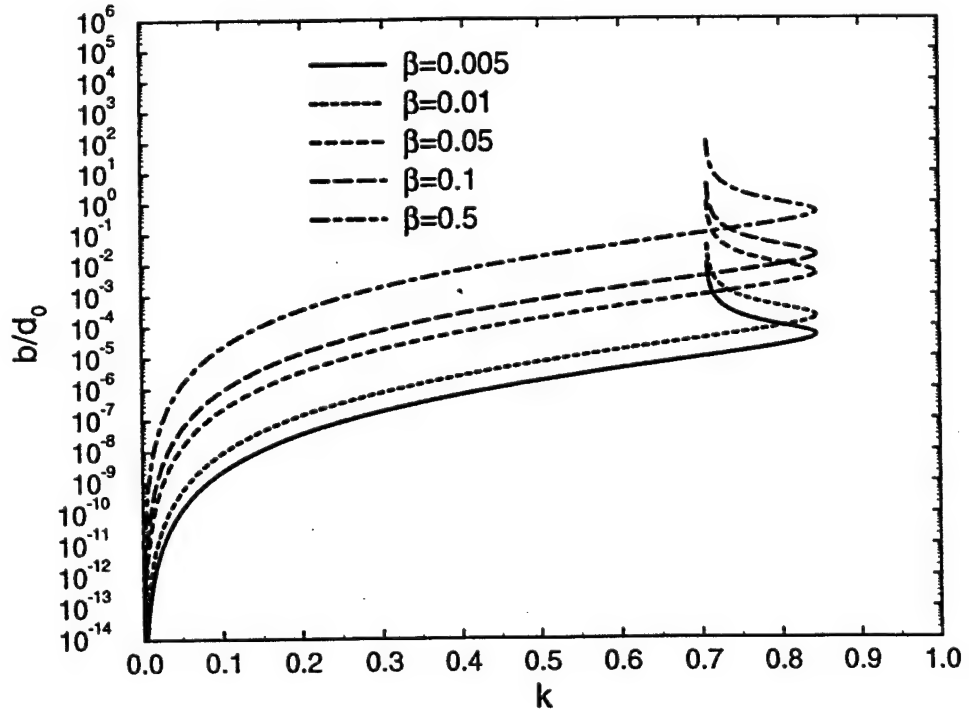

Figure 4.9: Variation of parameter b with k

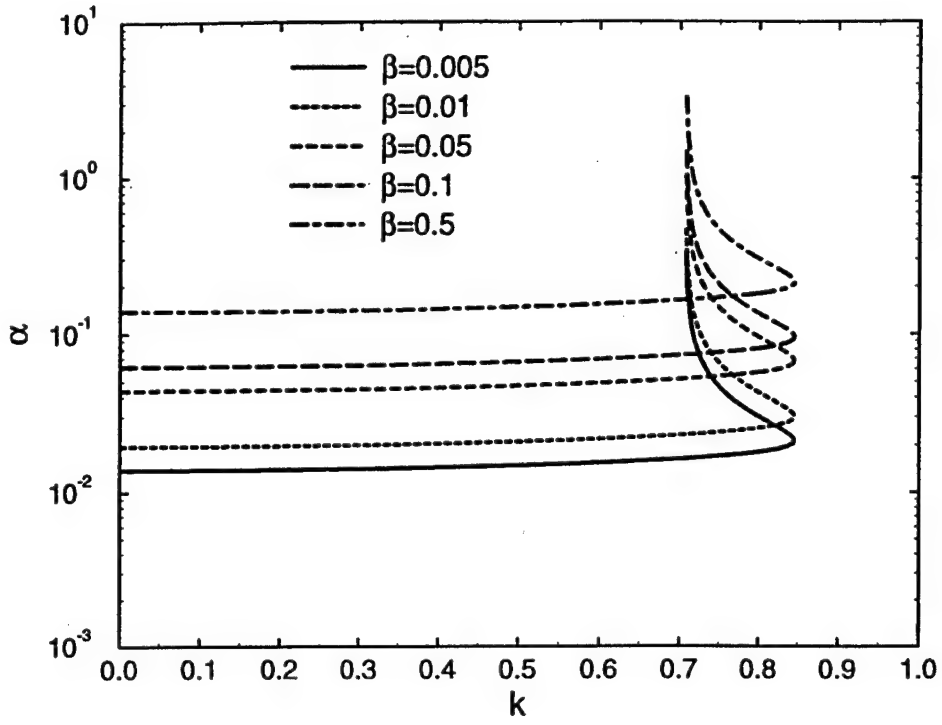

Figure 4.10: Variation of parameter α with k

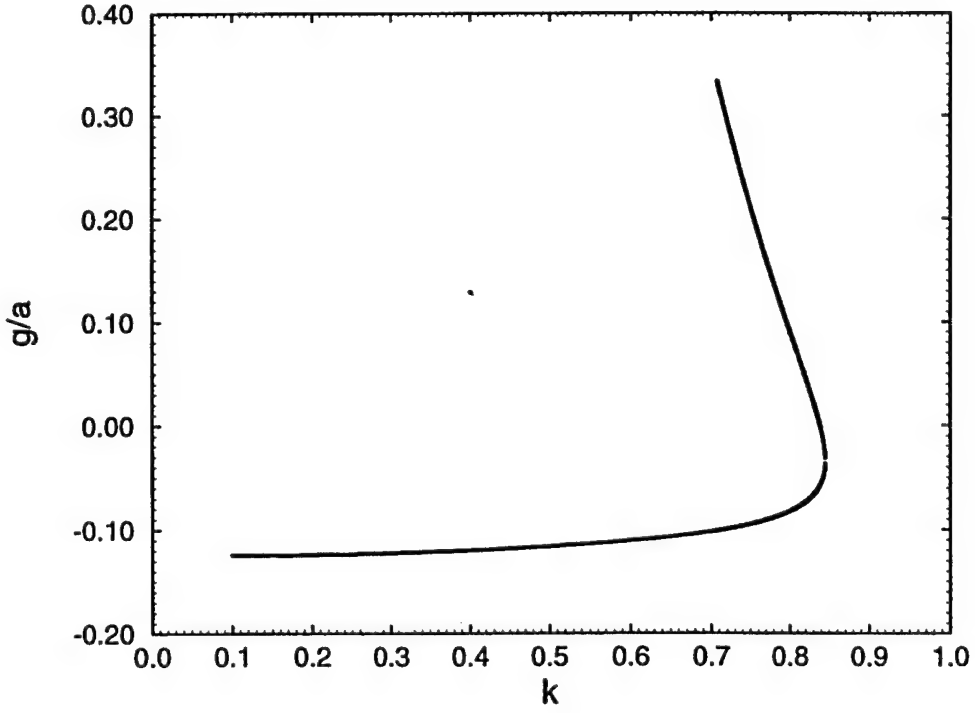

Figure 4.11: Variation of parameter g with k

Table 4.2: Solutions of the complete equation for $L_W = 381.7$ m

β	$a(m)$	$b(m)$	k	α	g	$\frac{U}{c} - 1$
0.0079	0.323	0.01134	0.7126	0.16524	0.3164	-0.01146
0.0130	0.340	0.0192	0.7160	0.16660	0.3062	-0.01245
0.3130	0.330	0.2362	0.8382	0.18593	0.00047	-0.0678

Given a wavelength $L_w = 381.7$ m, and let others parameters $F_r = 0.3$, $d_0 = 3$ m, $E = 10$ GPa, and $\eta = 1$ m be the same as those of the last case in the Table 4.1 for the simplied solution, solutions of Eq. 4.54, which obtained from Figs. 4.8 to 4.12, are shown in Table 4.2. Figure 4.13 shows the profiles of these nonlinear waves. When $\beta = 0$, this returns to the simple case. When only ice inertia is considered, $\beta = 0.0079$, i.e. Case 1 in Table 4.2. If there is an axial force in ice cover, say $\frac{N_{cr}}{3}$, that is Case 3 in Table 4.2.

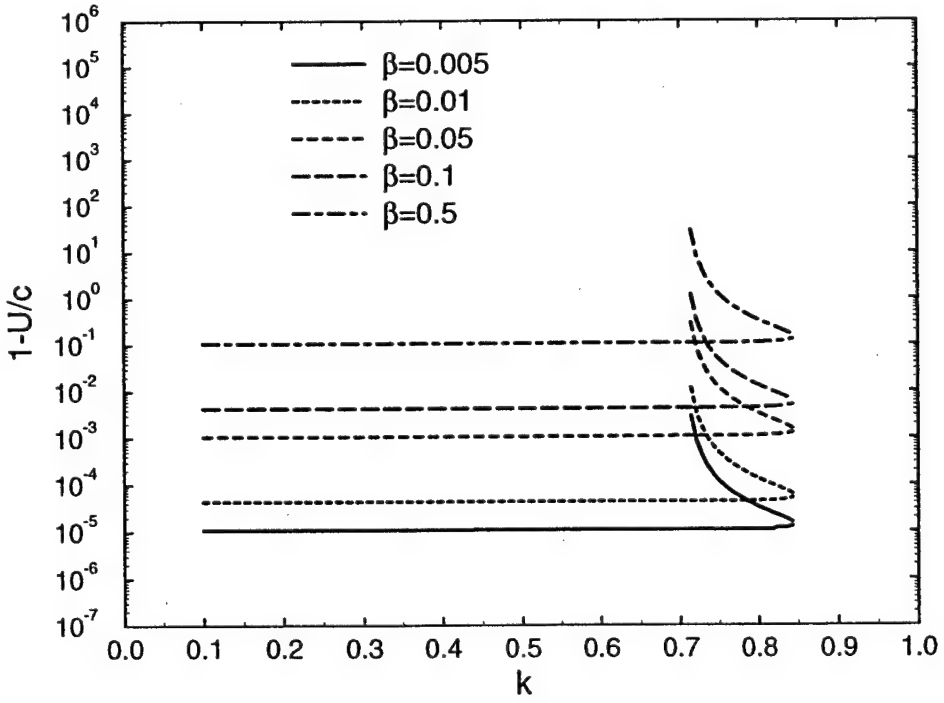

Figure 4.12: Variation of parameter U with k

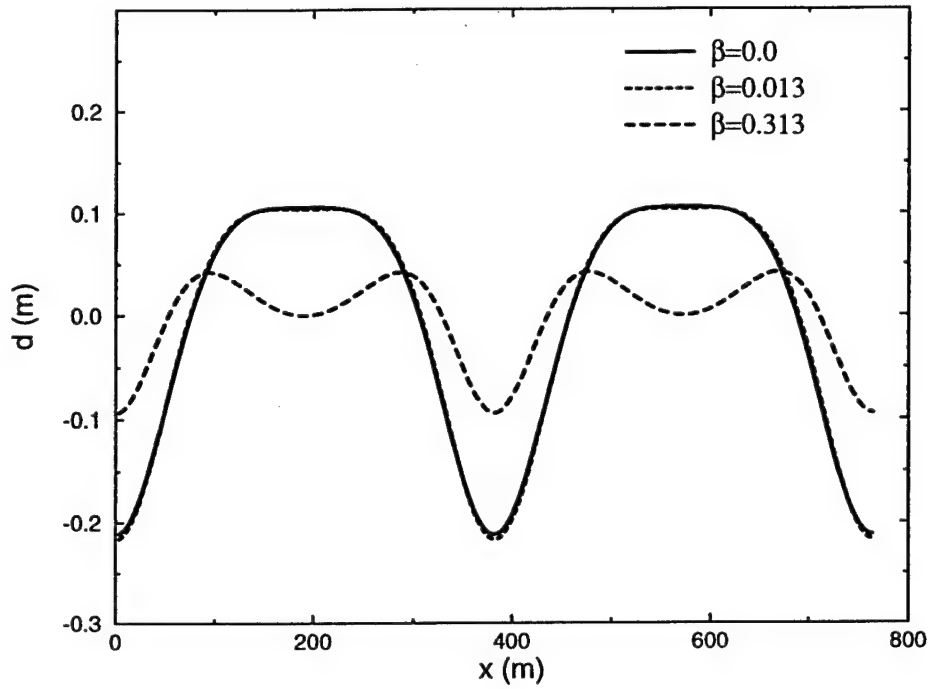

Figure 4.13: Profiles of nonlinear waves

4.2.4 Application

The maximum bending stress in the ice cover S_{Xmax} is at the bottom of the ice sheet, $z = -\frac{\eta}{2}$.

$$S_{Xmax} = \frac{E}{1-\nu^2}\frac{\eta}{2}\frac{\partial^2 d}{\partial x^2} \tag{4.78}$$

Based on Eqs. 4.55, B.23 and B.20, $\frac{\partial^2 d}{\partial x^2}$ can be obtained as Eq.4.79, after setting $t = 0$,

$$\begin{aligned}\frac{\partial^2 d}{\partial x^2} &= \frac{\alpha^2}{l^2}[20k^2 a\mathrm{cn}^6(\alpha\frac{x}{l},k) + (16(-1+2k^2)(-a) - 6k^2 b)\mathrm{cn}^4(\alpha\frac{x}{l},k) \\ &\quad +[12(1-k^2)(-a) + 2(-2+4k^2)b]\mathrm{cn}^2(\alpha\frac{x}{l},k) + 2b(1-k^2)] \end{aligned}\tag{4.79}$$

Therefore, Eq.4.78 gives

$$\begin{aligned}S_{Xmax} &= \frac{E}{1-\nu^2}\frac{\eta}{2}\frac{\alpha^2}{l^2}[20k^2 a\mathrm{cn}^6(\alpha\frac{x}{l},k) + (16(-1+2k^2)(-a) - 6k^2 b)\mathrm{cn}^4(\alpha\frac{x}{l},k) \\ &\quad +[12(1-k^2)(-a) + 2(-2+4k^2)b]\mathrm{cn}^2(\alpha\frac{x}{l},k) + 2b(1-k^2)] \end{aligned}\tag{4.80}$$

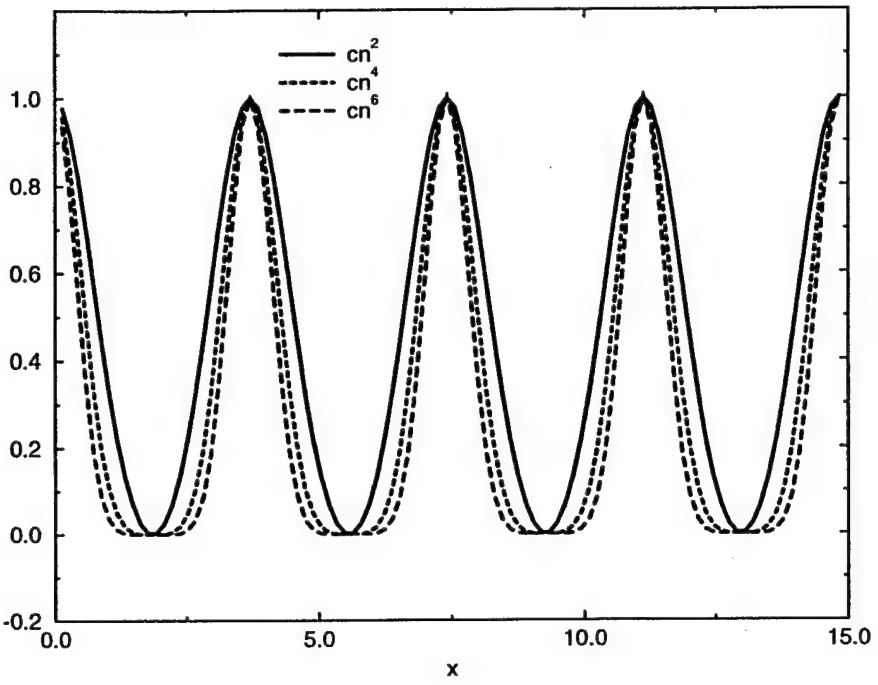

Figure 4.14: Variation of cnoidal functions with modulus $k = \frac{1}{2}$

The profiles of the functions, $\mathrm{cn}^2(x, \sqrt{\frac{1}{2}})$, $\mathrm{cn}^4(x, \sqrt{\frac{1}{2}})$, and $\mathrm{cn}^6(x, \sqrt{\frac{1}{2}})$ are shown in Fig. 4.14. Figure 4.14 shows that their wave lengths are the same, as stated by Eq. B.9. Let

$$\begin{aligned} G(x, L_W) &= \frac{\alpha^2}{l^2}[20k^2 a\mathrm{cn}^6(\alpha\frac{x}{l}, k) + (16(-1+2k^2)(-a) - 6k^2 b)\mathrm{cn}^4(\alpha\frac{x}{l}, k) \\ &\quad +[12(1-k^2)(-a) + 2(-2+4k^2)b]\mathrm{cn}^2(\alpha\frac{x}{l}, k) + 2b(1-k^2)] \end{aligned} \tag{4.81}$$

Equation 4.81 gives

$$S_{Xmax} = \frac{E}{1-\nu^2}\frac{\eta}{2}G_{max}(L_W) \tag{4.82}$$

The maximum value $G_{max}(L_W)$ is difficult to obtain explicitly. It can be obtained numerically by varying the value of x over one wave length. If the value of S_{Xmax} is found to be larger than the maximum flexural strength S_{Xb}, then the ice cover will crack. The longest wave, L_{Wmax}, to cause cracking can be then found. In summary, the procedure for determining L_{Wmax} is:

1. Select a k (This fixed L_W);

Table 4.3: Solutions of complete equation for breakuping ice cover

β	$L_w(m)$	$a(m)$	$b(m)$	k	α	g	$\frac{U}{c}-1$
0.0	381.7	0.3180	0.0	0.7071	0.1659	0.3333	-0.0106
0.013	387.5	0.3230	0.0186	0.7162	0.1645	0.3056	-0.0120
0.113	414.9	0.4310	0.1836	0.7827	0.1617	0.1309	-0.0237
0.213	440.8	0.5300	0.3598	0.8325	0.1601	0.0162	-0.0349
0.313	442.4	0.5787	0.4793	0.8432	0.1616	-0.0478	-0.0504

2. Vary x to find the maximum value of $S_{Xmax} = \frac{E}{1-\nu^2}\frac{\eta}{2}G_{max}(x, L_W)$ for this k from Eq. 4.82;

3. See if this matches or exceeds S_{Xb}. If not, try another k, and repeat steps 1 to 3.

Using the parameters of the last case in the Table 4.1, with $F_r = 0.3$, waves which cause the ice cover to fracture are shown in Table 4.3. The profiles of these waves are shown in Fig. 4.15.

If an axial force is absent, the effect of inertia of ice cover is insignificant as shown in Table 4.2 and Fig. 4.13. If the axial force is large enough, it can change the shape of the wave. Furthermore, the wave height required to cause the ice cover to fracture is significantly reduced, as shown in Fig.4.15.

Eqs. 4.55, B.33 and B.34 give

$$\begin{aligned} \mid \frac{\partial d}{\partial x} \mid &= \frac{\alpha}{l} \mid -a\frac{d}{dx}\mathrm{cn}^4(x) + b\frac{d}{dx}\mathrm{cn}^2(x) \mid \\ &\leq \frac{\alpha}{l} max(a,b)(\mid \frac{d}{dx}\mathrm{cn}^4(x) \mid + \mid \frac{d}{dx}\mathrm{cn}^2(x) \mid) \\ &\leq \frac{2\mathrm{K}(k)}{L_W} max(a,b)(4+2) \\ &\leq \frac{12\mathrm{K}(k)}{L_W} max(a,b) \end{aligned}$$

Since $a < 1$ m, $b < 1$ m, $\mathrm{K}(k) < 3$ as $k < 9$ and the order of wavelength is O(100) m, and the order of $\mid \frac{\partial d}{\partial x} \mid$ is O(0.1), the assumption used in deriving the plate equation Eq. 2.14 is again justified.

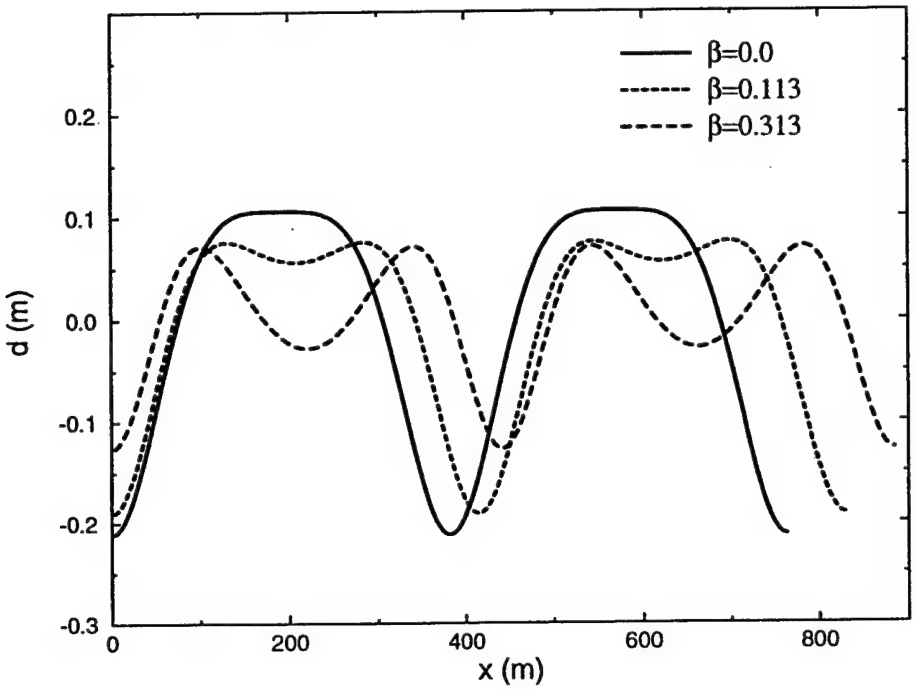

Figure 4.15: Profiles of the waves that can fracture the ice cover

4.3 Summary

In this chapter, a nonlinear analysis is carried out for the interaction of shallow water waves with a floating ice cover in a uniform channel. By retaining the nonlinear terms of order ε and δ (dimensionless wave amplitude and dimensionless ice cover stiffness), a nonlinear wave equation similar to the form of the Korteweg-de Vries (KdV) equation is obtained. The nonlinear periodic wave solutions similar to the cnoidal wave are derived for this nonlinear equation. The solution for a simplified form of this equation, neglecting the axial force and the ice inertia term, shows that the celerity of the shallow water wave is slightly reduced by the existence of the ice cover. The minimum wave height that is required to fracture the ice cover is typically in the range of 0.2 to 0.8 m, depending on the ice cover thickness and strength. The corresponding wavelength, i.e. the distance between the transverse cracks that formed by the propagating water waves, varies from 50 to 400 m. For typical ice cover conditions during the spring breakup period, the range is in the order of 50 to 150 m. These results agree closely with the existing field observations by Parkinson (1982), Gerard (1984), and Prowse (1986). The solution of the complete equation shows that the ice inertia term has an insignificant effect. However, an axial force could change the wave profile and reduce the wave height if the wavelength is fixed. Furthermore, the axial force reduces the minimum wave height that is required to cause ice cover fracture.

Chapter 5

Conclusions

In this study the interaction of shallow water waves with an ice cover in a river channel is analyzed using both linear and nonlinear theories. The linear analysis shows that the linear theory developed by Daly(1995), which neglected the effect of the axial force acting along the ice cover, is limited to small amplitude waves and can not be used to determined the condition for ice cover fracture. The inclusion of the axial force reduced the magnitude of the wave amplitude that is required to fracture an ice cover so that validity of the linear analysis is satisfied. However, the results obtained from the linear analysis do not agree with the existing field observations. A further analysis by including the nonlinear terms in the water wave equation is needed. In the nonlinear analysis, a nonlinear equation is obtained by retaining the first order terms in the nonlinear governing equations of the water wave and floating ice cover. The periodic wave solutions similar to cnoidal waves are obtained. These solutions show that the celerity of the water wave is slightly reduced by the ice cover. The minimum wave amplitude that is required to fracture the ice cover during the spring breakup period is in the order of 0.5 m. The corresponding wavelength, i.e. the spacing between transverse cracks induced by the water wave, is in the order of 50 to 150 m. These results agree closely with the existing field observations on the formation and propagation of breaking front in the field. This study provided a plausible explanation of the formation of the transverse cracks during the passage of a river wave, which is the key mechanism of the initiation of breakup ice runs and ice jams. Further field and laboratory studies should be carried out to validate the present finding.

Bibliography

[1] Abramowitz, M. and Stegun, I.A. (1972). *Handbook of Mathematical Functions*, U.S. Gover. Publications, New York.

[2] Beltaos, S. (1984). A conceptual model of river ice breakup, *Can. J. Civ. Engrg.*, 11(3): 516-529.

[3] Beltaos, S. (1985). Initial fracture patterns of river ice cover, *Contribution No 85-139*, Natural Water Research Institute, Burlington, Ontario, Canada.

[4] Beltaos, S. (1990). Fracture and breakup of river ice cover, *Can. J. Civ. Engrg.*, 17(2): 173-183.

[5] Beltaos, S. and Burrell, B. C. (1990). Restigouche river ice project, *Proc., 1990 Eastern Snow Conf.*, U.S. Army Cold Regions Research and Engineering Laboratory, Hanover N.H.: 159- 173.

[6] Billfalk, L. (1981). Formation of shore cracks in ice covers due to changes in water level, *Proc., IAHR Int. Symp. on Ice*, Quebec City, Quebec, Vol. II: 650-660.

[7] Billfalk, L. (1982). Breakup of solid ice covers due to rapid water level variations, *CRREL Rep. 82-3*, U.S. Army Cold Regions Research and Engineering Laboratory, Hanover, N.H.

[8] Byrd, P.F. and Friedman, M.D. (1971). *Handbook of Elliptic Integrals for Engineers and Scientists*, Springer-Verlag, New York

[9] Chaudhry, M. H. (1993) *Open-channel flow* , Prentice Hall, Englewood Cliffs, N.J.: 284-288

[10] Daly, S. F. (1993). Wave propagation in ice-covered channel, *J. Hydr. Engrg.*, ASCE, 119(8): 895-910.

[11] Daly, S. F.(1995). Fracture of river ice covers by river waves, *J. Hydr. Engrg.*, ASCE, 119(8): 41-52.

[12] Debnath, L. (1994). *Nonlinear Water Waves*, Academic Press, San Diego.

[13] Ferrick, M.G., Lemeiux, G., Mulherin, N., and Demont, W. (1986). Controlled river ice breakup, *Proc., IAHR Int'l Symp. on Ice*, V.III, Iowa City, Ia.: 281-305.

[14] Gerard, R., Kent, T. D., Janowicz, R., and Lyons, R. O. (1984). Ice regime reconnaissance, Yukon River, Yukon, *Cold Regions Engineering Specialty Conference, Edmonton, Alta.*, V.III: 1059-1073.

[15] Kerr, A.D. (1972). The continuously supported rail subjected to an axial force and a moving load, *Int. J. mech. Sci.*, Vol 14.

[16] Liu, L. Shen, H.T. Tuthill, A. (1998). A numerical model for river ice jam evolution, Vol. II, Proc., *14th IAHR International Symposium on Ice*, Potsdam, N.Y.

[17] Lawden, D.F. (1989). *Elliptic Functions and Applications*, Springer-Verlag, New York

[18] Mei, C.C. (1983). *The applied dynamics of ocean surface waves*, Wiley, New York.

[19] Pariset, E. and Hausser, R. (1966), Formation of ice covers and ice jams in rivers, *J. Hydr. Div.*, ASCE, NY6: 1-24.

[20] Parkinson, F.E. (1982), Water temperature observations during breakup on the Liard-Mackenzie river system, *Proceedings, Workshop on Hydraulics of Ice-Covered Rivers*, Edmonton, Alta., pp. 261-290

[21] Ponce, V.M., and Simons, D.B. (1977). Shallow wave propagation in open-channel flow, *J. Hydr. Div.*, ASCE, 103(12): 1461-1476.

[22] Prowse, T.D. (1986). Ice jam characteristic, Liard-Mackenzie river conference, *Canadian Journal of Civil Engineering* , 13(6): 653-665.

[23] Prowse, T.D. and Demuth, M.N. (1989). Failure modes observed during river ice breakup, *Proc., 46th Eastern Snow Conference*, Quebec City, Quebec: 237-241.

[24] Shen, et al. (1990). Dynamic transport of river ice, *J. Hydr. Res.*, 28(6), 659-671

[25] Shen, et. al (1993). Lagrangian discrete parcel simulation of river ice dynamics, *Int'l J. of Offshore and Polar Engrg.*, 3(4): 328-332.

[26] Shulyakovskii, L.G. (1972). On a model of breakup process, *Soviet Hydrology: Selected Papers*, Issue No. 1: 21-27.

[27] Skudrzyk, E. (1968). *Simple and Complex Vibratory Systems*, Pennsylvania State University Press, University Park.

[28] Steffler, R.M. and Hicks, E. F. (1994). Discussion of 'Wave propagation in ice-covered channels, *J. Hydr. Engrg.*, ASCE, 120(12): 1478-1480.

[29] Ugural, A.C. and Fenster, S.K. (1995). *Advanced strength of material and applied elasticity*, PRT Prentice Hall, Englewood Cliffs, NJ.

Appendix A

Notations

The following symbols are used in this report:

A = cross-sectional area of channel;

c = wave celerity;

$cn(x, k)$ =a Jocobian function;

d = depth of channel from bottom to ice cover;

d_0 = uniform flow depth;

d' = small perturbation to depth;

E = elastic modulus of ice;

E_W = fluid bulk modulus of elasticity;

F_r = channel Froude number;

g = acceleration of gravity;

H = piezomotric head;

H_0 = piezomotric head under uniform flow condition;

H' = perturbation to piezomotric head H_0;

I = moment of inertia of ice cover;

L = wavelength;

L_0 = longitudinal length scale;

L_w = nonlinear wave length ;

l = characteristic length of ice cover;

$l_0 = \frac{l}{L}$;

k = modulus of Jacobian functions;

$K(k)$ = complete elliptic integral of the first kind;

N = an axial force in ice cover;

$N_0 = \frac{N}{\rho g L_0^2}$, a nondimensional axial force;

P' = pressure deviation from hydrostatic beneath ice cover;

S_f = friction slope;

S_0 = channel bottom slope;

S_X = stress in ice cover;

T = wave period;

t = time;

u = mean flow velocity;

U = celerity of a nonlinear wave;

$\hat{U}$ = group velocity;

u_0 = mean flow velocity under steady flow;

u' =small perturbation to flow velocity;

x = longitudinal distance;

z = elevation of channel above datum;

α = nondimensional fluid bulk modulus;

β = nondimensional complex wave propagation factor;

β_I = imaginary part of propagation factor;

β_R = real part of propagation factor;

β^* = rescaled propagation factor;

δ = natural decrement; ice characteristic of ice stiffness

η = ice cover thickness;

η_0 = nondimensional ice cover thickness;

γ = nondimensional ice inertial;

$\lambda = \eta_0(\frac{d_0}{L_0})^2$;

ν = Poisson's ratio of ice cover;

ρ = fluid density;

ρ' = ice density;

σ = nondimensional wave number;

τ = average shear stress acting on bed and ice cover;

τ_0 = average shear stress under steady flow conditions; and

τ' = small perturbation to the average shear stress.

ε = small amplitude parameter.

Appendix B

Elliptical Functions

The detail of elliptical functions is available in books by Lawden (1989), Byrd and Friedman (1971) and others. A brief introduction to elliptic functions and theirs integrals is presented in this Appendix.

Consider the integral

$$x(y) = \int_0^y \frac{dt}{\sqrt{1 - k^2 \sin^2(t)}} \tag{B.1}$$

where the parameter k, is taken such that $0 \leq k \leq 1$. Eq. B.1 may be compared to

$$w(v) = \int_0^v \frac{dt}{\sqrt{1 - t^2}} \tag{B.2}$$

When we use $t = \sin(\theta)$ so that $w = \arcsin(v)$ or $v = \sin(w)$. This led Jacobi to define a new pair of inverse functions from Eq. B.1 as elliptic functions:

$$\mathrm{sn}(x, k) = \sin(y), \qquad \mathrm{cn}(x, k) = \cos(y) \tag{B.3}$$

where k is the modulus. In addition, a third elliptic function is defined as:

$$\mathrm{dn}(x, k) = \sqrt{1 - k^2 \sin^2(y)} \tag{B.4}$$

The period of $\mathrm{cn}(x, k)$ and $\mathrm{sn}(x, k)$ can be written as

$$\int_0^{2\pi} \frac{d\theta}{(1-k^2\sin^2\theta)^{\frac{1}{2}}} = 4\int_0^{\frac{\pi}{2}} \frac{d\theta}{(1-k^2\sin^2\theta)^{\frac{1}{2}}} \tag{B.5}$$

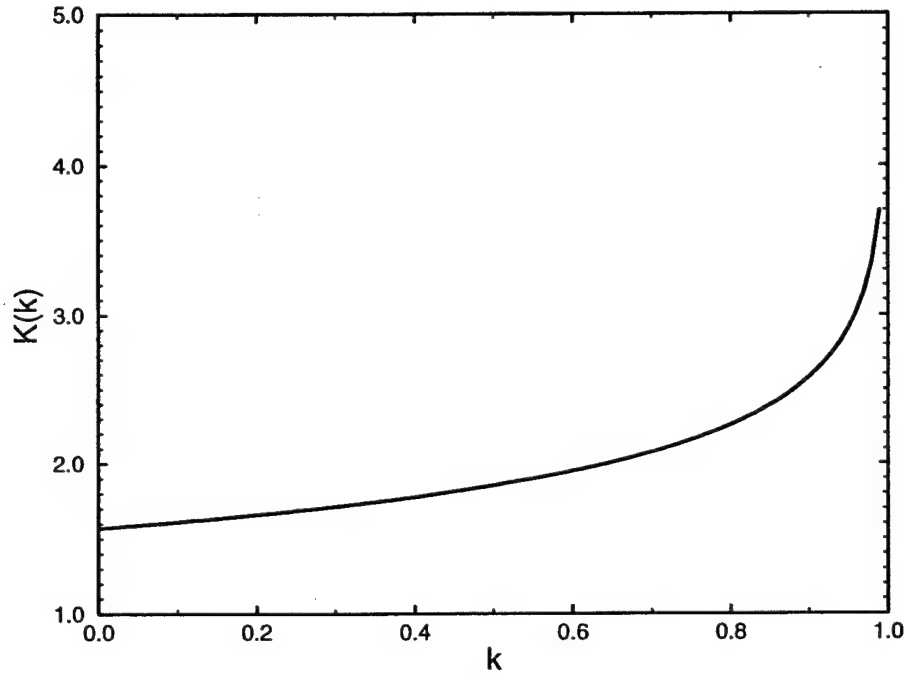

Figure B.1: The elliptic integral function of the first kind

The latter equation gives the complete elliptic integral of the first kind

$$\mathrm{K}(k) = \int_0^{\frac{\pi}{2}} \frac{d\theta}{(1-k^2\sin^2\theta)^{\frac{1}{2}}} \tag{B.6}$$

The values of $\mathrm{K}(k)$ in Fig. B.1 are available in a mathematical handbook, (Abramowitz and Stegun 1972).

The two special cases $k = 0$, and 1 enable integrals (B.1) and functions (B.3) to be reduced to elementary functions. If $k = 0$ then,

$$x = y, \qquad \mathrm{cn}(x,0) = \cos(\mathrm{y}) = \cos(x) \tag{B.7}$$

It is immediately clear that $\mathrm{K}(0) = \frac{\pi}{2}$. If $k = 1$ the integral can be evaluated to yield

$$x = \mathrm{arcsech}(\cos(y)), \qquad \mathrm{cn}(x,1) = \mathrm{sech}(x) \tag{B.8}$$

Both cn(x,k) and sn(x,k) are periodic functions for $0 \leq k < 1$.

The wavelength of $\mathrm{cn}(ax,k)$ is $4a^{-1}\mathrm{K}(k)$. The wavelength of cnoidal waves $\mathrm{cn}^2(ax,k)$, $\mathrm{cn}^4(ax,k)$ and $\mathrm{cn}^6(ax,k)$ are

$$2a^{-1}\mathrm{K}(k) \tag{B.9}$$

Using $\mathrm{cn}(x)$ as the abbreviation of $\mathrm{cn}(x,k)$, the following equations can easily be obtained from B.3 and B.4

$$\mathrm{sn}^2(x) + \mathrm{cn}^2(x) = 1 \tag{B.10}$$

$$\mathrm{dn}^2(x) + k^2\mathrm{sn}^2(x) = 1 \tag{B.11}$$

$$\mathrm{dn}^2(x) - k^2\mathrm{cn}^2(x) = 1 - k^2 \tag{B.12}$$

$$\frac{d}{dx}\mathrm{cn}(x) = \frac{dy}{dx}\frac{d}{dy}\mathrm{cn} = \sqrt{1 - k^2\sin^2(y)}\frac{d}{dy}\cos(y) \tag{B.13}$$

$$= -\mathrm{sn}(x)\mathrm{dn}(x) \tag{B.14}$$

$$\frac{d}{dx}\mathrm{sn}(x) = \mathrm{cn}(x)\mathrm{dn}(x) \tag{B.15}$$

$$\frac{d}{dx}\mathrm{dn}(x) = -k^2\mathrm{sn}(x)\mathrm{cn}(x) \tag{B.16}$$

Assuming

$$y(x) = \mathrm{cn}^2(x) \tag{B.17}$$

then

$$y'(x) = -2\mathrm{cn}(x)\mathrm{sn}(x)\mathrm{dn}(x) \tag{B.18}$$

$$y'^2(x) = 4\left((1-k^2)\mathrm{cn}^2(x) + (-1+2k^2)\mathrm{cn}^4(x) - k^2\mathrm{cn}^6\right) \quad \text{(B.19)}$$

$$\begin{aligned}\frac{d^2}{dx^2}\mathrm{cn}^2(x) &= 2\left(-\mathrm{cn}^2(x)\mathrm{dn}^2(x) + \mathrm{sn}^2(x)\mathrm{dn}^2(x) + k^2\mathrm{sn}^2(x)\mathrm{cn}^2(x)\right) \\ &= 2\left(-3k^2\mathrm{cn}^4(x) + (-2+4k^2)\mathrm{cn}^2(x) + 1 - k^2\right) \quad \text{(B.20)}\end{aligned}$$

$$\begin{aligned}y'''(x) &= 8[\mathrm{cn}(x)\mathrm{sn}(x)\mathrm{dn}^3(x) + k^2\,\mathrm{sn}(x)\mathrm{dn}(x)\mathrm{cn}^3(x) \\ &\quad -k^2\mathrm{cn}(x)\mathrm{dn}(x)\mathrm{sn}^3(x)] \quad \text{(B.21)}\end{aligned}$$

$$\begin{aligned}\frac{d^4}{dx^4}\mathrm{cn}^2(x) &= 8[15k^4\mathrm{cn}^6(x) + (-30k^4+15k^2)\mathrm{cn}^4(x) \\ &\quad +(17k^4-17k^2+2)\mathrm{cn}^2(x) + (-2k^4+3k^2-1)] \quad \text{(B.22)}\end{aligned}$$

$$\begin{aligned}\frac{d^2}{dx^2}\mathrm{cn}^4(x) &= \frac{d^2}{dx^2}y^2 \\ &= 2y'^2 + 2yy'' \\ &= -20k^2\mathrm{cn}^6(x) + 16(-1+2k^2)\mathrm{cn}^4(x) + 12(1-k^2)\mathrm{cn}^2(x) \quad \text{(B.23)}\end{aligned}$$

$$\begin{aligned}\frac{d^4}{dx^4}\mathrm{cn}^4(x) &= 6y''^2 + 8y'y''' + 2yy'''' \\ &= 840k^4\mathrm{cn}^8(x) + 1040(-2k^4+k^2)\mathrm{cn}^6(x) \\ &\quad +32(53k^4-53k^2+8)\mathrm{cn}^4(x) + 240(-2k^4 \\ &\quad +3k^2-1)\mathrm{cn}^2(x) + 24(1-k^2)^2 \quad \text{(B.24)}\end{aligned}$$

The complete integral of the second kind is denoted by E and is defined by

$$\mathrm{E}(k) = \int_0^{\mathrm{K}(k)} \mathrm{dn}^2 u\,du = \int_0^{\frac{\pi}{2}} (1-k^2\sin^2\theta)^{\frac{1}{2}}\,d\theta \quad \text{(B.25)}$$

The values of $\mathrm{E}(k)$ are available in (Abramowitz and Stegun 1972). Some special relations and values are listed as following:

$$\mathrm{sn}(0,k) = 0 \quad \text{(B.26)}$$

$$\mathrm{sn}(u+2\mathrm{K}(k),k) = -\mathrm{sn}(u,k) \quad \text{(B.27)}$$

$$\mathrm{cn}(0,k) = 1 \quad \text{(B.28)}$$

$$\mathrm{cn}(u+2\mathrm{K}(k),k) = -\mathrm{cn}(u,k) \quad \text{(B.29)}$$

$$\int_0^{2\mathrm{K}(k)} \mathrm{dn}^2(x,k)\,dx = 2\mathrm{E}(k) \quad \text{(B.30)}$$

$$\int_0^{2\mathrm{K}(k)} \mathrm{cn}^2(x,k)\,dx = \int_0^{2\mathrm{K}(k)} \left(\frac{1}{k^2}\mathrm{dn}^2(x,k) - \frac{1-k^2}{k^2}\right)dx$$

$$= \frac{2\mathrm{E}(k)}{k^2} - \frac{1-k^2}{k^2}2\mathrm{K}(k) \tag{B.31}$$

$$\begin{aligned}\int_0^{2\mathrm{K}(k)} \mathrm{cn}^4(x,k)dx &= \int_0^{2\mathrm{K}(k)} (\frac{2(2k^2-1)}{3k^2}\mathrm{cn}^2(x,k) + \frac{1-k^2}{3k^2} \\ &\quad -\frac{1}{6k^2}\frac{d^2}{dx^2}\mathrm{cn}^2(x,k))dx \\ &= \frac{2(2k^2-1)}{3k^2}\int_0^{2\mathrm{K}(k)} \mathrm{cn}^2(x,k)dx + \frac{1-k^2}{3k^2}2\mathrm{K}(k) \\ &\quad -\frac{1}{6k^2}(-2\mathrm{cn}(x,k)\mathrm{sn}(x,k)\ \mathrm{dn}(x,k))\ |_0^{2\mathrm{K}(k)} \\ &= \frac{2(2k^2-1)}{3k^2}\int_0^{2\mathrm{K}(k)} \mathrm{cn}^2(x,k)dx + \frac{1-k^2}{3k^2}2\mathrm{K}(k) \end{aligned} \tag{B.32}$$

Eq. B.18 yields

$$|\ \frac{d\mathrm{cn}^2(x)}{dx}\ | \leq 2 \tag{B.33}$$

$$|\ \frac{d\mathrm{cn}^4(x)}{dx}\ | = |\ 2\mathrm{cn}^2(x)\frac{d\mathrm{cn}^2(x)}{dx}\ | \leq 4 \tag{B.34}$$

To order to check Eq. B.24, The two special cases i.e $k = 0$ and $k = 1$ are considered.

$$\frac{d^4}{dx^4}\mathrm{cn}^4(x,0) = 256\mathrm{cn}^4(x,0) + (-240)\mathrm{cn}^2(x,0) + 24 \tag{B.35}$$

$$\frac{d^4}{dx^4}\mathrm{cn}^4(x,1) = 840\mathrm{cn}^8(x,1) + (-1040)\mathrm{cn}^6(x,1) + 256\mathrm{cn}^4(x,1) \tag{B.36}$$

Also, we can obtain from the MAPLE 4:

$$\begin{aligned}\frac{d^4}{dx^4}\cos^4(x) &= 24\sin^4(x) - 192\cos^2(x) + 40\cos^4(x) \\ &= 256\cos^4(x) + (-240)\cos^2(x) + 24 \end{aligned} \tag{B.37}$$

$$\begin{aligned}\frac{d^4}{dx^4}\mathrm{sech}^4(x) &= 256\mathrm{sech}^4(x)\tanh^4(x) - 528\mathrm{sech}^4(x)\tanh^2(x)(1-\tanh^2(x)) \\ &\quad +56\ \mathrm{sech}^4(x)(1-\tanh^2(x))^2 \\ &= 256\mathrm{sech}^4(x)(1-\mathrm{sech}^2(x))^2 \\ &\quad -528\mathrm{sech}^4(x)\mathrm{sech}^6(x)(1-\mathrm{sech}^2(x)) + 56\mathrm{sech}^8(x) \\ &= 840\mathrm{sech}^8(x) + (-1040)\mathrm{sech}^6(x) + 256\mathrm{sech}^4(x) \end{aligned} \tag{B.38}$$

Therefore,

$$\frac{d^4}{dx^4}\text{sech}^4(x) = \frac{d^4}{dx^4}\text{cn}^4(x,1) \tag{B.39}$$

$$\frac{d^4}{dx^4}\cos^4(x) = \frac{d^4}{dx^4}\text{cn}^4(x,0) \tag{B.40}$$

Appendix C

Figures in Linearized Models

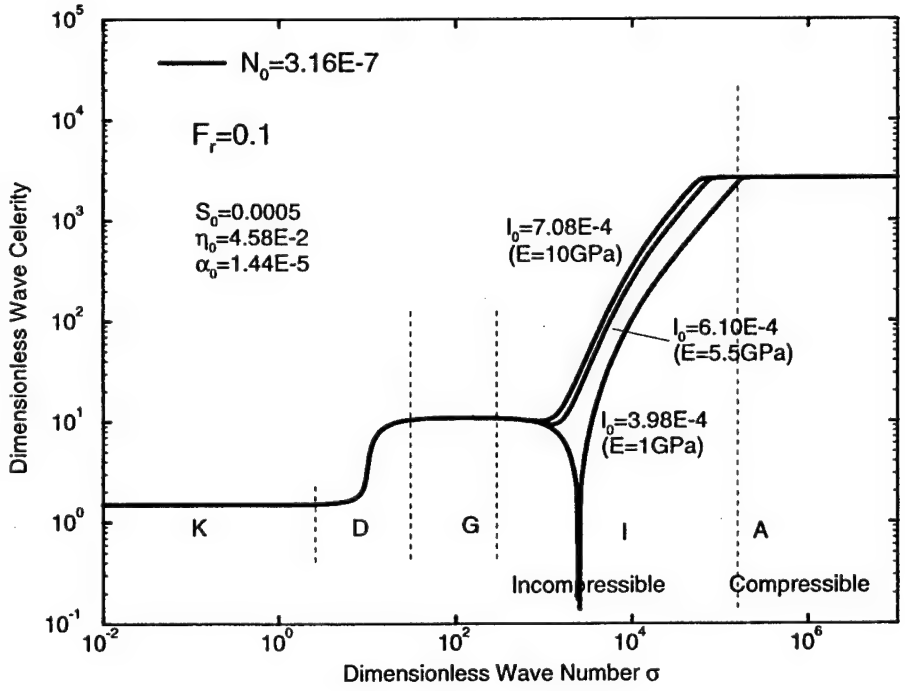

Figure C.1: Effect of elastic modulus on the influence of axial force on wave celerity

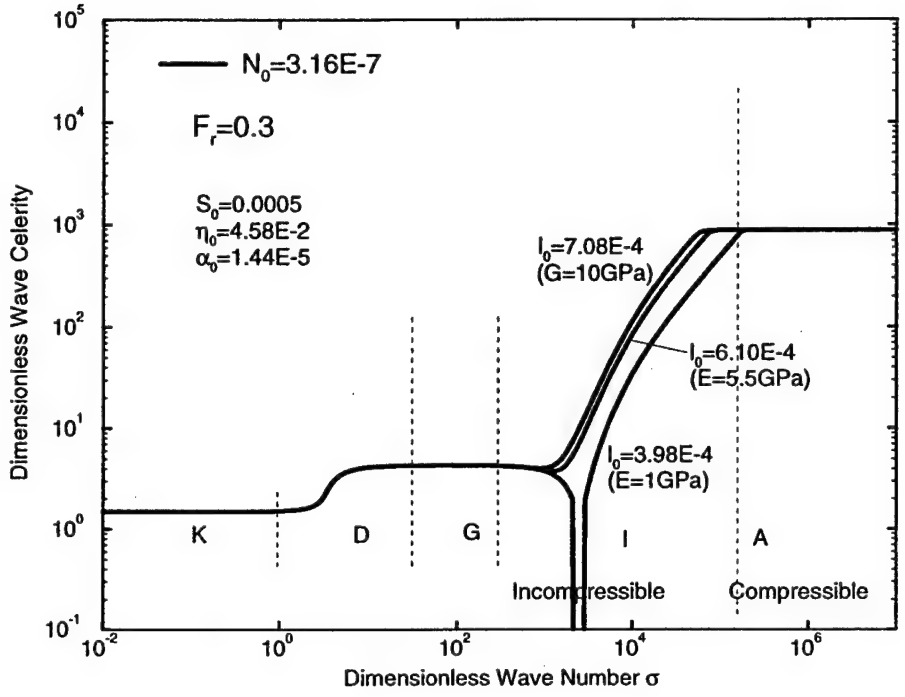

Figure C.2: Effect of elastic modulus on the influence of axial force on wave celerity

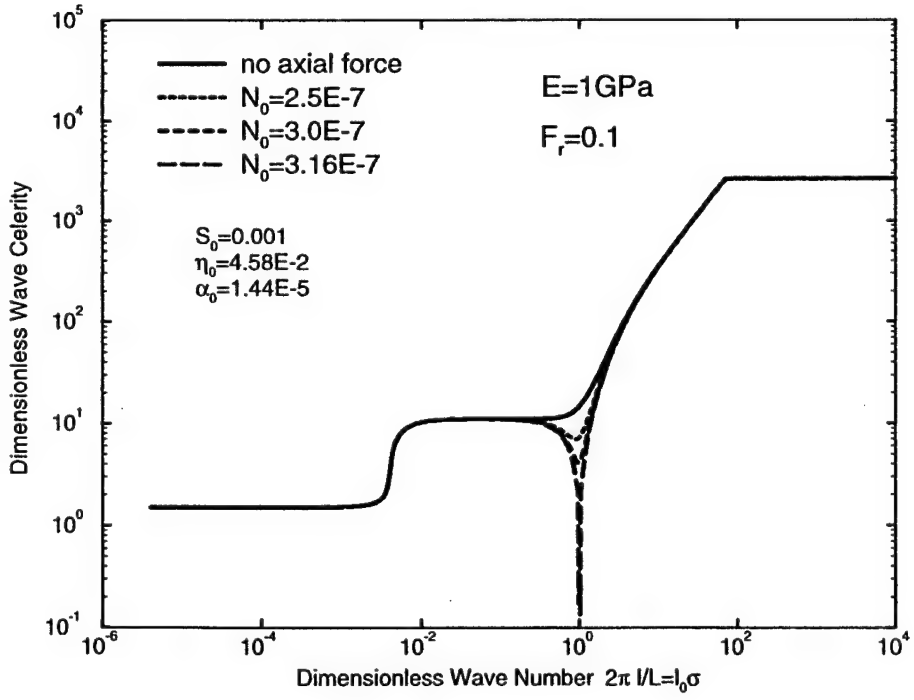

Figure C.3: Effect of the magnitude of the axial force on wave celerity

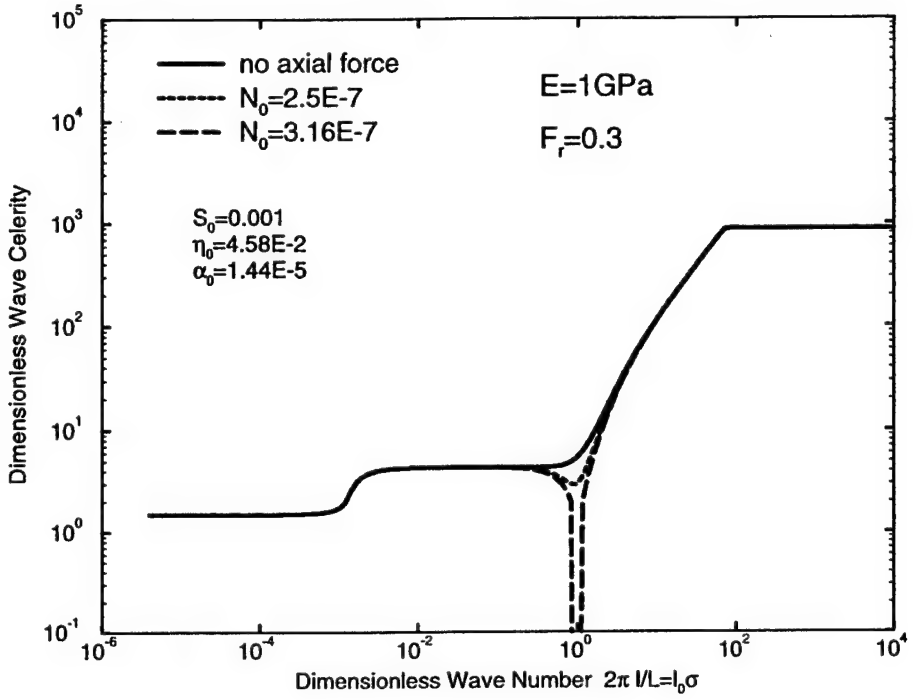

Figure C.4: Effect of the magnitude of the axial force on wave celerity

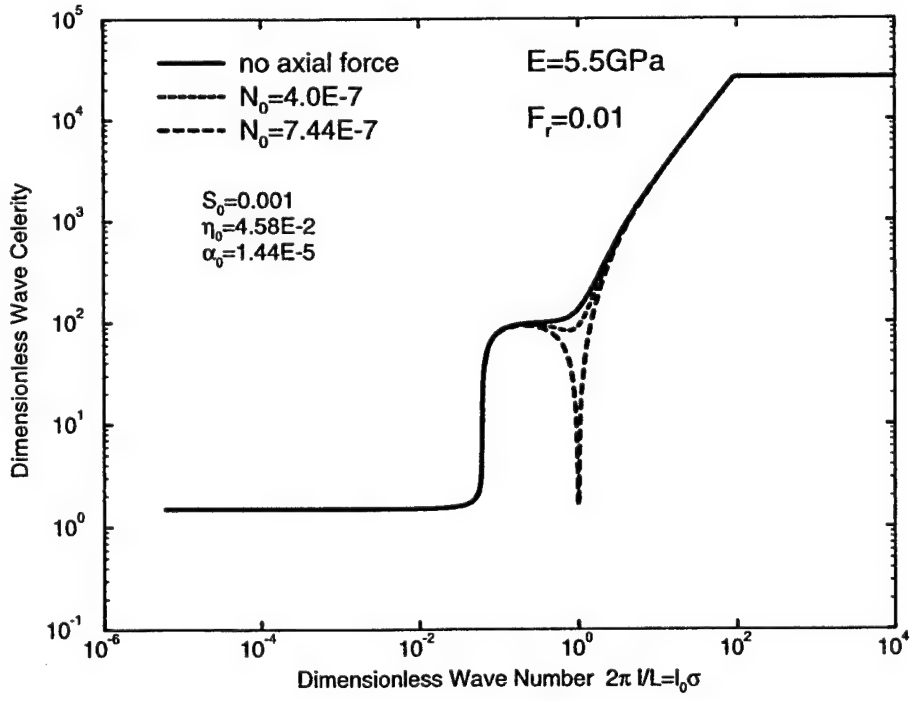

Figure C.5: Effect of the magnitude of the axial force on wave celerity

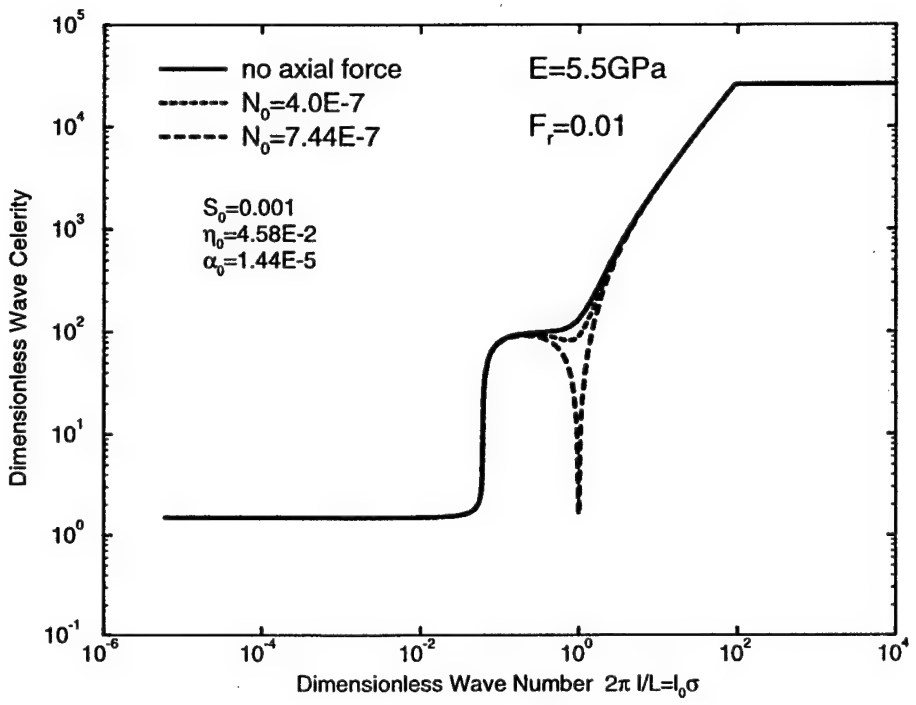

Figure C.6: Effect of the magnitude of the axial force on wave celerity

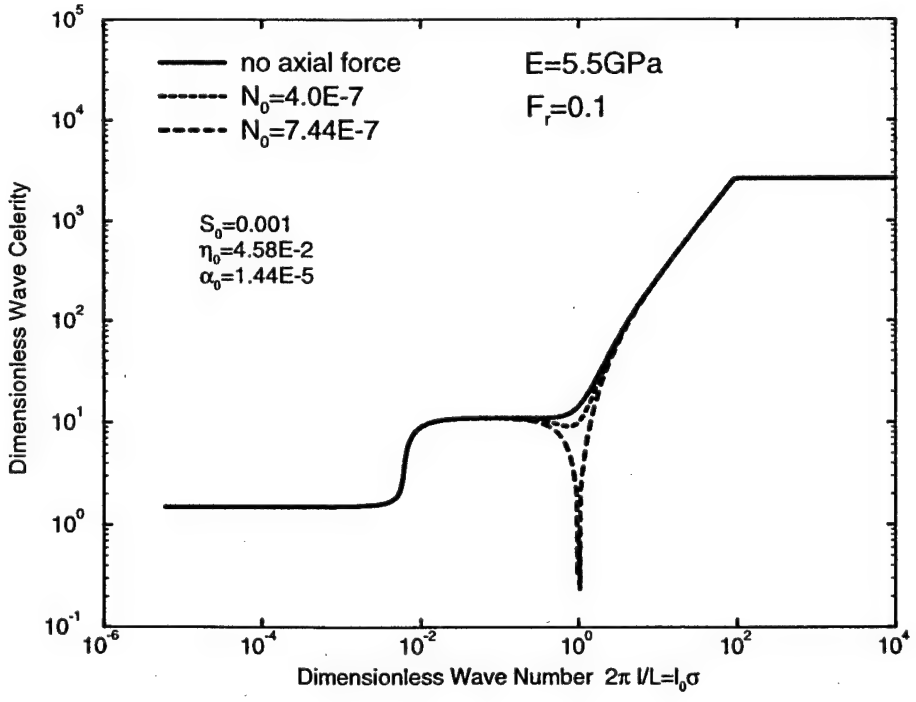

Figure C.7: Effect of the magnitude of the axial force on wave celerity

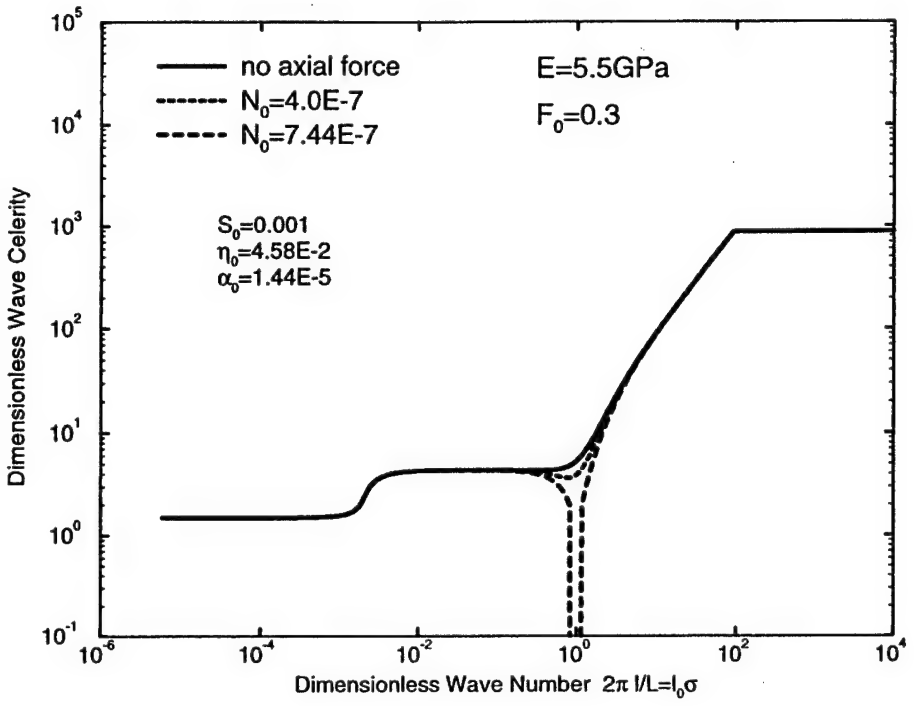

Figure C.8: Effect of the magnitude of the axial force on wave celerity

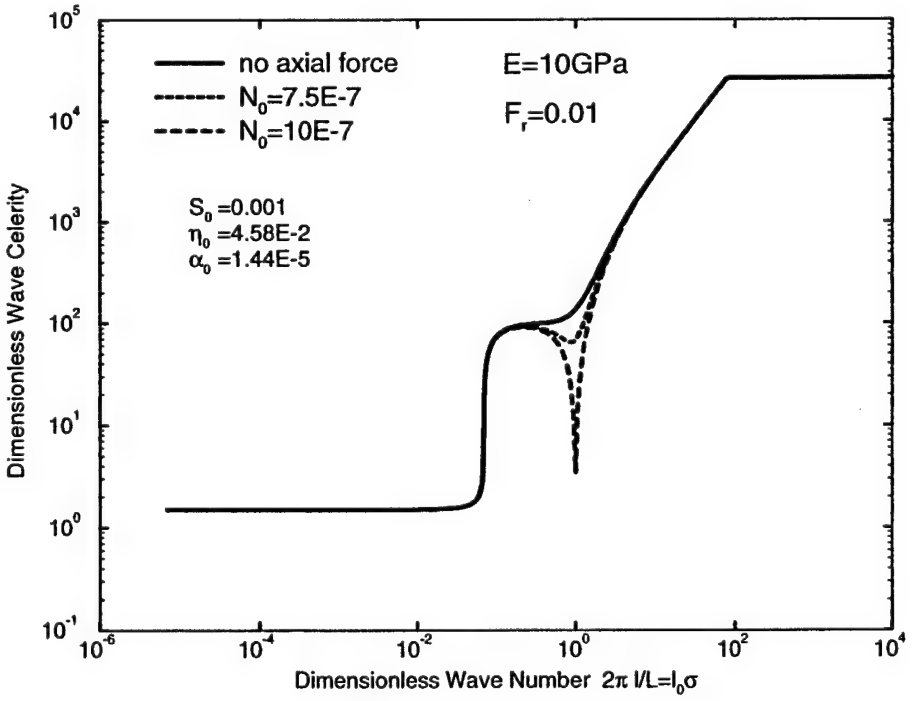

Figure C.9: Effect of the magnitude of the axial force on wave celerity

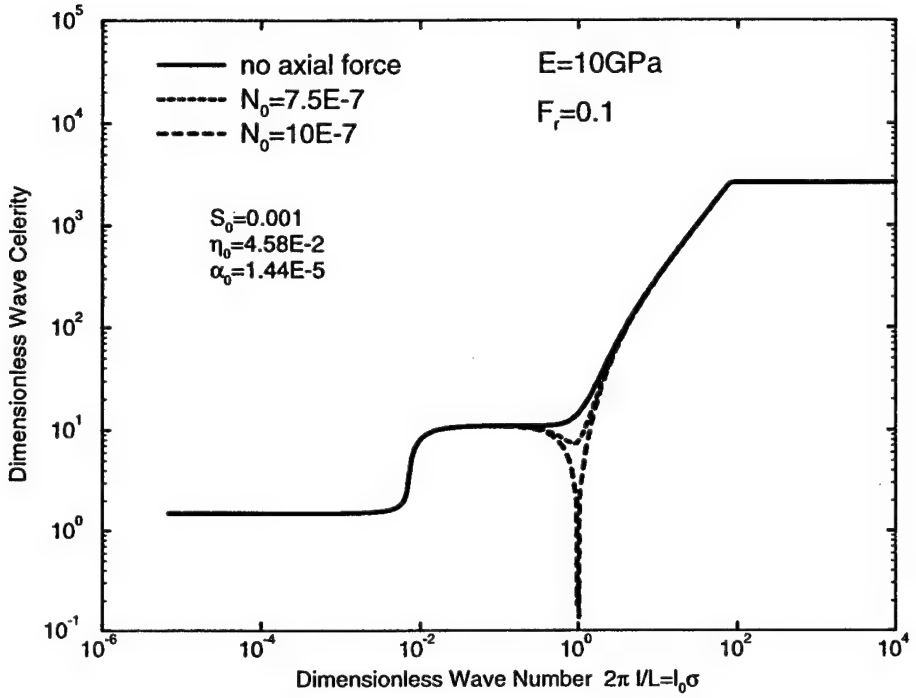

Figure C.10: Effect of the magnitude of the axial force on wave celerity

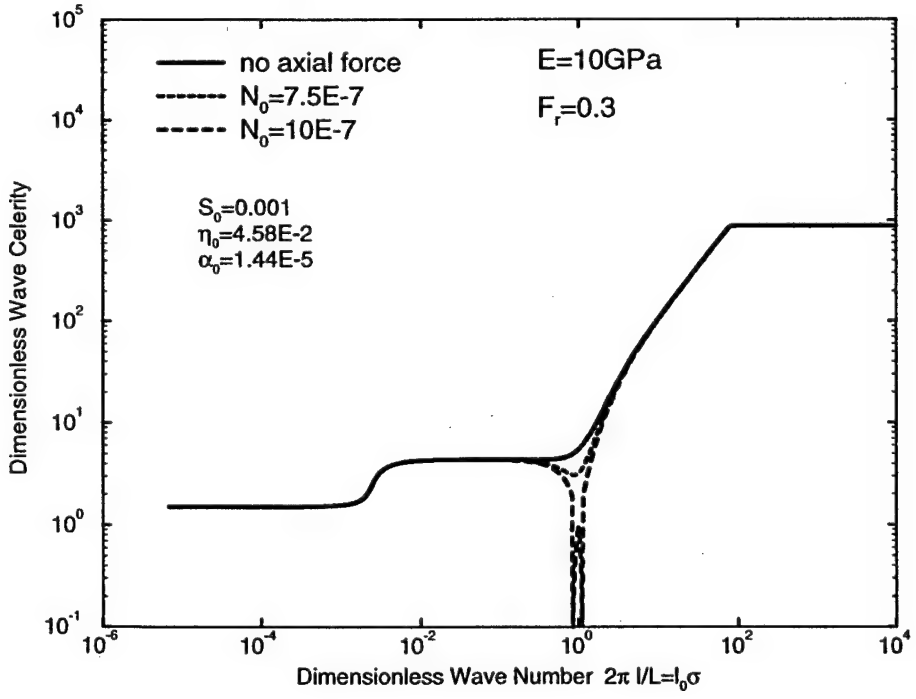

Figure C.11: Effect of the magnitude of the axial force on wave celerity

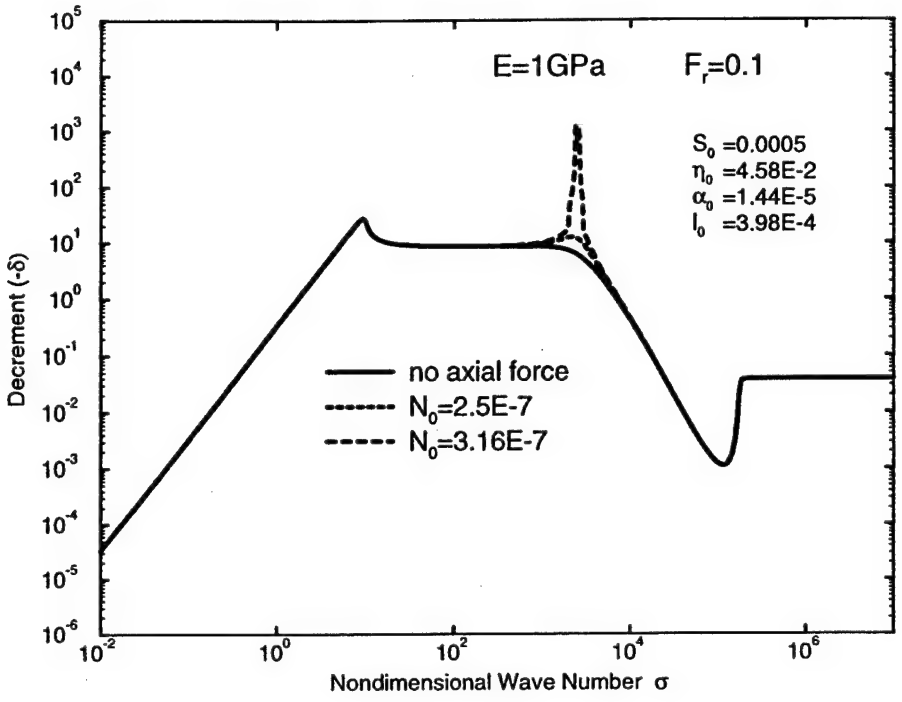

Figure C.12: Effect of axial forces on natural decrement

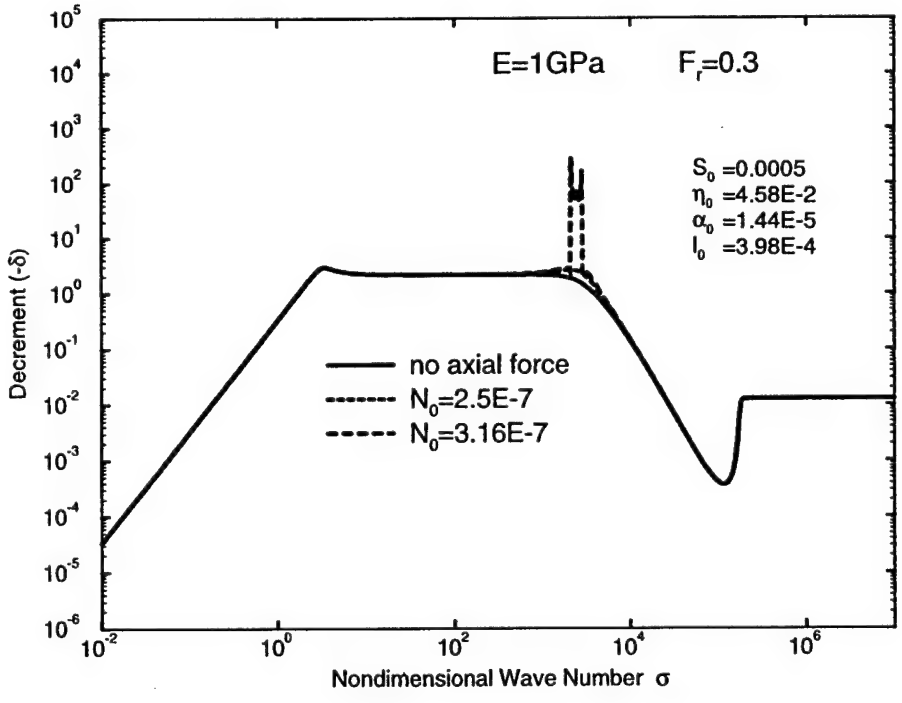

Figure C.13: Effect of axial forces on natural decrement

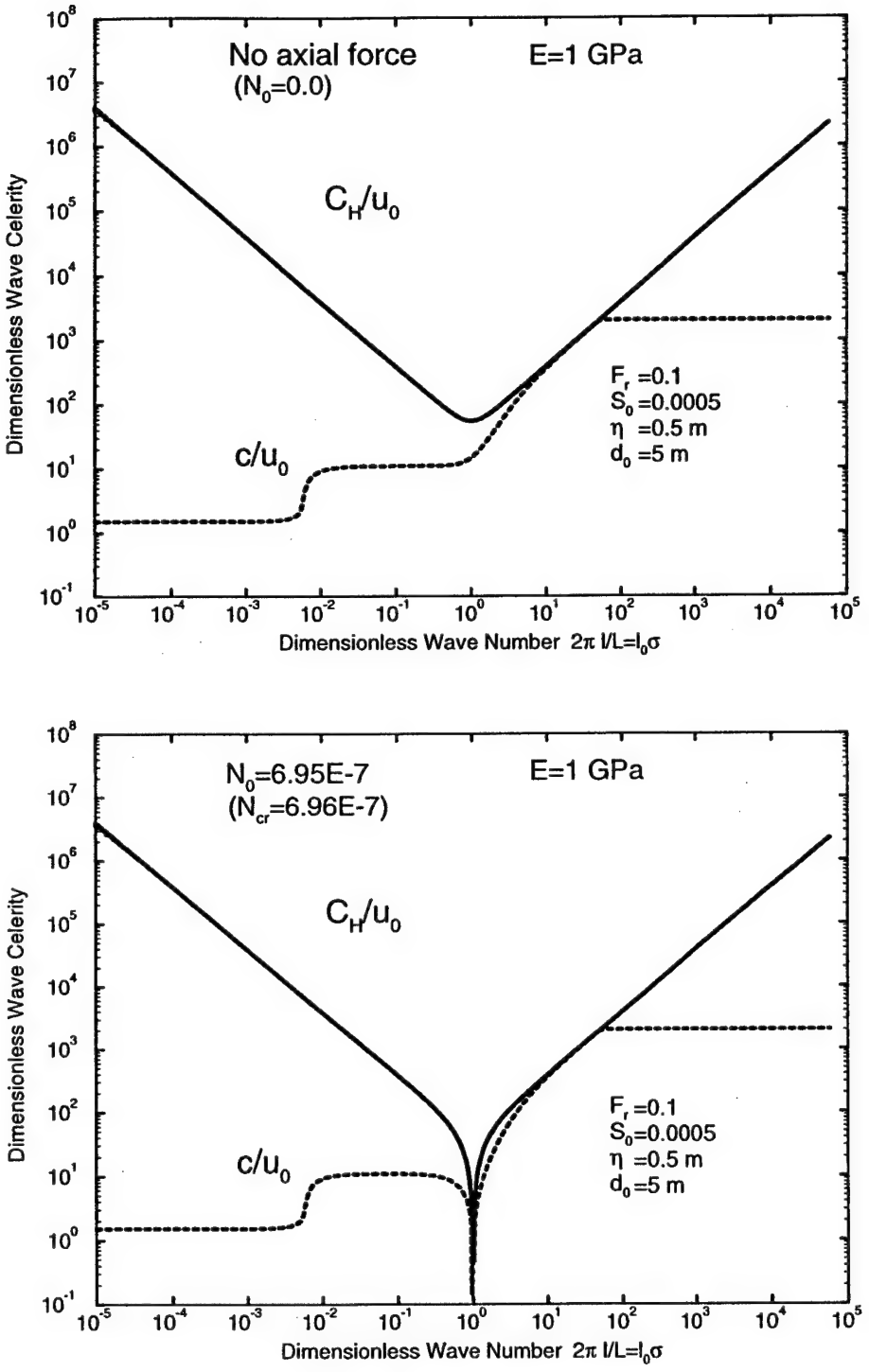

Figure C.14: Dimensionless free-wave celerity C_H and dimensionless wave celerity $\hat{c}$ in ice-covered channel as functions of dimensionless wave number

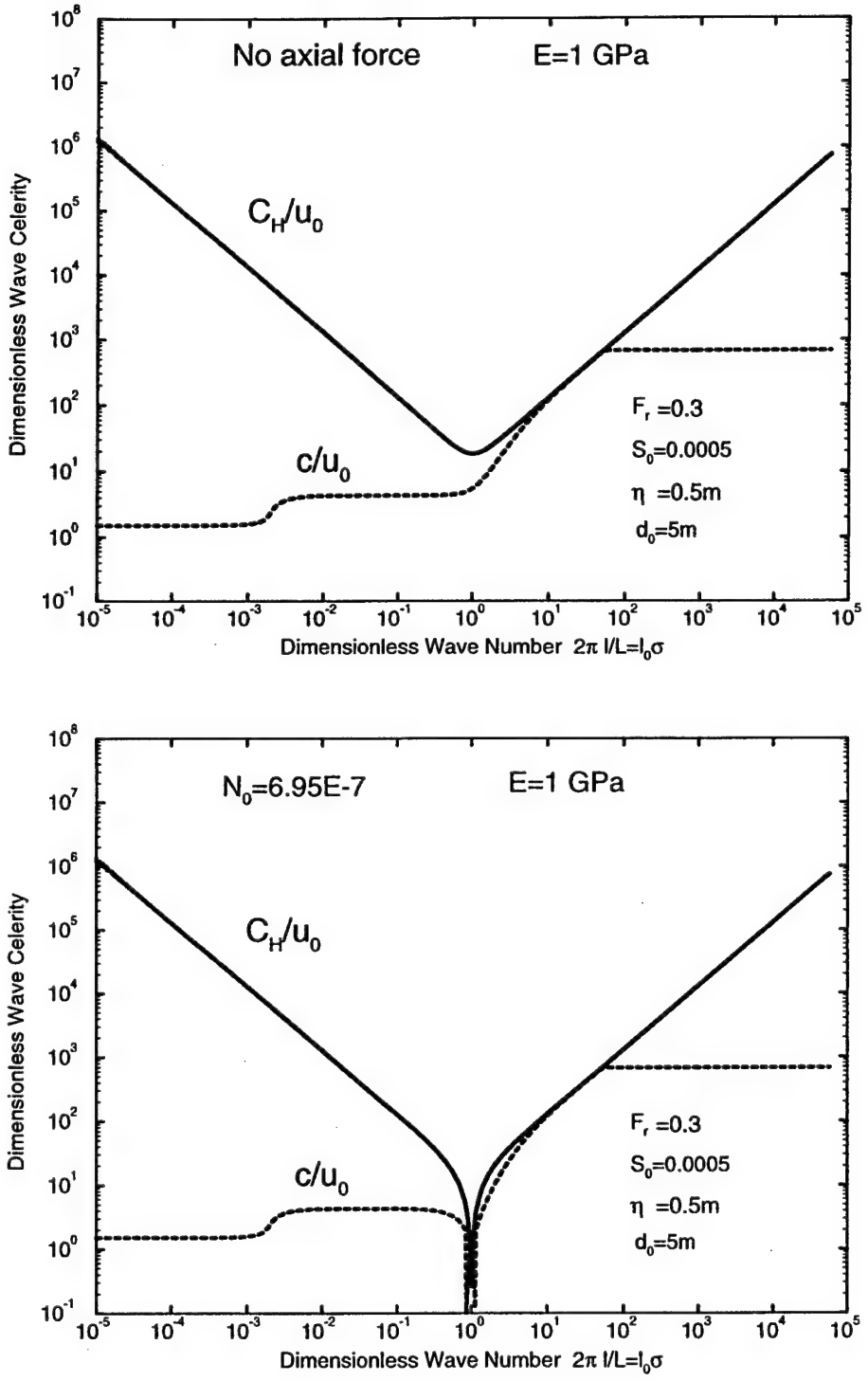

Figure C.15: Dimensionless free-wave celerity C_H and dimensionless wave celerity $\hat{c}$ in ice-covered channel as functions of dimensionless wave number

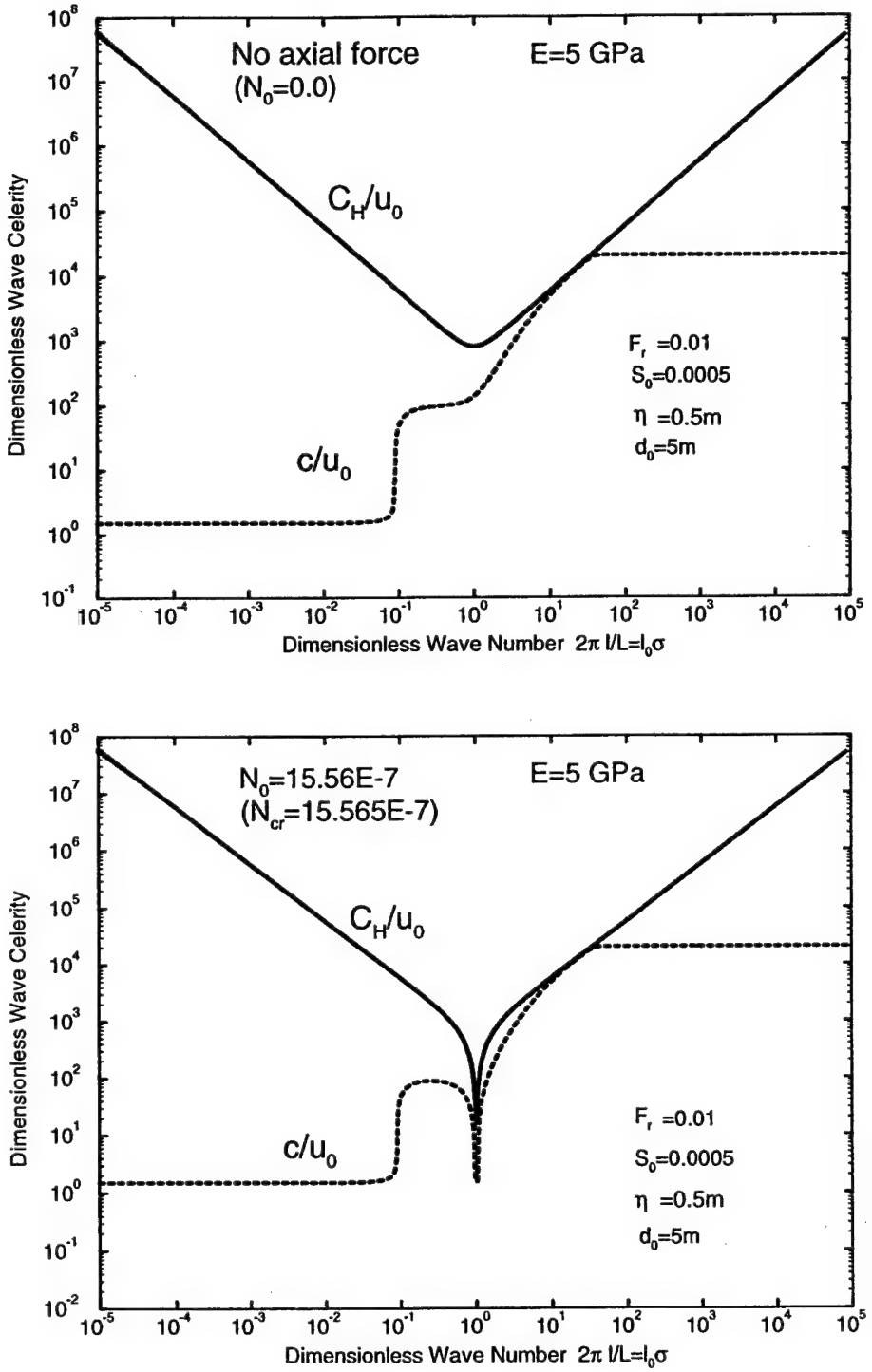

Figure C.16: Dimensionless free-wave celerity C_H and dimensionless wave celerity $\hat{c}$ in ice-covered channel as functions of dimensionless wave number

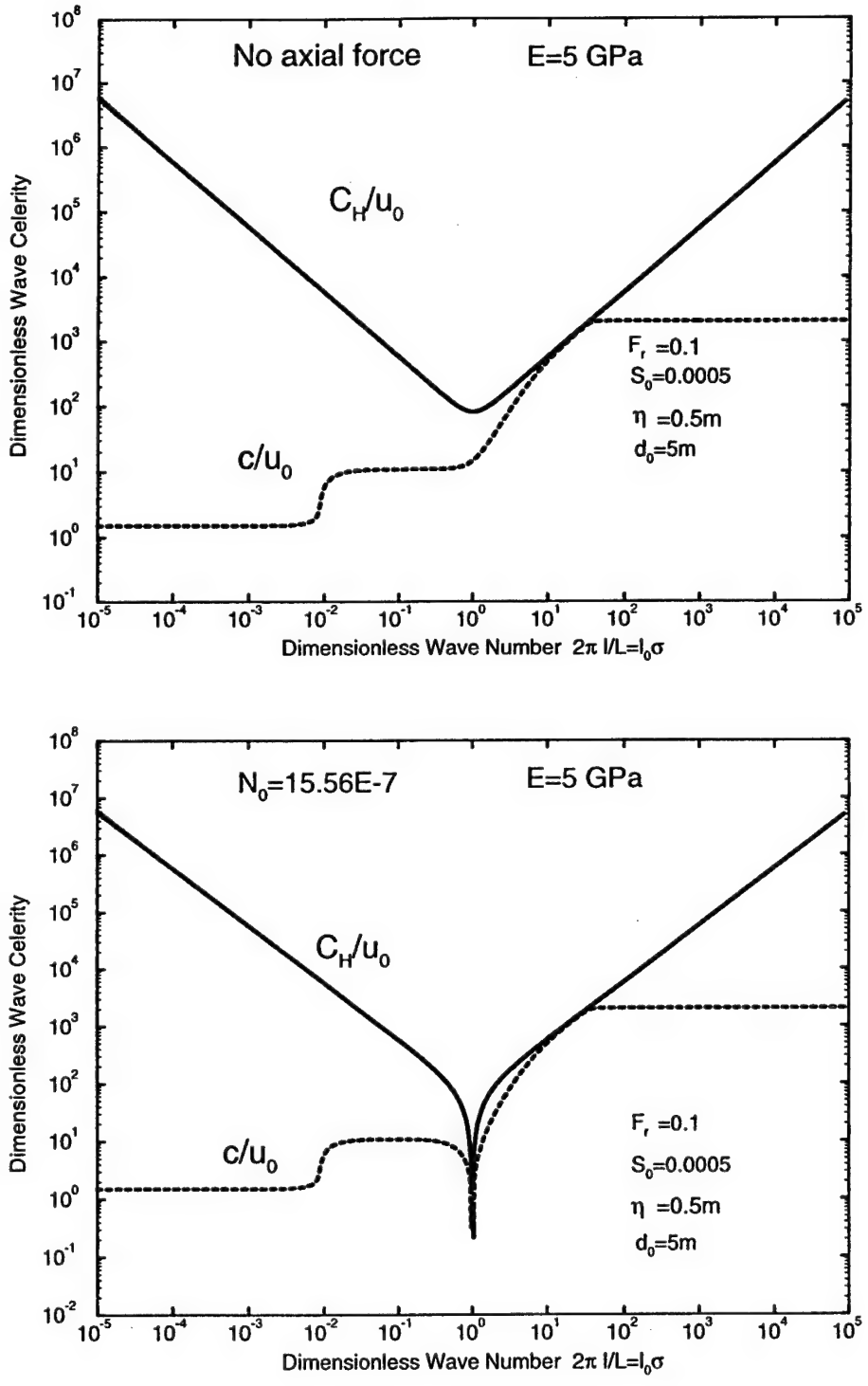

Figure C.17: Dimensionless free-wave celerity C_H and dimensionless wave celerity $\hat{c}$ in ice-covered channel as functions of dimensionless wave number

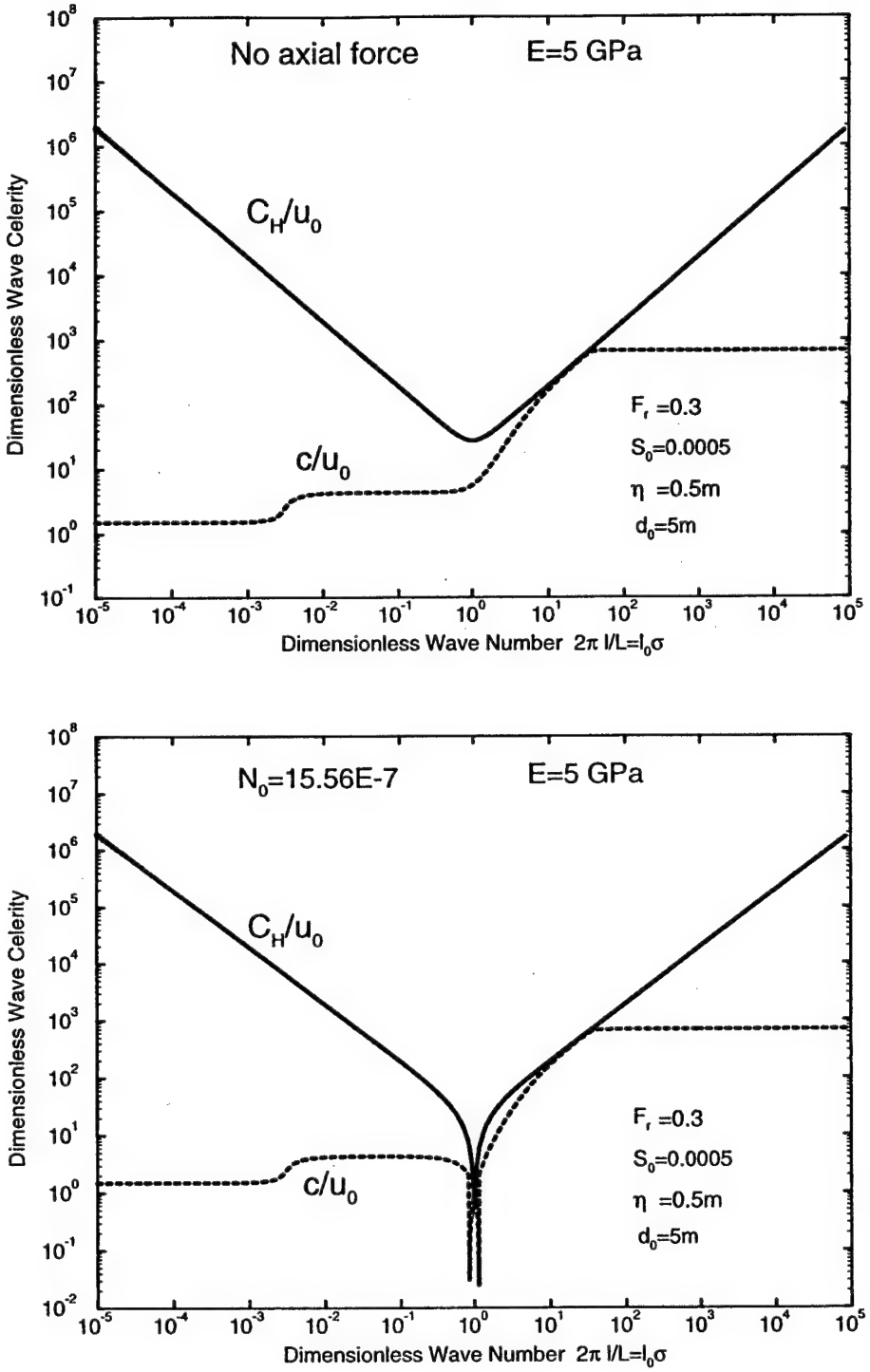

Figure C.18: Dimensionless free-wave celerity C_H and dimensionless wave celerity $\hat{c}$ in ice-covered channel as functions of dimensionless wave number

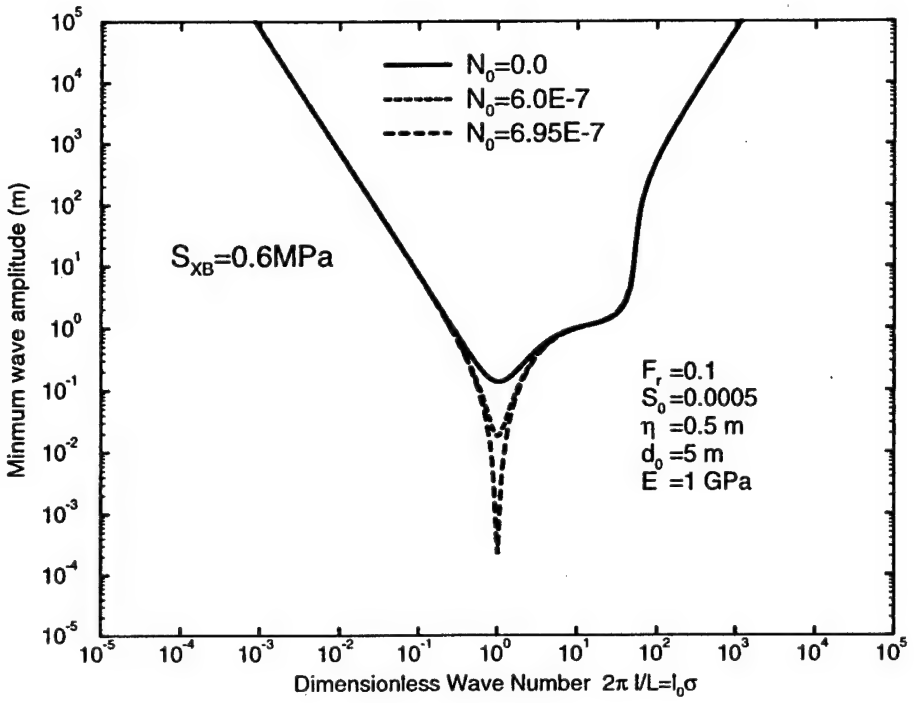

Figure C.19: Minimum wave amplitude (m) required to fail an ice cover of 0.5 thick

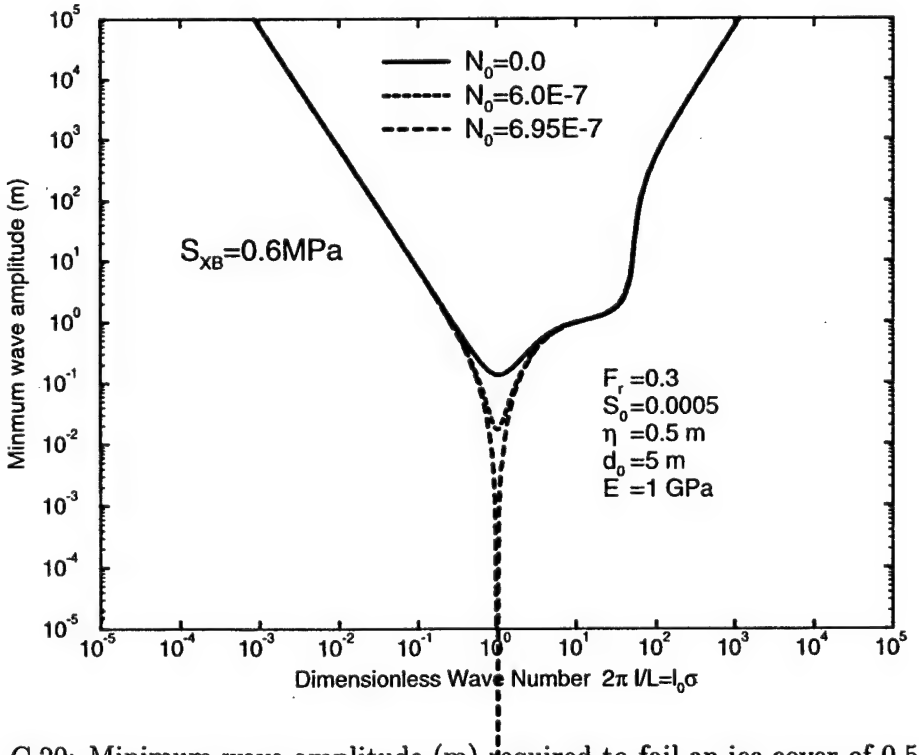

Figure C.20: Minimum wave amplitude (m) required to fail an ice cover of 0.5 thick

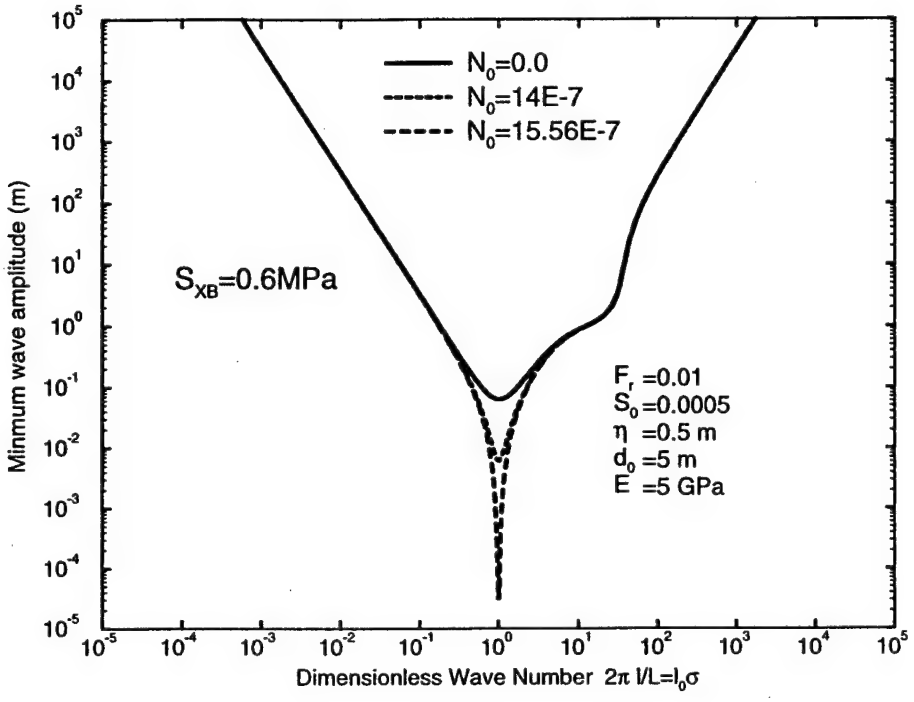

Figure C.21: Minimum wave amplitude (m) required to fail an ice cover of 0.5 thick

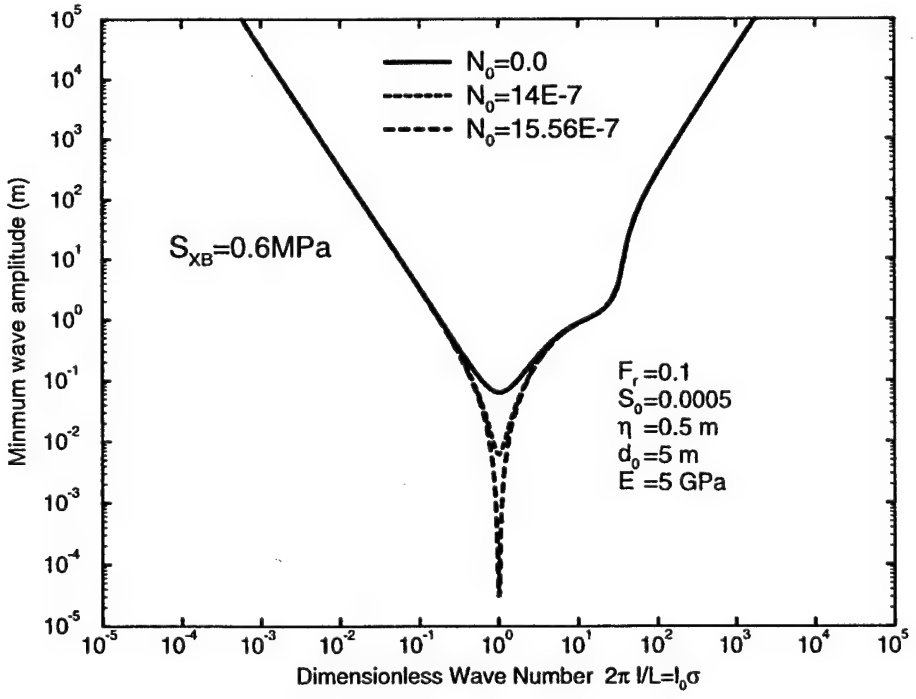

Figure C.22: Minimum wave amplitude (m) required to fail an ice cover of 0.5 thick

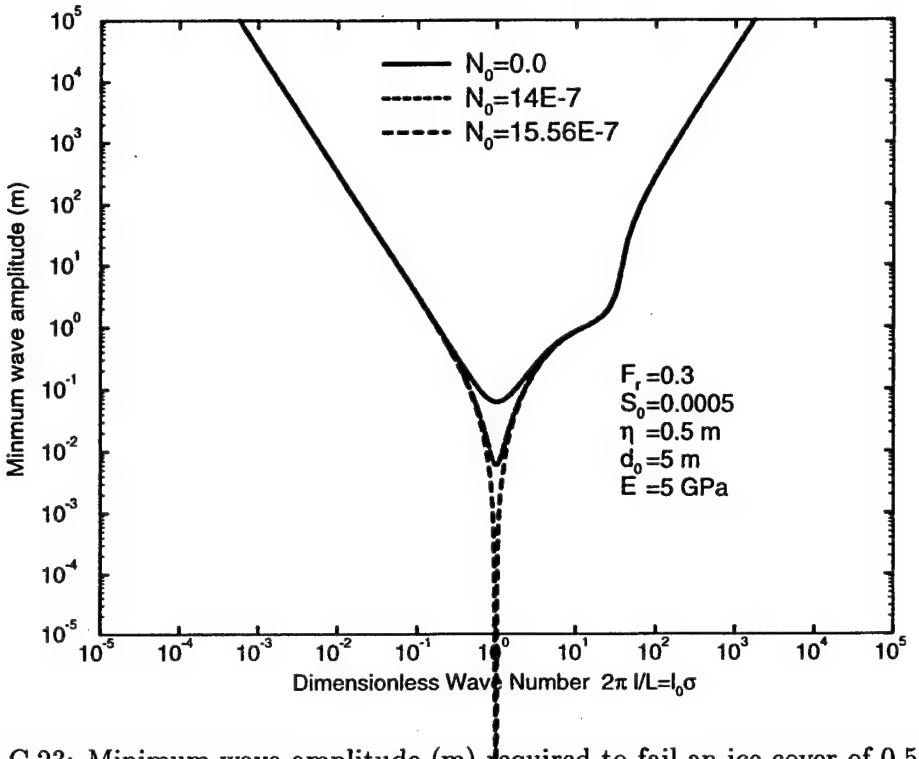

Figure C.23: Minimum wave amplitude (m) required to fail an ice cover of 0.5 thick

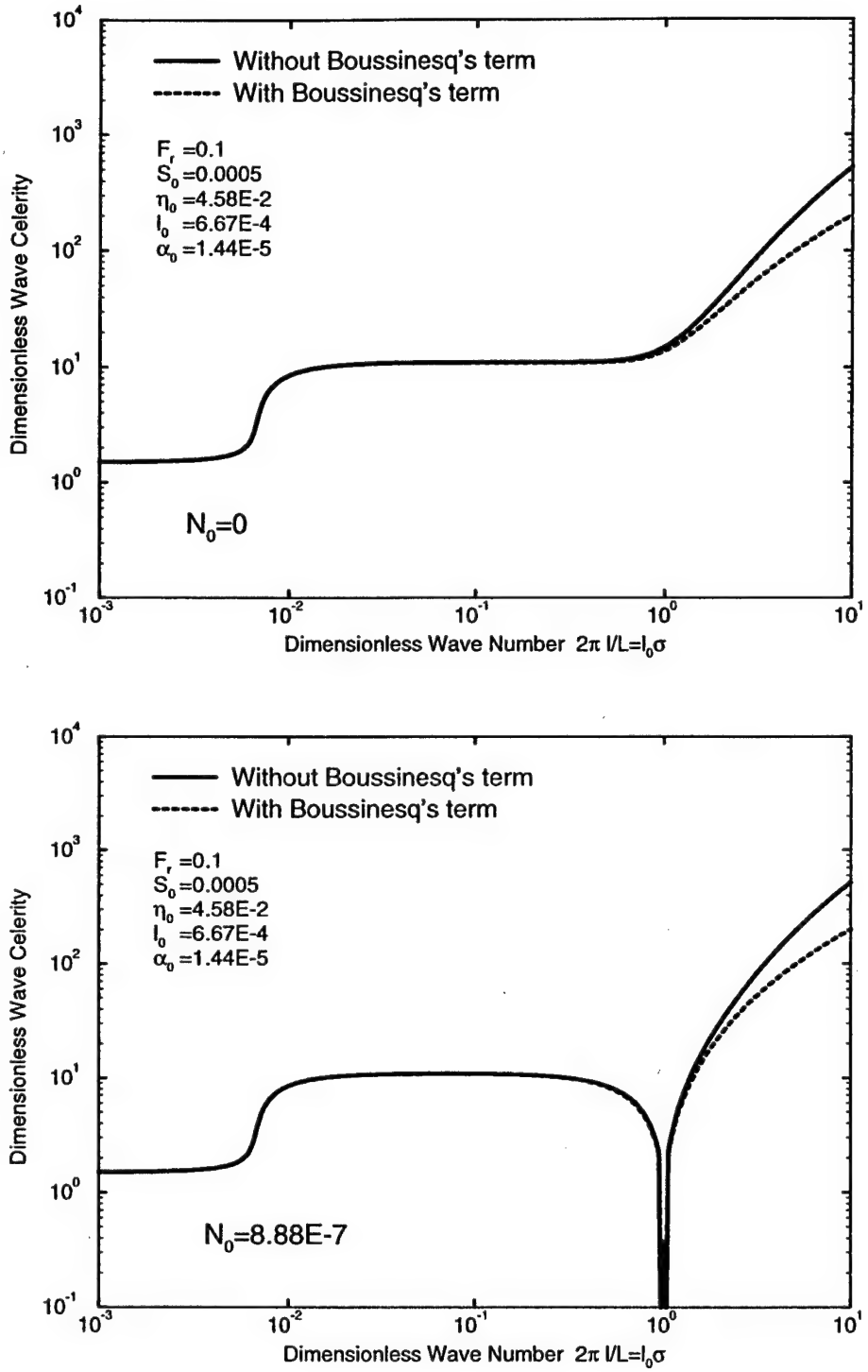

Figure C.24: (a)Effect of Boussinesq's term: without axial force; (b) with an axial force.

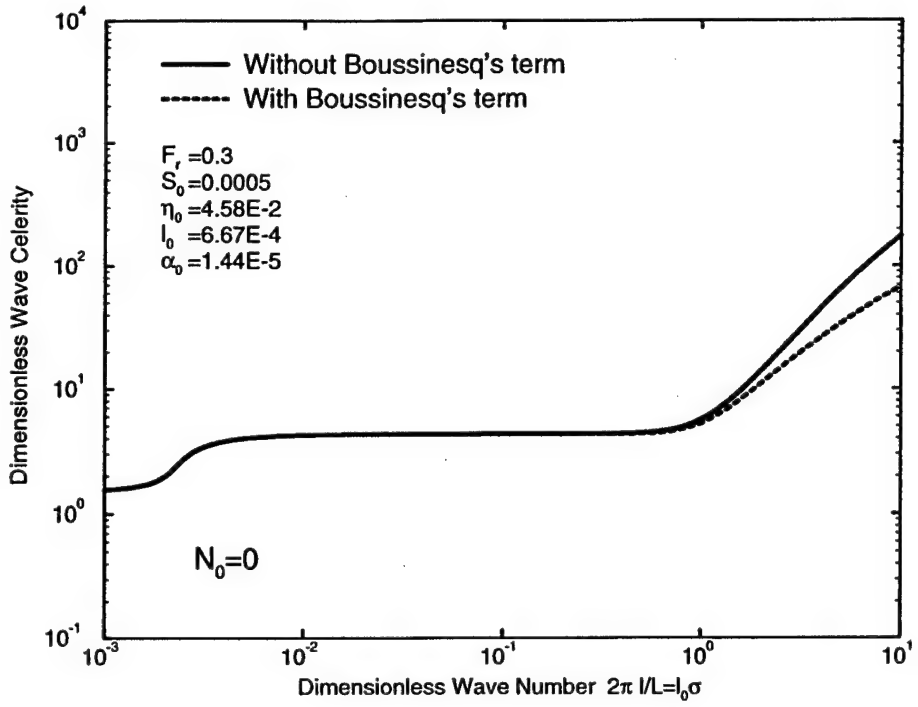

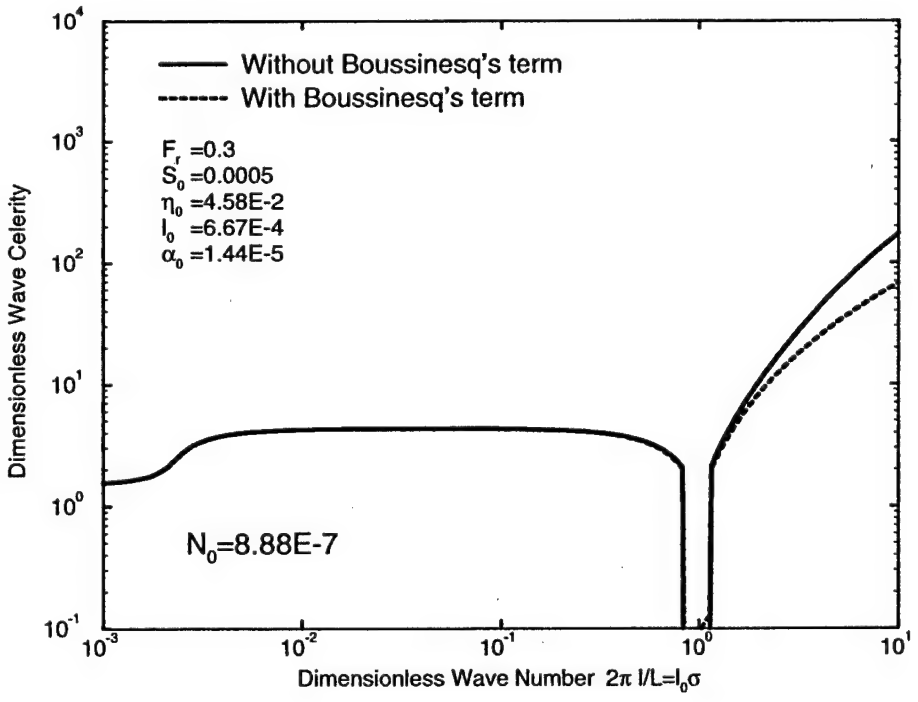

Figure C.25: (a)Effect of Boussinesq's term: without axial force; (b) with an axial force.

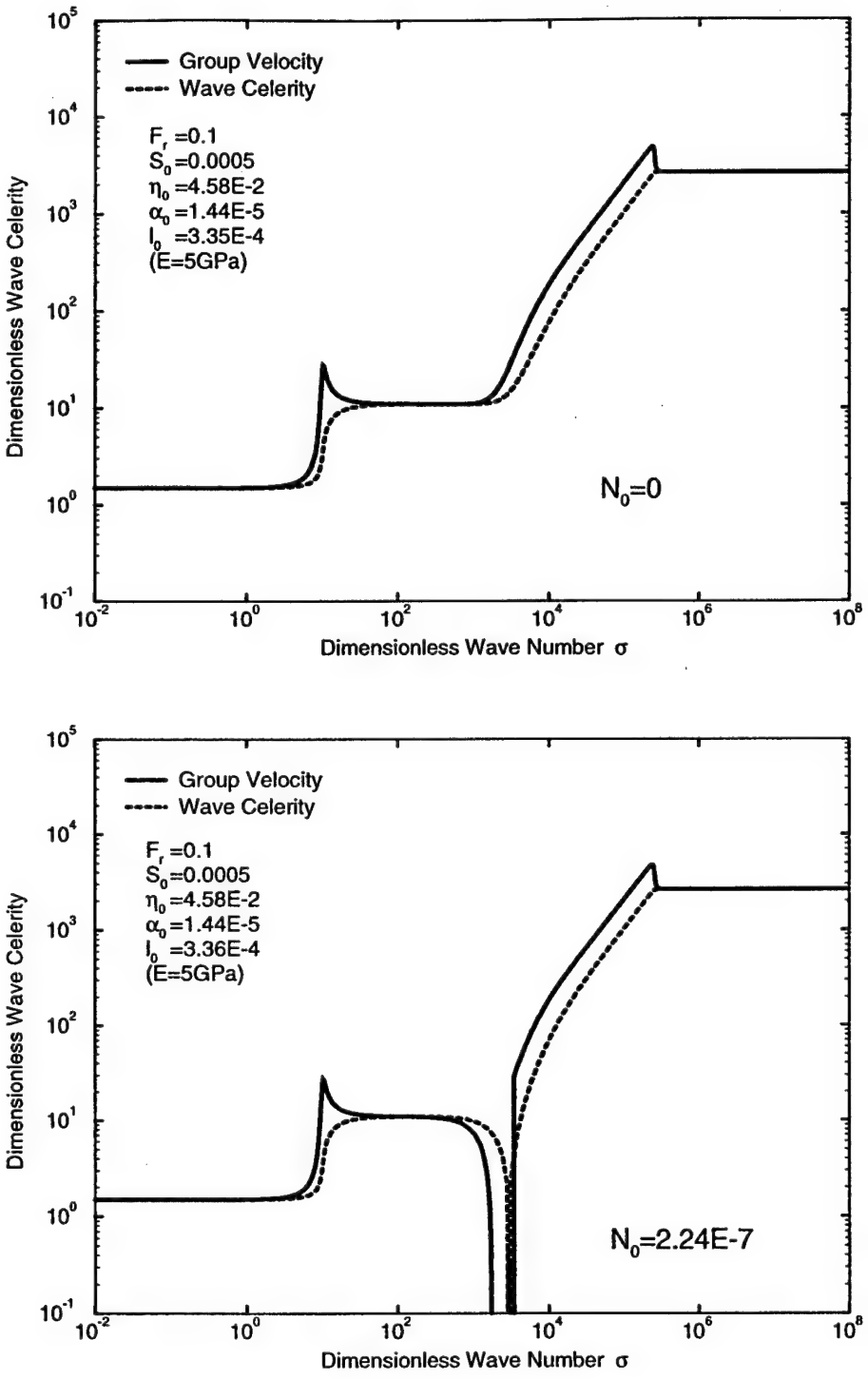

Figure C.26: Dimensionless wave celerity and group velocity as functions of dimensionless wave number

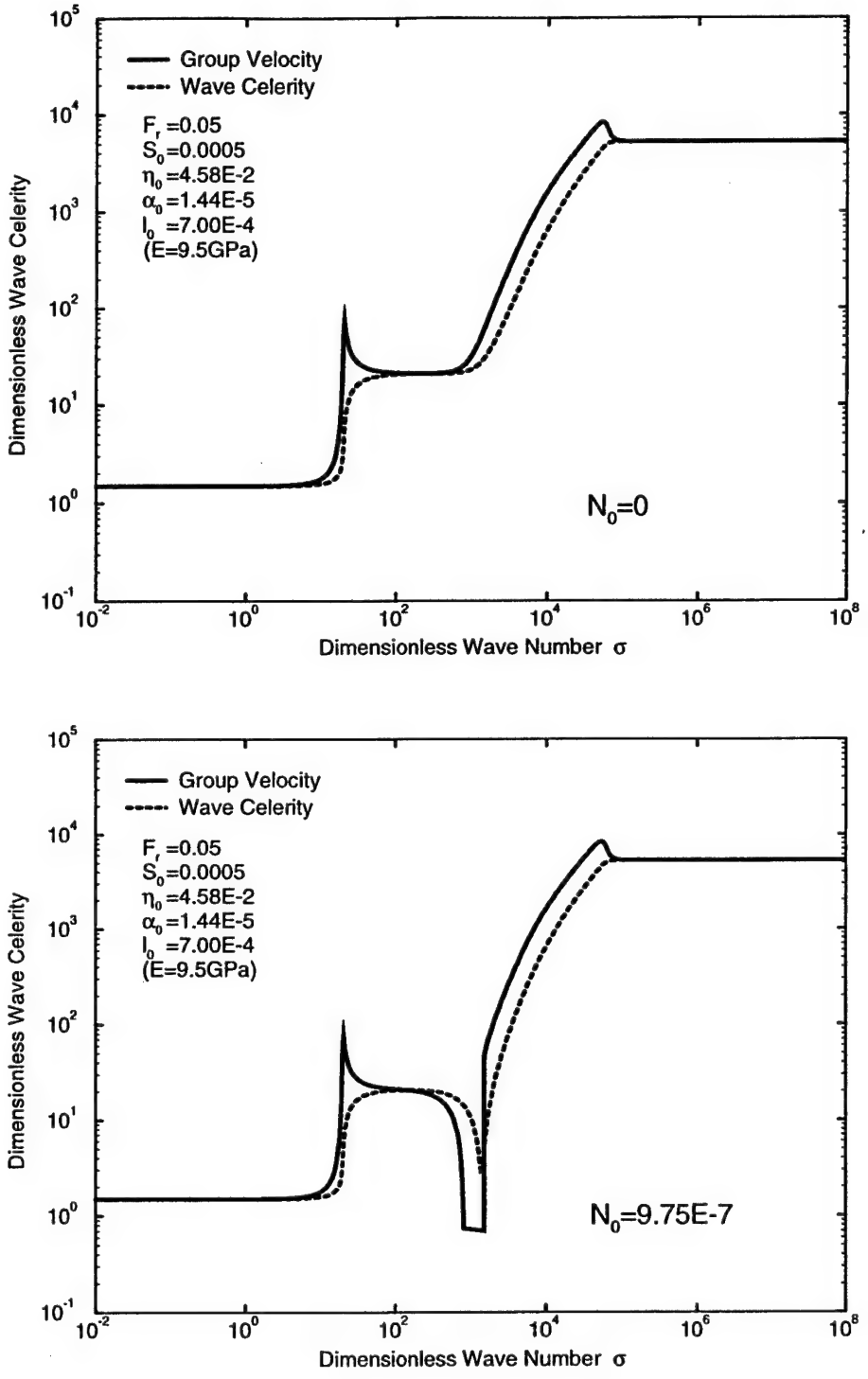

Figure C.27: Dimensionless wave celerity and group velocity as functions of dimensionless wave number

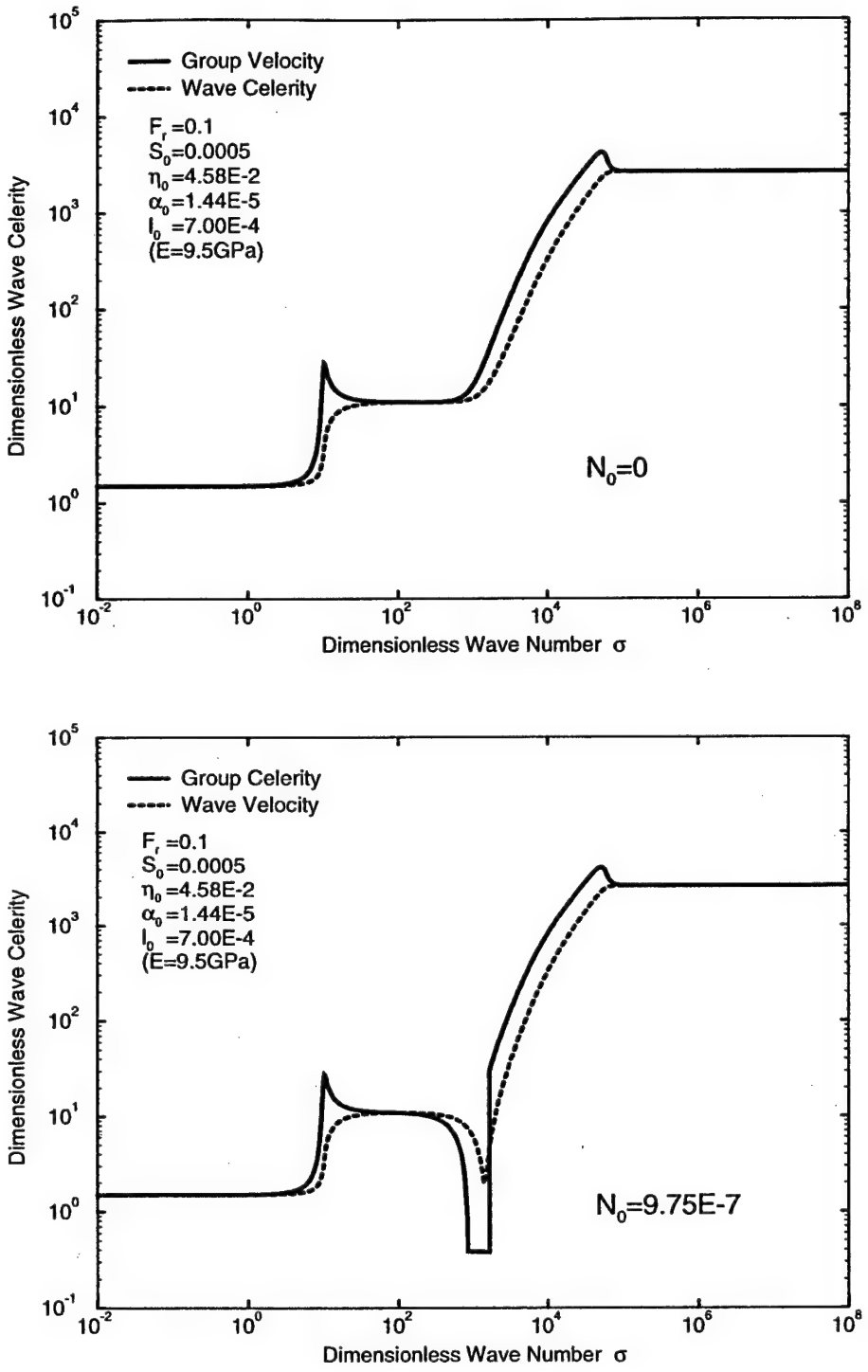

Figure C.28: Dimensionless wave celerity and group velocity as functions of dimensionless wave number

Appendix D

Figures in Nonlinear Model

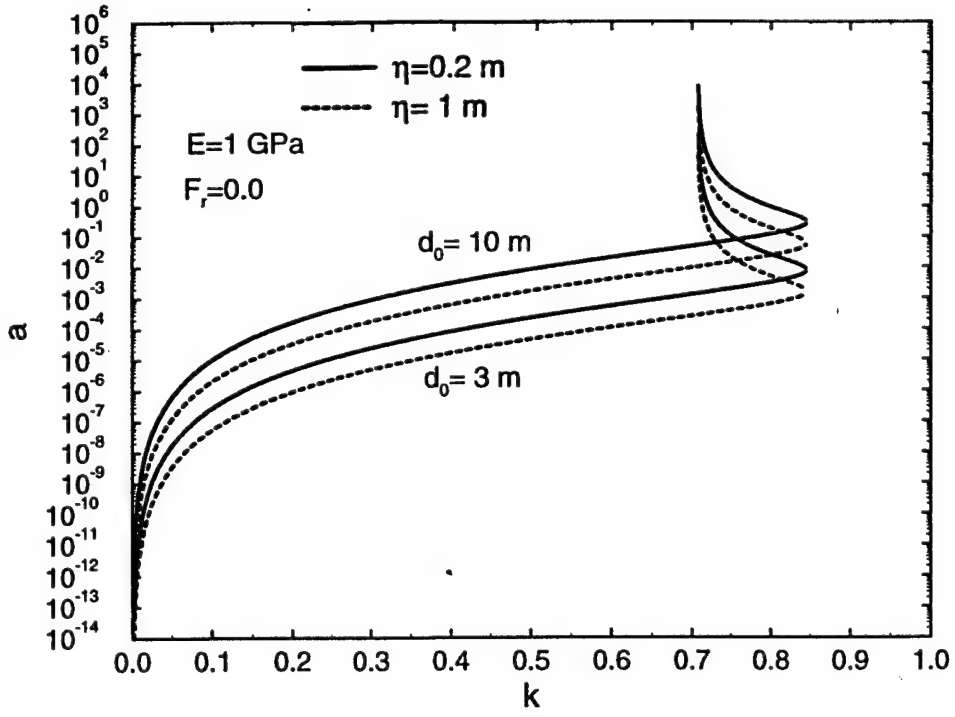

Figure D.1:

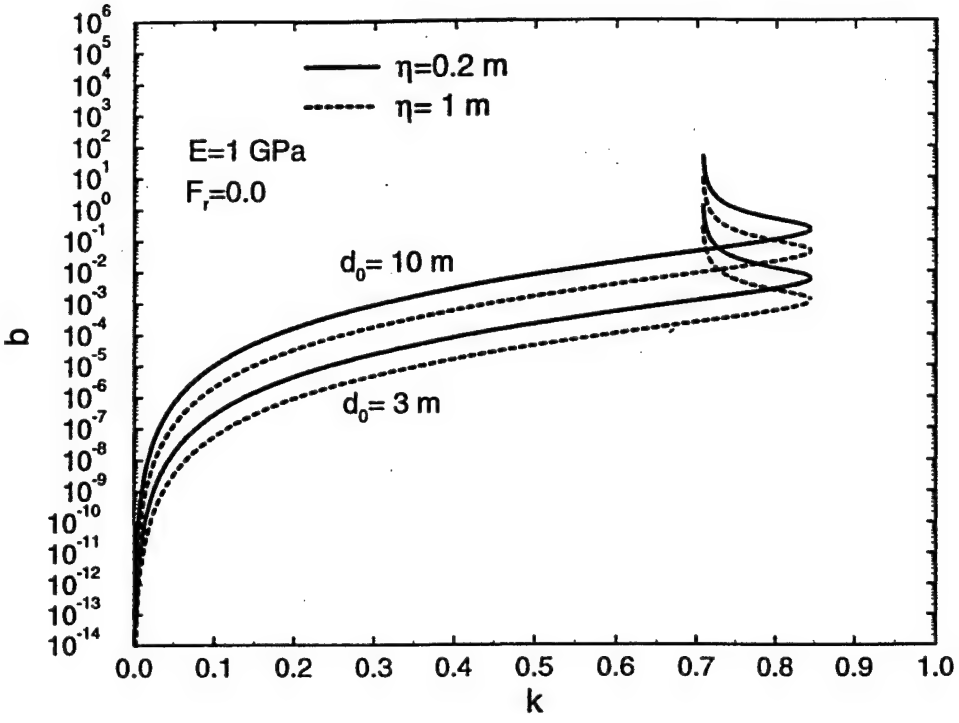

Figure D.2:

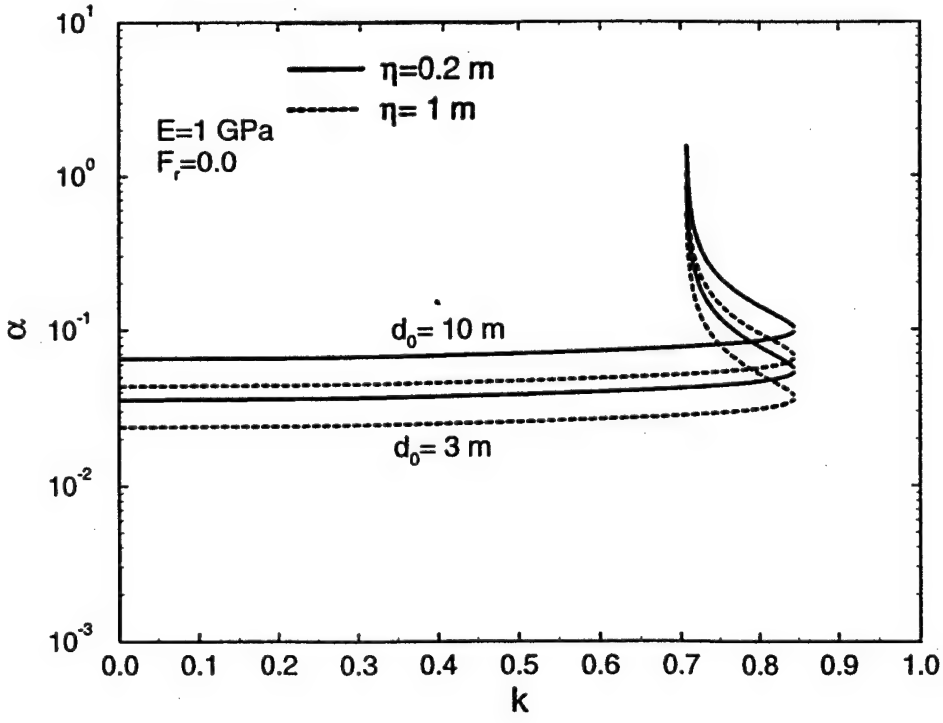

Figure D.3:

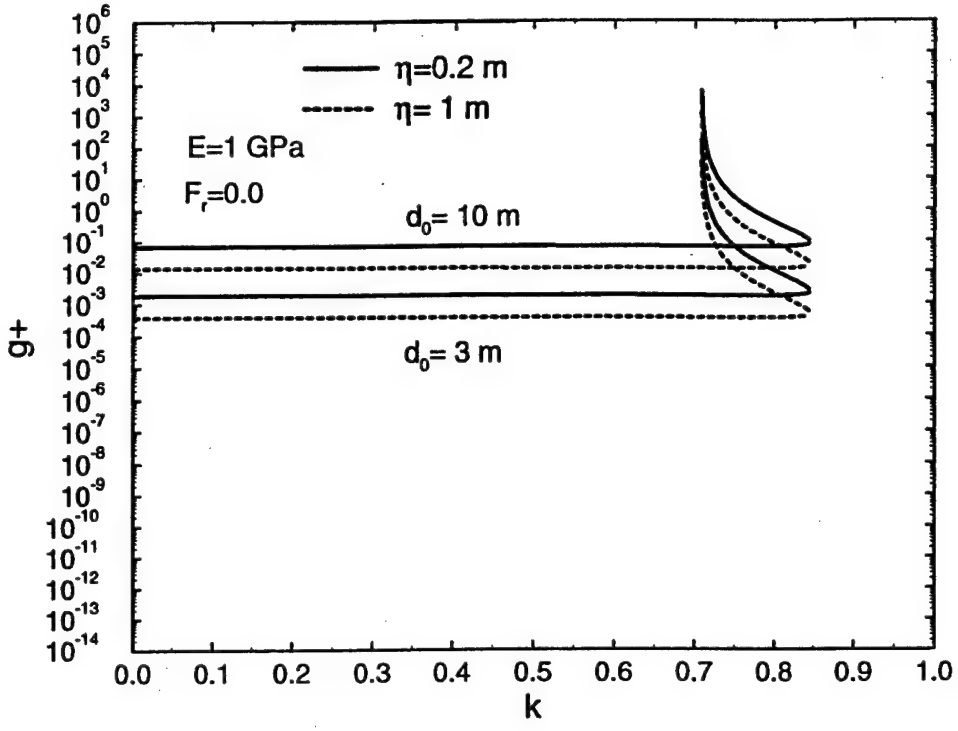

Figure D.4:

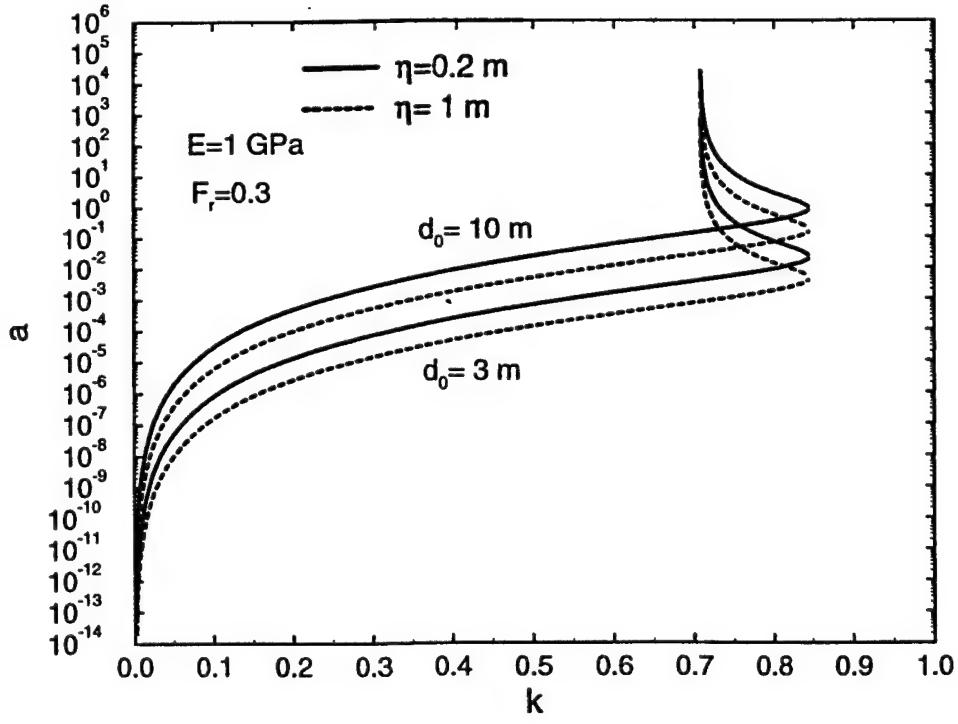

Figure D.5:

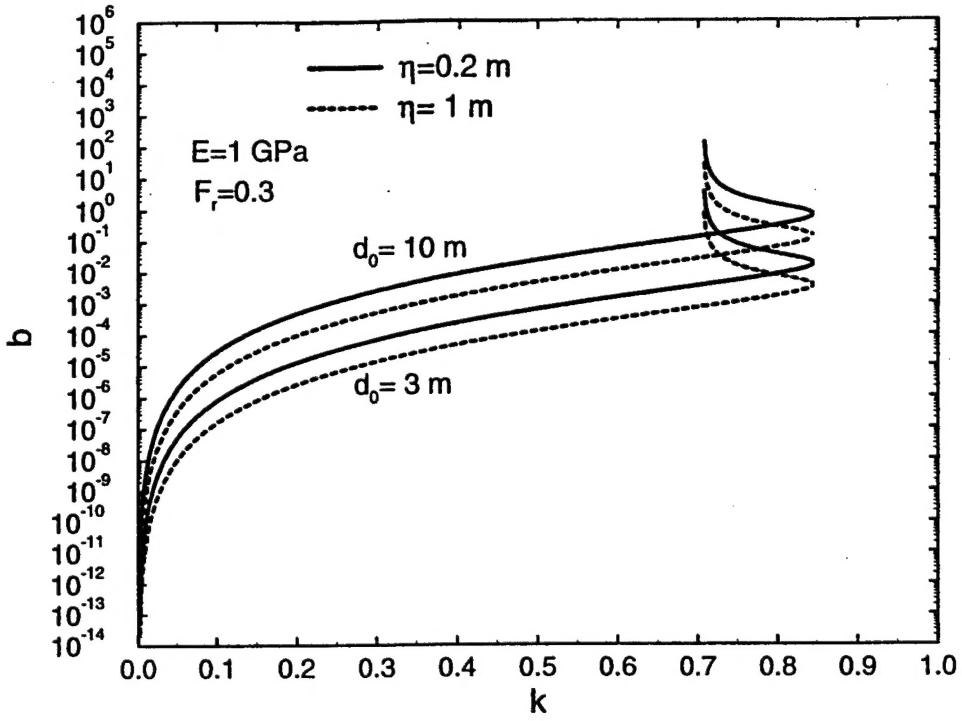

Figure D.6:

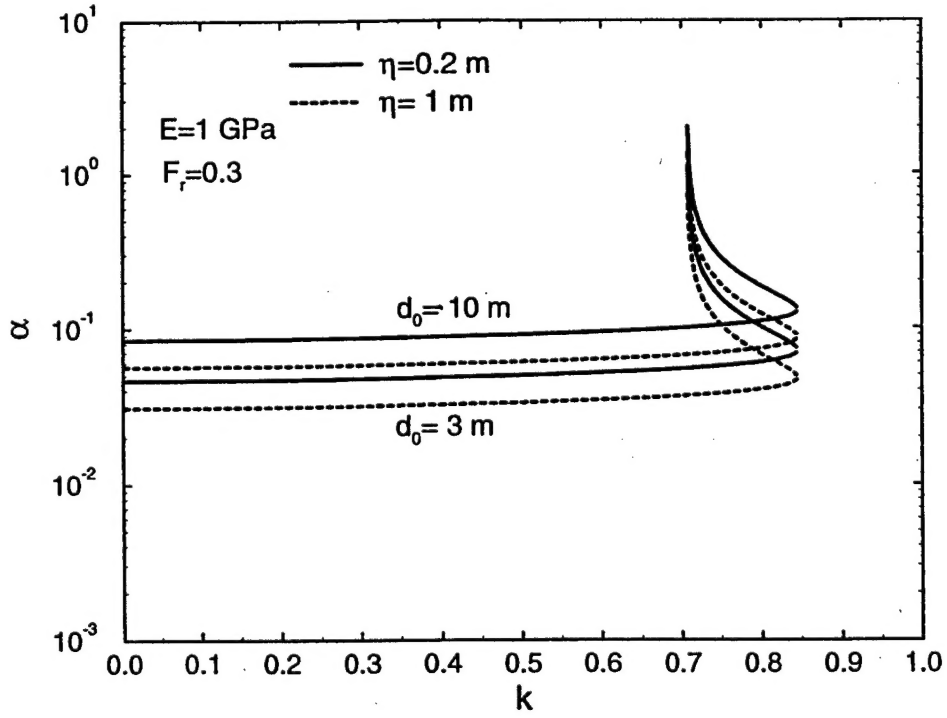

Figure D.7:

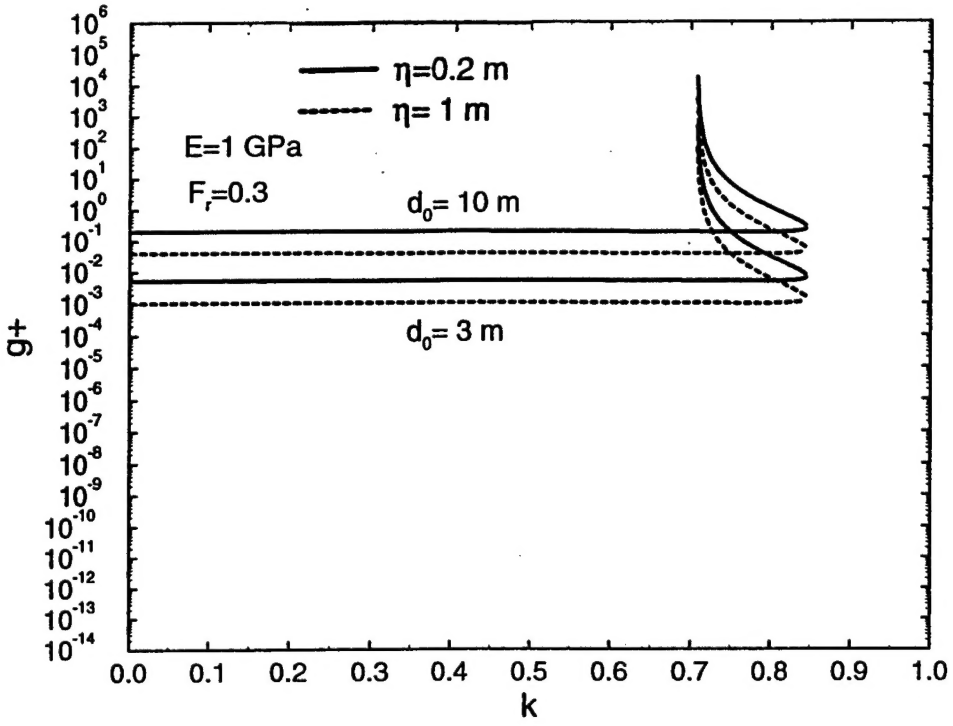

Figure D.8:

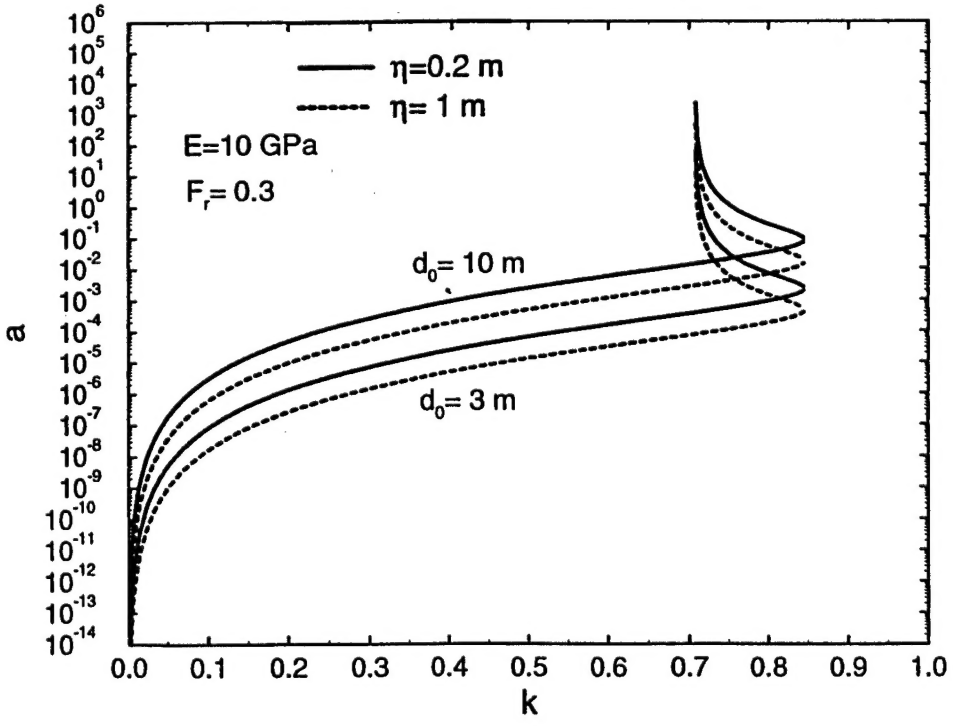

Figure D.9:

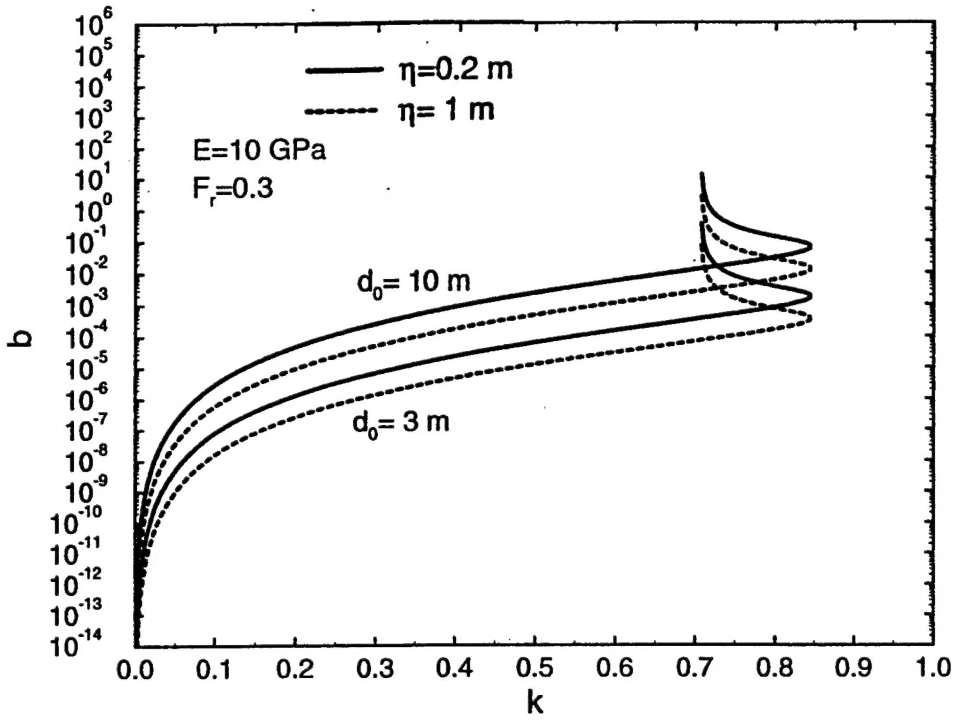

Figure D.10:

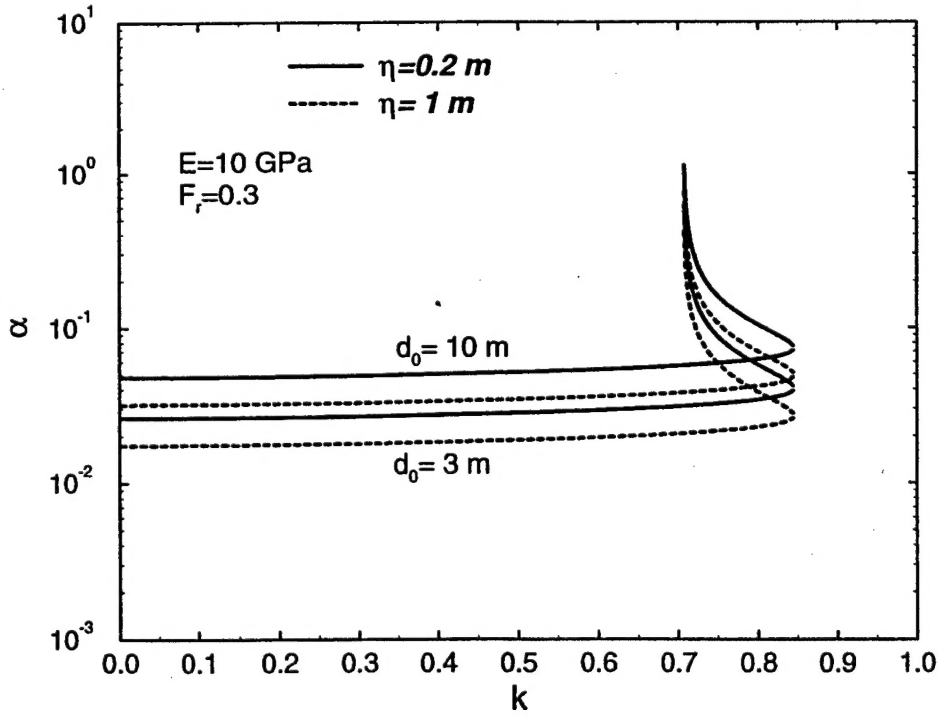

Figure D.11:

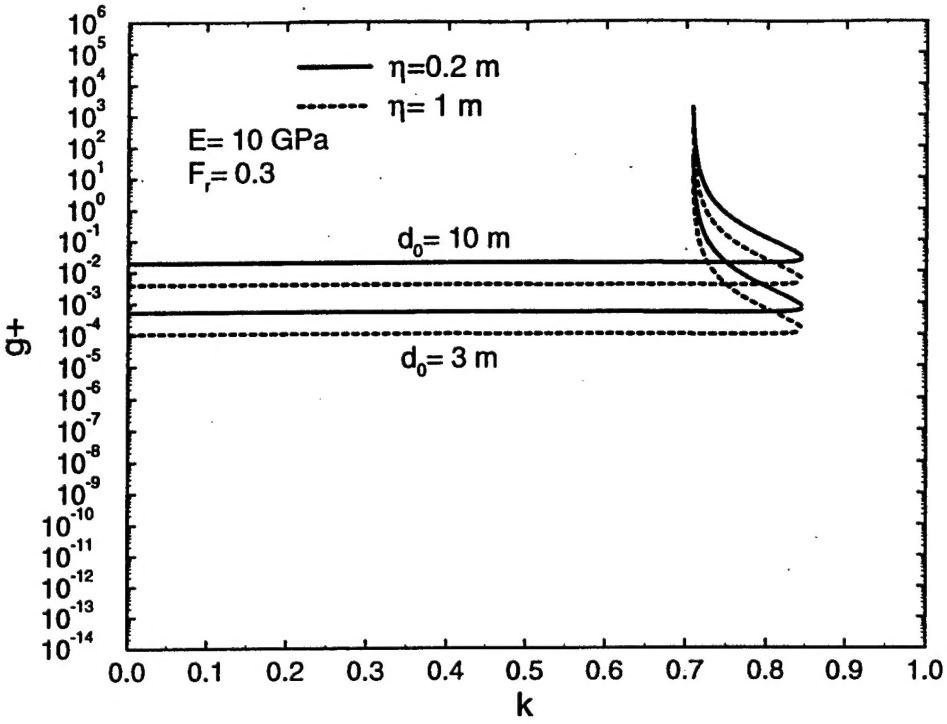
η=0.2 m
η= 1 m
E= 10 GPa
F_r= 0.3
d_0= 10 m
d_0= 3 m
g+
k
0.0
0.1
0.2
0.3
0.4
0.5
0.6
0.7
0.8
0.9
1.0

Figure D.12: